UNIVERSITY OF CALIFORNIA

Los Angeles

Integration and Control of Battery Energy Storage and Inverter to Provide Grid Services

A dissertation submitted in partial satisfaction of the requirements for the degree Doctor of Philosophy in Mechanical Engineering

by

Hamidreza Nazaripouya

2017

ABSTRACT OF THE DISSERTATION

Integration and Control of

Battery Energy Storage and Inverter

to Provide Grid Services

by

Hamidreza Nazaripouya

Doctor of Philosophy in Mechanical Engineering

University of California, Los Angeles, 2017

Professor Rajit Gadh, Chair

This dissertation develops and implements a methodology for integration, and real-time control of battery energy storage and grid-tie inverter to provide grid services and compensate for the intermittency of renewables in the power system with the minimum use of battery capacity.

Deploying Renewable Energy Sources (RES) has attracted significant attention in recent years. However, integrating RES into the grid makes the planning and operation of power systems more challenging due to the poor controllability and predictability of these resources. Technical concerns associated with large-scale integration of intermittent RES include power quality and power stability issues. In order to facilitate the deployment of RES into the power grid, the dissertation proposes control and integration of a battery energy storage system to compensate for the stochastic nature and rapid fluctuations of RESs. To this end, a new control methodology

and integration platform for battery energy storage system is developed which is unique due to its plug and play operation capability which is independent of system parameters, and fast acting characteristic for applications such as real-time solar power smoothing, dynamic voltage regulation, and real-time load uncertainty compensation, while it minimizes the use of battery capacity.

The developed methodology incorporates control techniques, machine learning algorithms, discrete signal processing, and optimization methods for smart operation of battery energy storage systems in the grid. A convex optimization approach is utilized to find the global optimal operating point for battery energy storage system to maximize the performance of the system and minimize the use of storage capacity. The optimal operating point is tracked by a model-free adaptive controller. A discrete signal processing approach adapts the control technique for practical implementation. Machine learning algorithms enable capturing and predicting renewables' and loads' stochastic behavior. In this context, in order to capture both linear and nonlinear patterns, Discrete Wavelet Transform (DWT), Auto-Regressive Moving Average (ARMA) models, and Recurrent Neural Networks (RNN) are combined as a hybrid method for super short-term solar power prediction. Second-order cone programming (SOCP) is employed to design a minimum-length, low-group-delay digital Finite Impulse Response (FIR) filter to compensate renewable intermittency and load uncertainty. An extremum seeking algorithm and adaptive PI controller are used to improve the grid voltage profile in the presence of RES and EVs without an explicit model of distribution circuit.

To prove the performance of the proposed concept, a testbed platform including 64kWh battery energy storage system and 36kW grid-tie inverter interacting with 25kW solar PV and 50kW DC fast charger is designed and implemented. Also a prototype of a hardware/software control unit is built which incorporates the proposed algorithms/techniques for real-time managing the power flow

of BESS and inverter in four quadrants. The control hardware is configured appropriately for interaction of the controller with the grid-tie inverter, battery management system, and measurement units. The control software is structured to manage the communication, safe operation and monitoring of the system. The main advantage of the proposed methodology is to minimize the use of battery capacity for applications such as voltage regulation, renewable compensation, and load compensation. The proposed controller has been tested over several dynamic scenarios including smoothing the solar power generation, voltage regulation and shaping power demand. The results obtained show a 45 percent reduction in the deployed battery capacity for solar smoothing [1] , an 11 percent reduction in the mean absolute value error of the super short-term solar prediction [2], and 20 percent improvement in voltage regulation for defined size of storage, compared with their counterparts in the literature.

The dissertation of Hamidreza Nazaripouya is approved.

Adrienne G Lavine

Tsu-Chin Tsao

Subramanian Srikantes Iyer

Rajit Gadh, Committee Chair

University of California, Los Angeles

2017

Dedicated with Love and Gratitude

to:

My Mother, My Father, & My Brother

Table of Contents

LIST OF ACORNYMS

AR	Auto-Regressive
ARMA	Auto-Regressive Moving Average
BESS	Battery Energy Storage System
BMS	Battery Management System
DC	Direct Current
DCFC	DC Fast Charging
DER	Distributed Energy Resource
DG	Distributed Generation
DOE	Department of Energy
DSP	Discrete Signal Processing
DWT	Discrete Wavelet Transform
ES	Extremum Seeking
ESC	Extremum-Seeking Control
EV	Electric Vehicle
FIR	Finite Impulse Response
GHC	Greenhouse Gas
GTI	Grid-tie Inverter
Li-ion	Lithium-ion
LTI	Linear Time-Invariant
LV	Low Voltage
MA	Moving Average
MAE	Mean Absolute Normalized Error

MAXE	Maximum of Normalized Error
MPPT	Maximum Power Point Tracking
MSE	Mean Squared Normalized Error
NARX	Nonlinear Auto-Regressive models with eXogenous inputs
NaS	Sodium Sulfur
OLTC	On-Load Tap Changer
PLC	Programmable Logic Controller
PMU	Phasor Measurement Unit
PV	Photovoltaic
RISE	Robust Integral of the Sign of the Error
RMS	Root-Mean-Squared
RNN	Recurrent Neural Networks
SCADA	Supervisory Control and Data Acquisition
SIP	Semi-infinite Programming
SMERC	Smart Grid Energy Research Center
SOC	State of the Charge
SOCP	Second-order Cone Programming
STD	Standard Deviation
SVR	Step Voltage Regulator
T&D	Transmission and Distribution
UPS	Uninterruptible Power Source
WT	Wavelet Transform

LIST OF FIGURES

LIST OF TABLES

ACKNOWLEDGEMENT

First and foremost I would like to thank Almighty God for granting me the capability and providing me health and opportunity to propose this work.

I offer my sincerest gratitude to my supervisor, Professor Rajit Gadh, for the patient guidance, encouragement and advice he has provided throughout my time as his student. I consider myself very fortunate for being able to work with a very considerate and encouraging professor like him.

My thanks also go to the members of my committee, Professor Tsao, Professor Lavine, and Professor Iyer for their acceptance of being in my committee as well as all valuable guidance and advice.

I would also like to express my thanks to the Mechanical Engineering Department of UCLA for providing me the opportunity to conduct my proposal in such an academic environment, and my friends and colleagues at UCLA for supporting me in both academic and social life.

I am grateful for the staffs, students, and visiting scholars at UCLA Smart Grid Energy Research Center (SMERC): Dr. Peter Chu, Dr. Ching-Yen Chuang, Dr. Mostafa Majidpour, Dr. Bin Wang, Dr. Yubo Wang, Dr. Wenbo Shi, Dr. Rui Huang, Behnam Khaki, Yu-Wei Chung, Tianyang Zhang, Zhiyuan Cao, Yingqi Xiongm, Dr. Armin Ghasem-Azar, Dr. Musa Yilmaz, and Dr. Tomi Medved for their supports and collaborations. Special thanks to the visiting scholar to SMERC, Prof. Hemanshu R. Pota, for his significant technical guidance.

This work has been sponsored in part by grants from the LADWP/DOE (fund 20699, Smart Grid Regional Demonstration Project) and the California Energy Commission (fund EPC-14-056, Demonstration of PEV Smart Charging and Storage Supporting Grid Operational Needs). I would like to thank them for providing this research opportunity

Above all, I wish to convey my heartfelt thanks and love towards my parents and brother to whom I owe everything. I am forever indebted to my mother, father, and brother for their understanding, endless support and encouragement when it was most required.

.

VITA

Educations

2011-2013 M.S in Power Systems, Louisiana State University (LSU), U.S.

2007-2010 M.S in Power Electronics, Sharif University of Technology, Iran.

2002-2007 B.S in Electrical Engineering, University of Tehran, Iran.

Professional Experiences

2013/02-2013/05 Technical Intern, Entergy Corporation, U.S

2009/10-2011/01 Head of Engineering Department, Arian Chemie Plant, Iran

2005/04-2005/10 Technical Intern, Niroo Research Institute, Iran

Journal Publications

[1] **H. Nazaripouya**, C. C. Chu, H. R. Pota and R. Gadh, "Battery Energy Storage System Control for Intermittency Smoothing Using Optimized Two-Stage Filter," in *IEEE Transactions on Sustainable Energy*, vol. PP, no. 99, pp. 1-1

[2] Bin Wang, Yubo Wang, **Hamidreza Nazaripouya**, Charlie Qiu, Chi-Cheng Chu and Rajit Gadh, "Predictive Scheduling Framework for Electric Vehicle with Uncertainties of User Behavior", IEEE Internet of Things Journal, vol. 4, no. 1, pp. 52-63, Feb. 2017.

Conference Publications

[1] **H. Nazaripouya,** B. Wang, Y. Wang, P. Chu, H. R. Pota and R. Gadh, "Univariate time series prediction of solar power using a hybrid wavelet-ARMA-NARX prediction method," IEEE/PES Transmission and Distribution Conference and Exposition (T&D), Dallas, TX, 2016, pp. 1-5.

[2] Y. Wang, B. Wang, Tianyang Zhang, **H. Nazaripouya**, C. C. Chu and R. Gadh, "Optimal energy management for Microgrid with stationary and mobile storages," 2016 IEEE/PES Transmission and Distribution Conference and Exposition (T&D), Dallas, TX, 2016, pp. 1-5.

[3] Bin Wang, Rui Huang, Yubo Wang, **H. Nazaripouya**, Charlie Qiu, Chi-Cheng Chu, Rajit Gadh, "Predictive scheduling for Electric Vehicles considering uncertainty of load and user behaviors," 2016 IEEE/PES T&D, Dallas, TX, 2016, pp. 1-5.

[4] **H. Nazaripouya**, Y. Wang, P. Chu, H. R. Pota and R. Gadh, "Optimal sizing and placement of battery energy storage in distribution system based on solar size for voltage regulation," 2015 IEEE Power & Energy Society General Meeting, Denver, CO, 2015, pp. 1-5.

[5] Y. Wang, **H. Nazaripouya**, C. C. Chu, R. Gadh and H. R. Pota, "Vehicle-to-grid automatic load sharing with driver preference in micro-grids," IEEE PES Innovative Smart Grid Technologies, Europe, Istanbul, 2014, pp. 1-6.

Patents

1- R. Gadh, **H. Nazaripouya**, P. Chu, "Battery Energy Storage Control System", UCLA Case No. 2016-213-2-LA-FP, Application No: PCT/US2017/033030 May 17, 2017, (Pending)

2- R. Gadh, **H. Nazaripouya**, P. Chu, "Plug and Play Battery Energy Storage Control System for Voltage Regulation", Sep 10, 2017, submitted to UCLA Office of Intellectual Property and Industry Sponsored Research (OIP-ISR)

Awards

1- UCLA Dissertation Year Fellowship Award, 2017

2- IEEE SFV Section Rookie of the Year Award, 2015

3- IEEE Presentation Award (IAS, Power and Energy Society), 2015

4- UCLA Graduate Student Fellowship Award, 2013

Grants

$50,000 NSF I-Corps Grant, 2017 – To investigate commercialization of the UCLA patent resulting from PhD

1 Introduction

Electrical energy is considered a basic need in the development of cities and rural areas as well as improvement of the quality of life [3]. An increasing growth rate in the population in recent years and use of the new products which depend on electricity, the demand for this type of energy is elevating rapidly. At the same time, conventional sources used to produce electrical energy such as fossil fuels are quickly diminishing. A need for developing more electric generation capacity, concerns about fossil fuel depletion and rising energy costs as well as environmental concerns over air pollution and greenhouse gas (GHG) emissions have encouraged the public to move towards renewable energy [4], [5], [6].

Renewable energy sources, like hydropower, geothermal, wind, and solar, have attracted a huge amount of attention due to their sustainability and low impact on the environment [7], [8], [9]. These energy sources neither produce waste nor pollute air, while they are almost omnipresent [10].

Among the renewable energy sources, the adoption rate of photovoltaic (PV) panels is increasing rapidly as they are relatively easy to install on the roofs of individual houses and their cost decreases dramatically. Solar energy is an unlimited and clean source of energy without any harmful gas emissions [6], [11]. However, variability of solar irradiance makes the PV power output uncontrollable and unpredictable which is one of the major barriers for large scale deployment of solar power generation. In the literature, this variable power generation is known as an “intermittency problem,” that hampers the solar panels’ ability to steadily generate power. The static behavior of solar panel systems is the primary reason for the output variability of PVs, thus, any instantaneous change in irradiance absorbed by PVs directly reflects in their output power [10], [12], [13].

There are various challenges that may stem from the uncontrollable nature of solar PVs such as reverse power flow, grid stability, power quality (voltage sags, rise, flicker, and frequency fluctuations), and protection coordination. These difficulties will especially affect the distribution side of the grid where household PVs are immediately connected. Electric utility companies are concerned about potential challenges of large scale penetration of PVs in the power grid.

One of the practical and effective solutions to improve the behavior of renewable energy sources from a grid perspective is the deployment of energy storage systems [14], [15], [16]. Among all feasible types of energy storage technologies, a battery storage system can be considered as fairly developed and widely used. Therefore, battery energy storage systems (BESS) are seriously being researched in the field of distributed generation with the goal of enhancing power quality [17], power stability [18], and power reliability [19].

A BESS has the advantage of mitigating the uncertainty caused by the intermittency nature of solar PV panels. The battery storage system can act as an energy buffer to regulate the output power of solar PV panels. As a reservoir, it can also store the surplus energy produced by renewable sources during light loads (off-peak times) and sending it back to the grid at peak times as a way of balancing supply and demand.

The combination of renewable energy sources and battery storage systems in a smart grid has the capability to improve power quality and stability, increase the reliability of the grid, and reduce the energy bill for the customers [20].

This dissertation after overviewing different challenges associated with the intermittent nature of solar energy resource and also studying the status of solar PV and battery energy storage in US and abroad, proposes a framework to make a solar PV system more dispatchable. It also propose methods to regulate the voltage in the presence of intermittent renewable resources. The framework

includes a method for super short-term prediction of solar power generation based on historical data to improve the controllability of solar power generation. It also includes a methodology for control of battery energy systems to smooth the solar power generation. Finally it equip the framework with a controller manages the BESS active and reactive power flow to regulate the voltage under the load and generation variation.

This dissertation is structured as follows. In chapter 2, the motivation to integrate renewable energy resources and battery storage systems into a modern electric system with the goal of addressing energy demand and environmental concerns are discussed. In chapter 3, a literature review is performed to investigate key challenges presented by widespread propagation of renewable energy in traditional power systems, including power fluctuation, power quality, and protection coordination issues. It also discusses about the consideration for integrating renewable energy resources and energy storage into the power grid. Chapter 4 studies the current status of energy storage and renewable energy in the U.S. and abroad.

Testbed topology design and implementation including a platform consists of battery storage system, inverters, solar PV panels, dynamic loads (electric vehicles) is presented in chapter 5.

Subsequently, this document suggests embedding solar power prediction techniques in dispatching a photovoltaic generation to facilitate real time control of solar power generation and compensating the intermittency, in chapter 6.

Chapter 7 propose a systematic way to optimize the size of the battery capacity for smoothing the solar power to a desired level. This goal is achieved by designing a two-stage filter solution. The first stage is a fast response digital FIR filter that makes a trade-off between smoothing of the solar output and battery capacity. The second stage filter is designed to level the battery charging

load. The proposed approach is demonstrated by simulation results and also over a real case implementation.

Chapter 8 proposes a new methodology to achieve voltage regulation in distributed power systems in the presence of solar energy sources and battery storage systems. The proposed algorithm in this chapter finds the minimum size of battery storage and the corresponding location in the network based on the size and place of the integrated solar generation. The proposed method formulates the problem by employing the network impedance matrix to obtain an analytical solution instead of using a recursive algorithm such as power flow. In this chapter the minimum size and the best place of battery storage is achieved by optimizing the amount of both active and reactive power exchanged by battery storage and its Grid-tie Inverter (GTI) based on the network topology and *R/X* ratios in the distribution system.

Finally, Chapter 9 proposes and implements a model-free optimal methodology to regulate the voltage in distribution systems by controlling the power flow of BESSs. In this chapter an alternative method for voltage regulation is presented that does not require phase measurement, communication, and a system model which are barriers in behind-the-meter applications of BESSs. The proposed method formulates the problem of voltage regulation in form equilibrium map with optimum, without any restriction on system configuration, amount of reverse power flow and/or losses. Without an explicit model of distribution circuit this method coordinates the ratio of active and reactive power in real time, and adaptively controls the amount of exchanged power, using the extremum seeking control technique. Simulation results and experimental results verify the effectiveness of the proposed approach.

2 Motivation

At the end of 2016, global PV installations reached 299 GW_{DC}, up from 225 GW_{DC} in 2015 with an annual increase of 74 GW_{DC} [21]. Only in the first quarter of 2017 the U.S. market installed 2,044 MW_{DC} of solar PV considering as the second-largest source of new electric generating capacity additions brought on-line, responsible for 30 percent of new generation [22]. Every day we hear that more Americans across the country are turning to solar, and this tendency is not just limited to solar panels appearing on the rooftops of homes, but it includes adopting non-residential and utility-scale solar. The United States is especially well suited for a solar energy program as it can benefit from its ample solar energy resources, particularly in the sun-drenched southwestern states.

U.S. Department of Energy (DOE) claims the cost of solar power will fall 75% between 2010 and 2020, reaching $1/watt while the Energy Department's SunShot Initiative aims to make solar energy fully cost-competitive with traditional sources of energy by 2020 [23]. Therefore, the integration of solar sources is expected, in the near future, to experience rapid growth. Currently many American utilities, governed by state or provincial incentives and/or mandated by green-generation portfolio requirements, are encountering installations of large PV plants, owned either by private power producers or the utility, with capacities in the range of several MVAs. Due to this huge amount of integration requests and demands, utilities have been urged to develop comprehensive engineering studies to analyze the effect of PVs on the distribution system. Typically, these areas of study can be categorized according to possible adverse impacts on the power quality, and operation of distribution feeders [24].

The impact studies on the photovoltaic distributed-generation (PV-DG) plants typically focus

on steady-state investigations, such as voltage and power flow analyses. However, many utilities request in depth studies, including the potential dynamic impact of intrinsically variable PV units on transient feeder voltages under various loads and generation conditions. In addition, the integration of PV sources lead to interactions with distribution equipment, such as an increase in the operation of line-voltage regulators and substation tap changers, and changes in status (on/off) of capacitor banks or operation of network protectors, which should be taken into account.

On the other hand, as PV generation becomes increasingly common, the intrinsic intermittency characteristic of solar resources creates another major challenge for those responsible for designing and implementing the next generation smart grid. In the case of grid-tied solar generation, the output can change extremely fast; therefore, a large quantity of installed photovoltaic devices may cause many problems for the distribution system operator.

As a solution, battery energy storage systems are proposed to help with solar sources integration into the grid. Battery storage system along with power electronic devices has the capability of absorbing and delivering both active and reactive power with sub-second response times. With this capability, battery energy storage systems can mitigate various problems posed by intermittent solar power generation such as ramp rate, frequency, and voltage issues [25]. Beyond these applications, energy storage systems can be dispatched in energy markets to provide ancillary services for further economic justification. Figure 1 shows the AC-coupled battery and solar PV system. In this topology battery energy storage can directly interact and exchange energy with the grid. This configuration allows battery energy storage system to contribute in compensation of solar power intermittency as well as providing grid services.

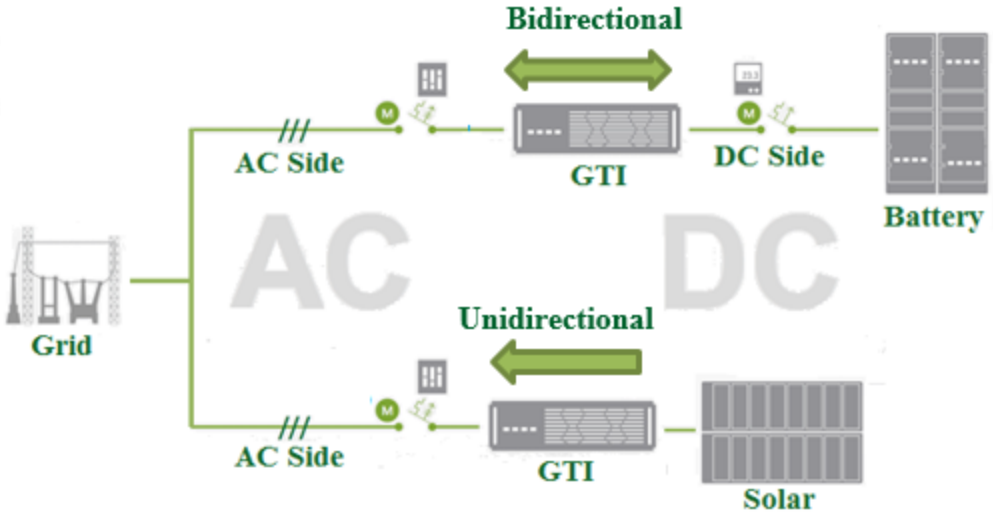

Figure 1 Schematic of AC coupled solar PV and battery system

This dissertation presents an overview of the existing challenges associated with integration of solar resources into the distribution power system. Then it studies the integration of battery energy storage system with solar PV panels to compensate the intermittency of these resources [26]. When there is a sudden change in power generated by solar, the energy storage unit automatically smooths the variations by instantaneously exchanging energy with the grid. The energy storage by levelling the ramps up and down of the power production enables the injection of a smoother power profile to the grid. This capability increases the power quality of solar energy resources and help grid to cope with the sudden change in the solar power.

In addition, this document addresses the voltage regulation issue in the presence of high penetration of solar energy resources. One of the power quality issue in power system is voltage sag/rise. Voltage sag happens when demand exceeds the capacity of the system to deliver the required energy. Voltage rise happens when the local generation exceeds the consumption and reverse power flow occurs. The voltage sag/rise causes malfunctioning or shutting down the electric

equipment if it is sufficiently long and large. In distribution system, the line impedances might mostly be resistive and the ratio of the resistance to reactance (R/X) be considerably large. Therefore, the impact of active power on voltage is not negligible. Energy storage systems integrated into grid through power electronic devices as source of active and reactive power can operate in four-quadrant (charging, discharging, leading or lagging). This allow them to effectively regulate the voltage in distribution system by coordinating both active and reactive power in the grid [27].

3 Literature Review and Problem Description

The motivation to overcome problems, such as environmental concerns, depletion of fossil fuels, air pollution, and increasing the population growth rate and the demand to electricity has accelerated the progress of employing renewable energy sources and has made them the most popular option for providing the required energy. There are still several technical and non-technical challenges that many scientists, researchers, companies, and utilities are investigating to make this evolution possible with maximum efficiency and minimum side effects. A quick survey of the literature shows a large amount of publications on this topic that validates the importance of the issue in the future modern electric network.

This chapter explains different existing challenges and considerations associated with solar and battery storage integration based on research and publications in the literature.

The challenges are generally classified as technical and non-technical. The technical challenges can be categorized as follow:

1. Power fluctuations, which include a) Short term power fluctuations and b) Long term or seasonal power fluctuations
2. Power qualities, which include a) Frequency fluctuations, b) Voltage fluctuations, and c) Harmonics
3. Protection system coordination

The non-technical challenges can be categorized as follow:

1- Lack of technically skilled man power

2- Lack of transmission line to accommodate renewable energy sources

3- Excluding renewable energy source technologies from the competition by giving them

priority to dispatch which discourages the installation of new power plants for the purpose of reserves [28].

Moreover, there are several considerations that should be addressed to integrate renewable energy sources and energy storage systems effectively into the power grid. These considerations include:

1. Placement
2. Communication

This chapter focuses mainly on the technical challenges and considerations.

3.1 Technical Challenges

3.1.1 Power Fluctuation

By increasing the penetration of renewable energy sources, the intermittent nature of generated power causes challenges such as stability, reliability and power fluctuations in the main electrical grid. Here short term and long term impacts of this phenomenon are discussed.

3.1.1.1 Short Term Power Fluctuations

One of the major problems associate with PV integration into the grid is the fluctuation of PV output power. This phenomenon has a negative impact on the electric network performance to which these systems are connected, especially when there is a high level of penetration. On the other hand, these fluctuations make it difficult to predict the output power of PVs and, as a result, difficult to consider them in generation scheduling in the network. Figure 2 and Figure 3 show two sample results of these fluctuations.

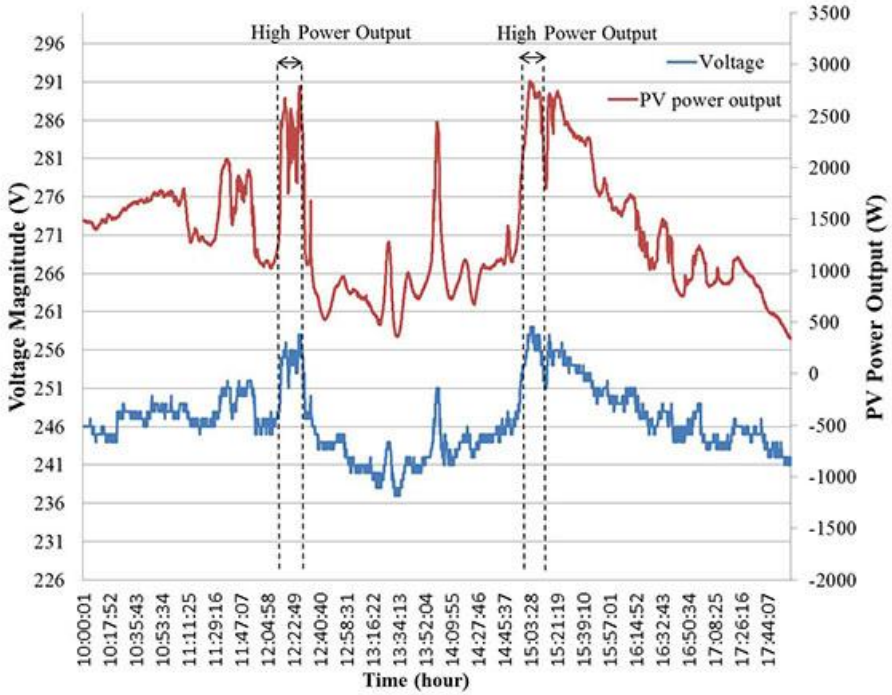

Figure 2 Voltage and power fluctuation of PV output [29]

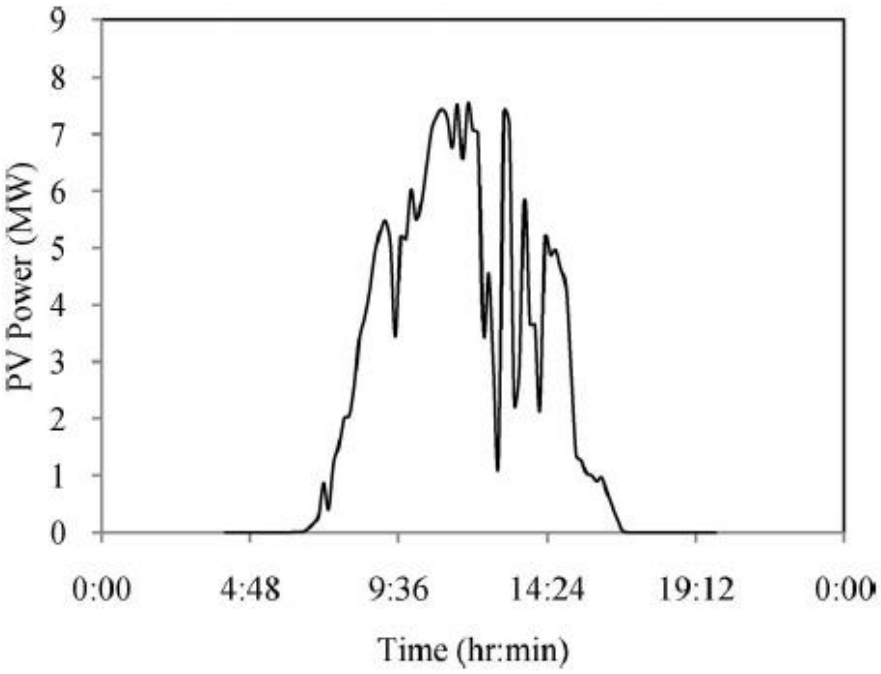

Figure 3 Power fluctuation of during one day [13]

Several researchers have focused on modeling PV power fluctuations for better understanding this problem. For example, the authors in [30] propose the probabilistic modeling of short term fluctuations of photovoltaic injected power in order to evaluate the overvoltage risk in low voltage grids. Solar power generation prediction in a laboratory-level micro-grid is proposed in [31]. In [32] the authors propose a method to estimate the Standard Deviation (STD) of the total power's output fluctuation in high-penetration photovoltaic power generation systems (HP-PVS), and then the impact of HP-PVS on the load frequency control is discussed.

Three methods have been proposed in [13] for solving power fluctuations: 1) use of battery storage systems, 2) use of dump loads, and finally 3) curtailment of the generated.

Several publications focus on power compensation techniques for grid connected photovoltaic systems that are integrated with battery storage systems [33], [34], [35]. A fast response energy storage system integrated with RES can effectively mitigate the intermittent power generation [24]. The energy storage unit can automatically smooth the RES power variation by instantaneously exchanging energy in reverse. Figure 4 below shows the result of solar power smoothing by energy storage in Borrego Spring microgrid [25].

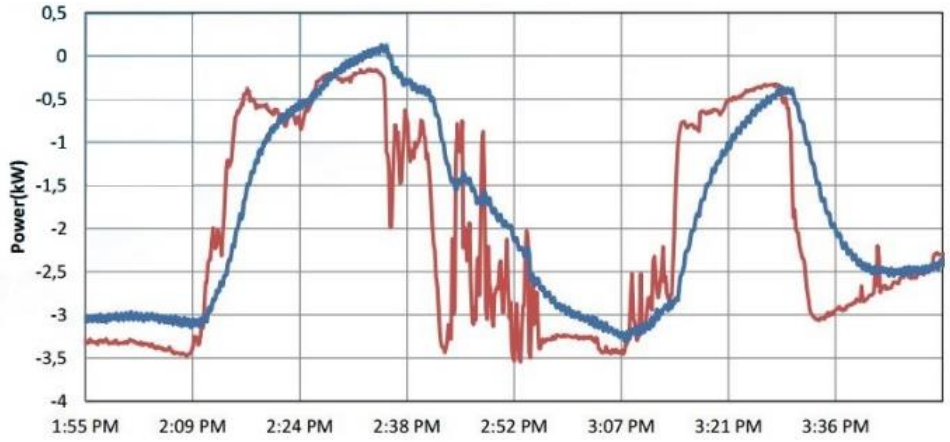

Figure 4 Solar power smoothing by energy storage in Borrego Spring microgrid [25]

3.1.1.2 Long Term Power Fluctuation

The results obtained from an investigation performed by the New Energy and Industrial Technology Development Organization (NEDO) on 553 residences in Ota City, Japan, demonstrate the seasonal power fluctuations of photovoltaics [36]. Figure 5 shows the PV energy generated daily over one year.

The PV output pattern of the first week of April (spring), August (summer), November (autumn), and February (winter) were chosen to depict the influence of seasonal changes on PV output. The PV energy generated daily during the four seasons is shown in Figure 6.

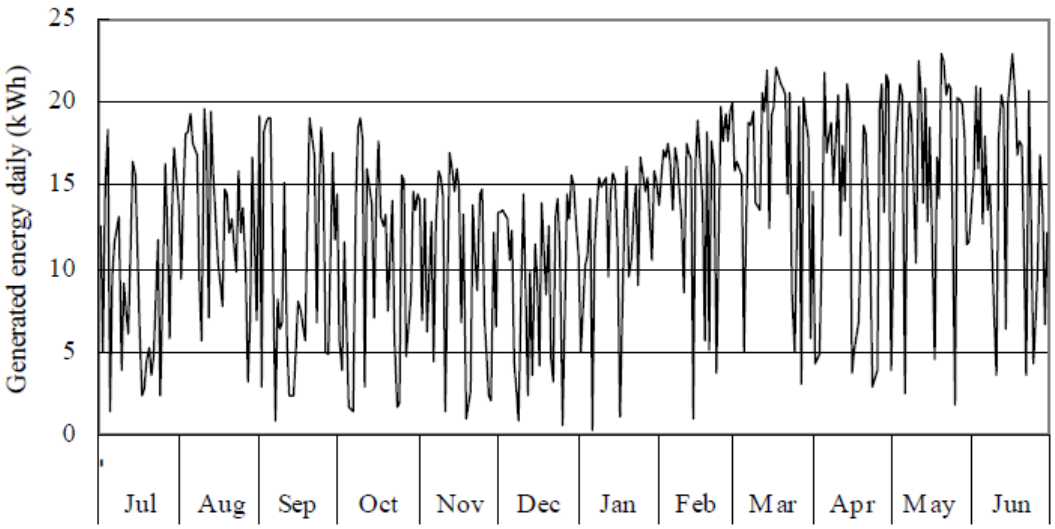

Figure 5 PV energy generated over a year daily base [36]

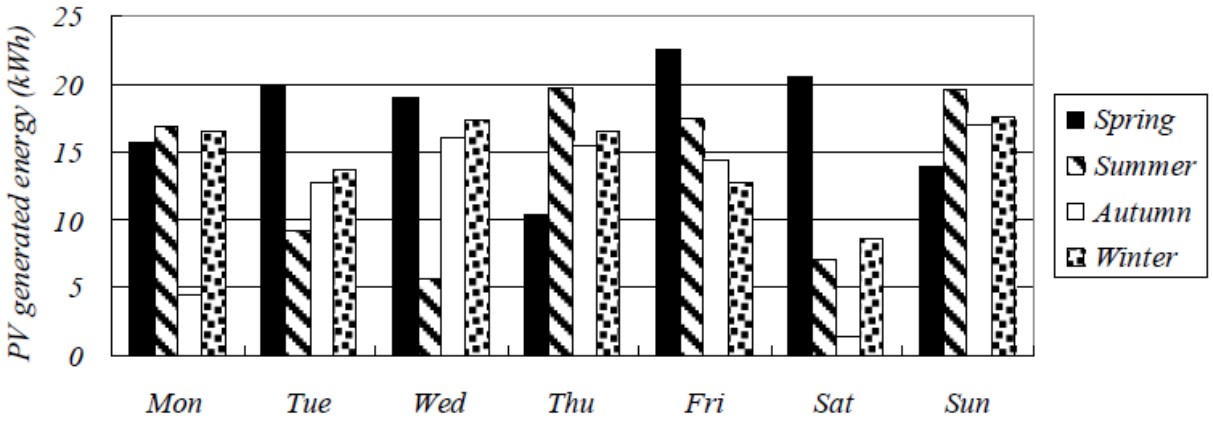

Figure 6 PV generated energy with selected data from the four seasons [36]

Although there are several publications which investigate, model, predict, and propose solutions for short term power fluctuations of PVs, few of them investigate the long term and seasonal aspect. For example, the German authors in [37] considering the fluctuating feed of a solar power plants with a measuring data set of several years which has a resolution of quarter-hour values, present the influence of a central storage in a rural distribution network with a high penetration of photovoltaic systems. They show the possibility of the reduction of solar power gradients by deploying proper size of energy storage and making the solar power supply less weather dependent.

3.1.2 Power Qualities

Analyzing the impact of PV systems on electrical energy systems, significant research studies are being promoted on different aspects of the issue. Power quality is one of those fundamental aspects.

Technical considerations such as frequency deviation, voltage deviation, voltage waveform, voltage unbalance, power factor, and short circuit levels should be taken into account when a small

PV power plants connected to the distribution network. These considerations are essential to ensure the reliable operation of the distribution networks operating in parallel with the PV power plant. Otherwise, there would be the possibility of tripping protection systems and power outage due to sudden changes in voltage or frequency [38]. To this end, normally different parameters, such as voltage, current, power, power factor, unbalance, and harmonic distortion, are measured and analyzed. The influence of PVs on different criteria of power quality is discussed in this chapter.

3.1.2.1 Voltage and Frequency Fluctuation

The authors in [39] conducted an analysis on the impact of photovoltaic power generation on a low-voltage distribution network. The evaluated distribution network is a radial system with a nominal phase voltage of 230 V, located in the South Moravia Region, in the Czech Republic. The maximum power demand through the distribution transformers during the measuring period was 175 kVA, with an average 65 kVA. There was a PV source connected to the system with a rated power of 15 kW. Figure 7 and Figure 8 show the reported Root-Mean-Squared (RMS) value of voltage in point of PV power plant connection (point A) along with the PV power data for three consecutive days. In order to investigate the behavior of distribution networks under variations of solar radiation, these days are chosen based on the solar radiation. Figure 7 and Figure 8 compare the system behavior in both cloudy and sunny days.

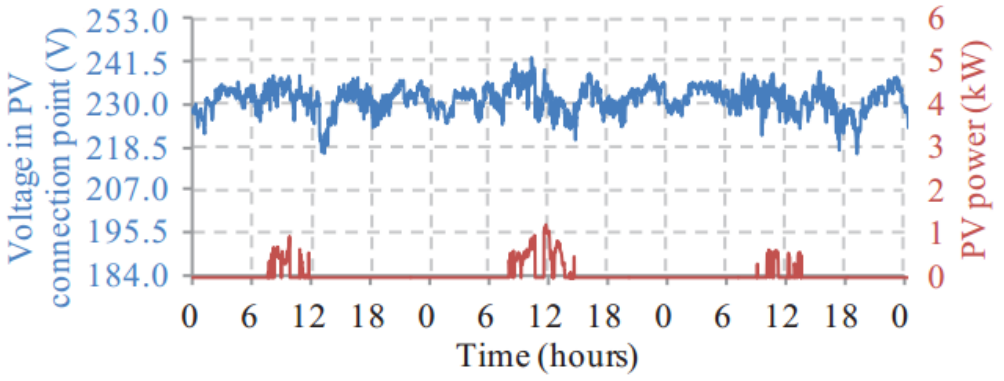

Figure 7 1 min. average voltage RMS value and PV power during three cloudy days in point A, phase A [39].

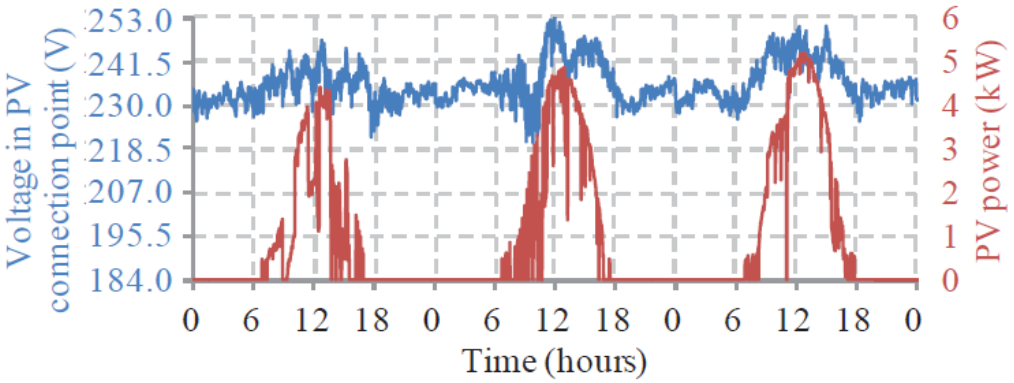

Figure 8 1 min. average voltage RMS value and PV power during three sunny days in point A, phase A [39].

The measured voltage in the point of PV connection shows 3.11 V increase per one kW of PV source in the network. Therefore, depending on the network size and the size of the installed PV power source, the RMS voltage is subject to change.

Authors in [40] presents a dynamic power quality analysis on a 1.8 MW grid-connected PV system in a radial 16 bus test system under different weather conditions and varying solar irradiations. It validates that highly penetrated grid-connected PV systems can cause power quality problems, such as voltage flickering and rise, as well as power factor reductions.

The authors in [41] propose a control scheme for PV inverter reactive power to accommodate higher level of PV penetration and regulate the voltage. The proposed controller dynamically changes the reactive power during solar power fluctuating state with rapidly varying solar irradiance to mitigate voltage fluctuations. In contingency state when the PV terminal voltage violates the allowable operating range, the controller uses the PV inverter as reactive power sink/source to bring the voltage back within the range. Results demonstrate the proposed approach reduces the number of OLTC operations, smooths out voltage fluctuations, and mitigates voltage violation in the LV grid.

3.1.2.2 Harmonic

A power quality analyses on a large scale photovoltaic system is performed in [42]. The evaluated system is a 1MVA centralized PV plant connected to a medium voltage distribution system in Brazil which is the largest PV system in operation in the Brazilian electric system, called "Usina Solar Tanquinho". The system comprises a large central 500 kW inverter plus fifty distributed 10 kW inverters. The measurements are basically on the fifty inverters side. The obtained results are illustrated as follows.

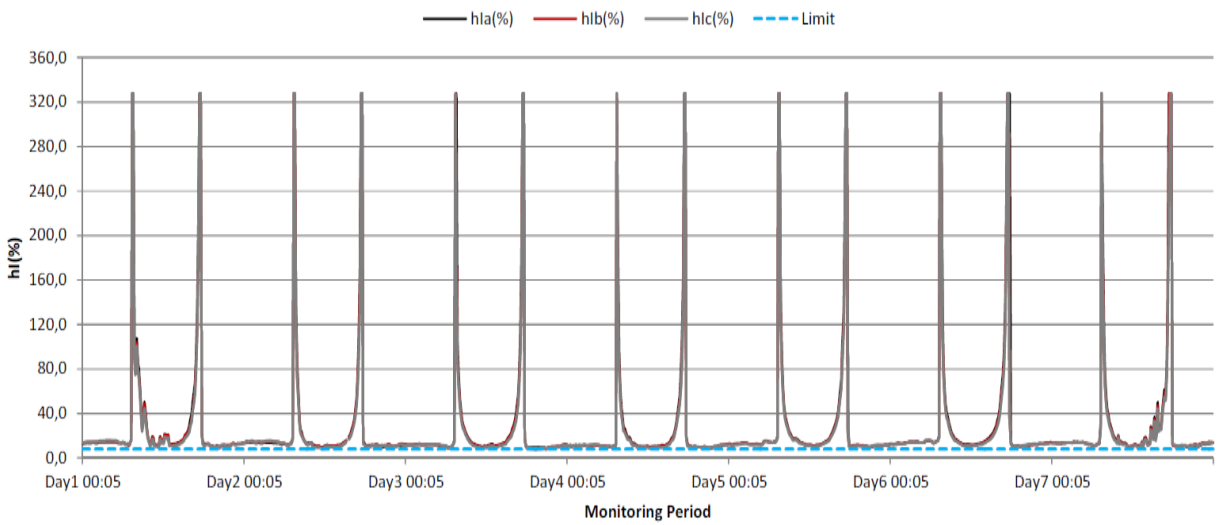

Figure 9 Measured harmonic current [42]

In Figure 9, although based on IEEE 519 the allowed current harmonic is 8.0%, there is a constant violation from the limit, sometimes by as much as 320%.

A power quality improvement in a 3-phase grid connected PV system is presented in [43]. In this study, the PV generation is forced to reach a maximum power operation by employing the variable step perturb & observe (VS-PO) Maximum Power Point Tracking (MPPT) scheme. A battery energy storage system via a bi-directional DC/DC converter is used to maintain the DC bus voltage level at a constant value. The reactive power and load current harmonics, generated by the nonlinear, load are compensated with a 3-phase hybrid filter connected to the utility grid.

3.1.3 Protection system coordination

PV sources have the potential to relieve burdens on the power distribution system, but it also poses challenges to well-known traditional protection mechanism in distribution systems, especially at the high levels of penetration. For example, PVs could contribute to fault currents on top of power grid.

The conventional nature of power distribution system is radial with downstream feeders being fed by a single source. In such a system, the protection scheme is composed of fuses, overcurrent relays, and reclosers that are designed based on the single direction fault current from the single source to the location of the fault. However, with the fast expansion of renewable sources, a couple of challenges would arise in terms of feeder protection [44]. The first challenge is the Bi-directional fault current; that is, by having multiple sources on the distribution network, all of them could contribute to the fault current which leads to bi-directional fault current. Hence, traditional relays which are insensitive to direction might become improper [44], [45]. The second challenge is reducing or increasing the fault current captured by relays, which upset the relay coordination [46], [47]. Finally, this integration can cause changes in the levels of fault currents [48], [49]which are due to the intermittent nature of photovoltaic sources. As a result the fault current levels may constantly change, making it difficult to coordinate conventional protection, which is only works with fixed settings.

3.2 Considerations

3.2.1 Communication

Communication systems are vital technologies for the integration of renewable energy sources and energy storage systems into the grid. In order to accommodate power transfer and reconfigure the network topology for more efficient power flow, bi-directional communication is the fundamental infrastructure. Many types of equipment in the grid should be monitored and controlled, such as meters, sensors, voltage detectors, etc., The communication infrastructure plays an important role in Decision Support Systems (DSS) and applications such as Supervisory Control and Data Acquisition (SCADA), energy management systems (EMS), protective relaying,

distribution feeder automation, generating plant automation, and physical security [50]. These applications are essential for the protection, operation, and monitoring of renewable energy generators and energy storage systems in power systems.

There are several available communication options for the integration of renewable energy resources and energy storage to the grid. These options include a combination of technologies, such as fiber optics, power line communications, copper-wire line, and a variety of wireless technologies. Utilities are interested in running as many applications as possible over their networks; therefore, issues of bandwidth, latency, reliability, security, scalability, and cost are still challenging topics. Although significant effort has been made to develop the smart grid infrastructure for better data interchange [51], [52], distinct characteristics of the electric grid pose new considerations to the communication systems for grid integration of renewable energy resources and energy storage systems [50]. These considerations include: 1) Reliability, coverage, and flexibility, 2) Addressing and localization, 3) Islanding detection, 4) Power consumption of the end device, and 5) Standardization of protocols.

In [53], a communication network design is proposed based on the pattern of the distribution network. A mathematical model of the communication network using different physical communication media is developed to offer an optimum solution for solving the communication tasks in various distribution network structures. A distributed communication schema is proposed in [54] for individual devices such as generators, photovoltaic systems, energy storage systems, microgrid point of common coupling switch, and supporting applications to improve interoperability, and plug-and play operation. The authors in [55] aim to improve communication reliability of a SCADA system in PV power plants, using an effective security strategy that includes a redundancy mechanism.

3.2.2 Placement

Integrating a PV and storage systems into the distribution network raises new issues and challenges for those who are responsible for planning the distribution system. The challenge is to find the suitable trade-off between the reliable and safe delivery of electrical energy to the end users and achieving maximum financial goals for the private investors in a timely manner. However, the installation and operation of renewable sources and storage cause complexity in electrical distribution systems. As it was mentioned, traditional radial distribution systems are not designed for bi-directional power flow. Therefore, important aspects of system performance, such as operations, protection, and system costs, can be affected by adding additional sources into the distribution systems. Currently, there is no industry standard to determine the amount and the corresponding location of renewable sources and storage on a feeder to avoid adverse effects.

The authors in [56]study and propose an approach using a genetic algorithm to find the optimal sizes and placements of Distributed Generators (DGs) in a Jeju island microgrid.

A methodology is proposed and tested in [57] that optimizes the sizing and placement of renewable sources on electrical distribution feeders based on technical and economic considerations; tests are conducted on an IEEE 34-bus system.

The optimal placement of a PV power plant on the distribution network based on minimizing active and reactive power losses is explained in [58]. The PV system and loads are modeled with electric production/consumption curves compiled daily with discrete hour intervals.

The same problem is considered in [59] with a concentration on the voltage stability factor, while [58] targets reliability.

Authors in [60] investigate optimal placement and sizing of energy storage in a distribution system to minimize total energy loss. They model a distribution network as a continuous tree with the linearized DistFlow model, and formulate the problem as an optimal power flow problem. It is proved that it is optimal to place storage devices near the leaves of the network away from the substation while the scaled storage capacity monotonically increases toward the leaves.

4 Status of Solar Energy and Battery Storage System

4.1 Solar Energy

By increasing the awareness of solar PV's potential to alleviate pollution and reduce CO_2 emission as well as increasing the competitiveness of solar PV and rising the demand for electricity, the solar PV market is expanding rapidly. Around 75 GW_{dc} of solar PV capacity is integrated worldwide during 2016 which is equivalent to installation of more than 31,000 solar panels every hour. This number is more than the cumulative world capacity five years earlier [61]. The integration of solar energy technologies has grown exponentially over the last decade at the global level. For instance, the global installed solar PV capacity, including grid-connected and off-grid, increased from 1.4 GW in 2000 to approximately 227 GW in 2015 as shown in Figure 10 [62]. Continual policy support in countries, such as Germany, Italy United States, Japan and China, is associated with the motivation behind the recent growth of solar technologies. Figure 11 shows several dominant countries in the PV market. Among them, some are experiencing a significant market growth in 2015; in particular, the PV market's growth pushes India for the first time into the top 5 countries with 2,1 GW as shown in Figure 12. UK also grew significantly in 2015, and with installed 4.1GW PV systems keep its position as the first country for PV installations in Europe [63].

In 2016, the top five solar PV markets belong to China, United States, Japan, India and United Kingdom, respectively. However, regarding the cumulative capacity, China, Japan, Germany, United States and Italy are among the top five countries.

In 2016, China by adding 34.5 GW solar PV capacity increased its total capacity by 45 percent, far more than that of any other country [61]. However, the rapid growth of solar PV capacity in

china has caused grid congestion problems due to the inadequate capacity of transmission system. Therefore, curtailment of solar PV started to become a serious concern.

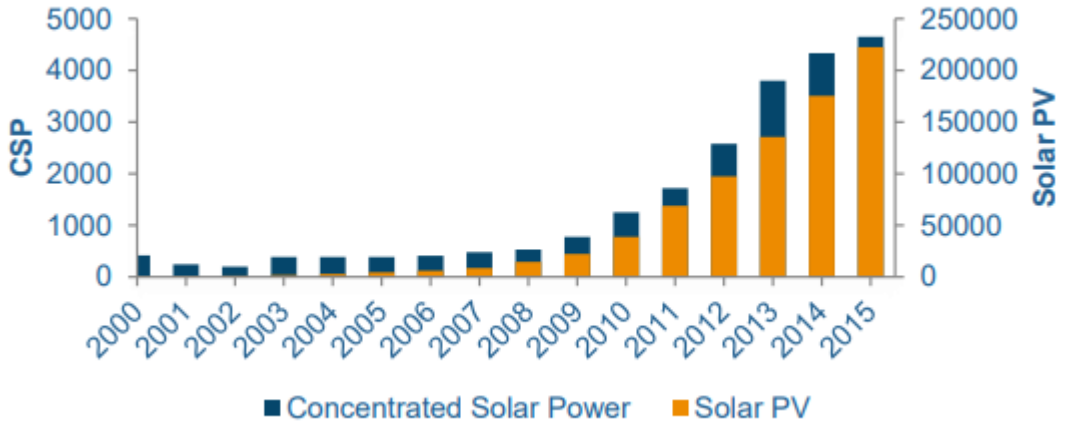

Figure 10 Total installed capacity of PV global trend [62]

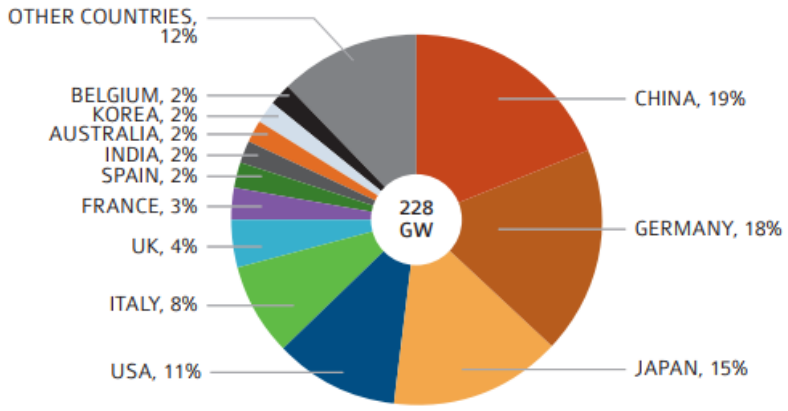

Figure 11 Country share in th cumulative PV global capacity end 2015 [63]

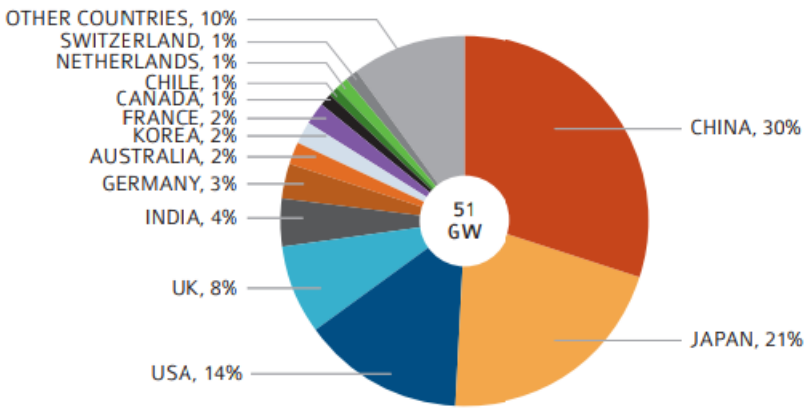

Figure 12 Global PV market in 2015 [63]

Japan by adding around 8.6GW solar PV capacity in 2016, and cumulating 42.8 GW capacity in total, passed Germany and stood second in rank for cumulative solar PV capacity. This country experience growing demand in residential sector. Also solar-plus-storage gain significant attention. As early of 2016 approximately 50,000 residential consumers had storage with their PV systems. Again in Japan, difficulties of securing grid connections are one of the reasons to slow down the PV market's growth [61].

India is the third largest market in Asia, ranked fourth globally for additions and seventh for cumulative capacity. Although in India rooftop solar market has expanded significantly in recent years, it is still far away from its target of 40GW by 2022. In India currently the grid congestion and curtailment are the most immediate challenges [61].

The European Union is the first region which passes the 100 GW milestone in 2016. This region finish the year 2016 with around 106 GW, more than 32 times its 2006 capacity. Most of the installation was in the United Kingdom, Germany and France which together integrated about 70% of the region's new grid-connected PV capacity [61].

The United States by bringing more than 14.8GW of solar capacity, almost double the installation in 2015, is a second after china for new solar PV installation. In 2016, for the first time solar PV represented the leading source of new generation capacity in the US, beating natural gas and wind in new capacity additions [64]. California again by adding 5.1GW solar capacity led, followed by Utah (1.2 GW) and Georgia (1 GW), which became the third largest state market even without additional mandates, subsidies or tax incentives beyond federal tax credits [61].

In US, although all sectors including residential, non-residential, and utility segments have expanded, primarily the growth occurred in the utility sector. Several US utilities established their own solar programmers as the cost of solar PV deployment has rapidly dropped over the years and different factors, such as fast customer adoption, improving financial conditions, public market successes, and grassroots support for solar, have contributed to the success of distributed solar PV for the general population and the investment community.

In 2016, for the first time, the US federal government launched an initiative to promote solar power and energy efficiency for low-and moderate income Americans [65]. At the sub-national level also several policies targeted towards low-income populations. For example, in California, Massachusetts and the District of Columbia, there are programs to increase access to renewable energy for low-income communities. In addition, 12 states initiated community net metering programs to help low-income residents access solar PV. These programs extend the benefits of solar PV to renters and not only property owners. During the year 2016, among new state initiatives, New York support solar PV deployment in low-income communities by USD 3.6 million in funding, and Illinois' Future Energy Jobs Bill promotes solar PV deployment for low-income communities.

In 2016, five states including California, Hawaii, Vermont, Nevada, and Massachusetts produced more than 5% of their total net generation from distributed and utility-scale solar PV [21].

Since 2005, when the congress passed the investment tax credit, the residential PV market has expanded 95 times by approximately 51% growth per year. At the end of 2016, there were over 1.25 million residential PV systems in the United States. Figure 13 shows the US residential PV market from 2005 to 2016.

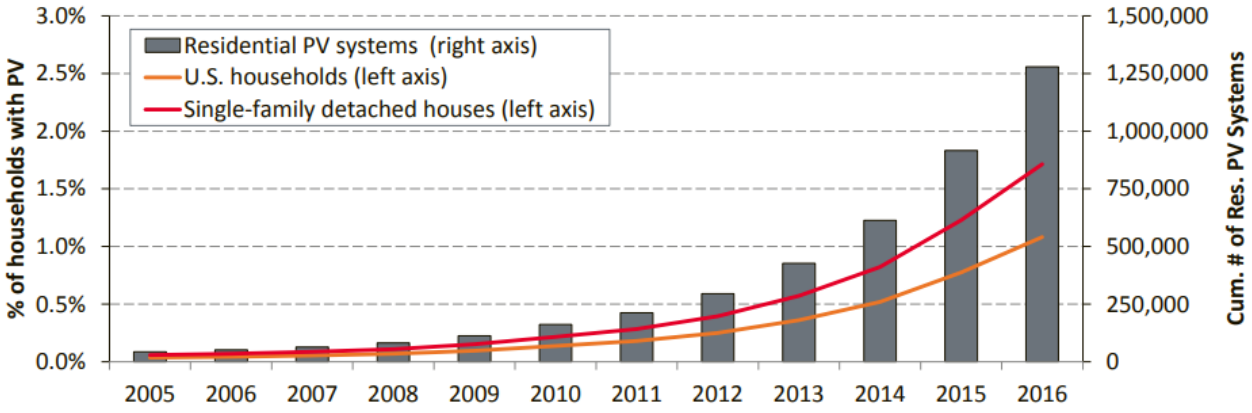

Figure 13 US residential PV market

The ongoing growth of solar PV capacity was driven by the continued decline in prices for this technology. Between 2007 and 2014, price of PV module declined by around 79 percent; the biggest yearly reduction was seen in 2011, when the price dropped by around 40 percent compared with 2010 [62]. In 2016, the median system prices dropped by 4 percent. From 2015 to 2016 the average gross costs of a residential system fell by 9 percent. Figure 14 depicts the average monthly solar PV module prices by manufacturing country, and technology between 2009 and 2014.

The Utility-owned PV prices also dropped significantly. The system price data from nine regulated utilities for projects larger than 5MW show that the capacity weighted average price of a utility-owned PV system fell 78% from \$5.90/W_{DC} to \$1.32/W_{DC} between 2009 and 2016.

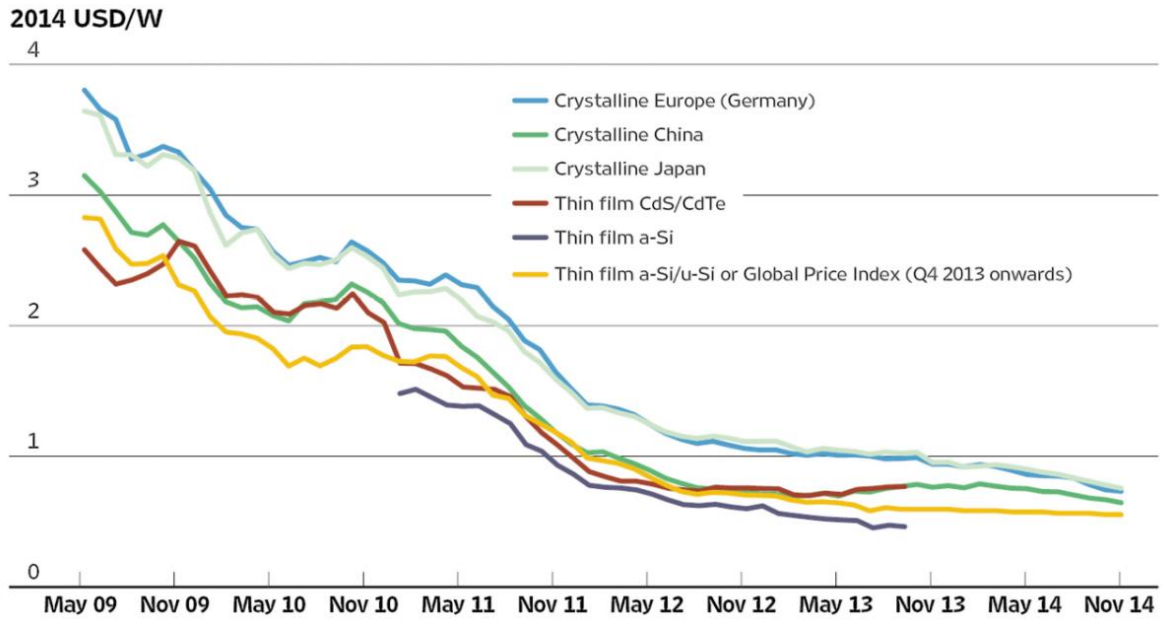

Figure 14 Trend of solar PV module prices by technology and manufacturing country

4.2 Battery Storage System

Currently there are several varieties of electrochemical battery technologies that are available for commercial applications. These technologies have been successfully employed in both centralized and decentralized applications with different sizes. However, challenges such as safety, lifetime, system cost, energy density, charging capabilities, and power performance prevent their widespread utilization. The more robust and common technologies are Lithium-ion (Li-ion), Sodium Sulfur (NaS), and lead acid batteries, including lead carbon batteries. Li-ion batteries are considered the best option for relatively short discharges (under two hours), but not deep-discharges, so this type of battery is more suited for use as an Uninterruptible Power Source (UPS) or in power-management operations, such as frequency regulation. NaS batteries can maintain longer discharges (four to eight hours), but are somewhat behind Li-ion battery technology in terms of energy and power; therefore, they may be more appropriate for price arbitrage operations and

load leveling. Lead acid batteries, despite their relatively low price, mature technology, and good battery life, suffer from low energy density and short time cycles, which make them difficult for large-scale deployment. In addition, sodium-ion batteries are another novel chemistry that is being developed. Table I shows some statistics about different types of battery technologies [66].

Table 1 Battery installation Statistics [66]

Battery Type	Number of 1MW+ Deployments	Largest installation (MW)
Lithium Ion	15	40
Sodium Sulfur	11	4
Lead Acid	9	36

Utilities, system operators, regulators, and private companies have already started to explore possible values that can be provided by battery energy storage systems for the U.S. electricity grid. The results in [67] show that energy storage is capable of providing thirteen general services to the power system. These thirteen services are listed and described in this document.

1-Energy Arbitrage: The electricity can be purchased when the Locational Marginal Price (LMP) is low for example during nighttime hours, and sale back to the wholesale market when LMPs are highest. In this classification, load following is considered as a subset of energy arbitrage. Load following manages the difference between actual demand, actual generation, and day-ahead scheduled generation.

2-Frequency Regulation: the frequency of the power grid can be maintained within the allowable tolerance by automatic and immediate response of power to a frequency change in the system. Frequency regulation is essential to ensure that system-wide generation is matched with

system-level load on a moment-by moment basis to avoid grid instability as a result of frequency spikes or dips.

3-Spin/non-spin reserves: Spinning reserve is the online generation capacity that is able to immediately respond to an unexpected contingency event such as an unplanned generation outage. Non-spinning reserve is generation capacity that is not instantaneously available but it can respond to contingency events within a short period, typically less than ten minutes.

4- Voltage regulation: Voltage on the transmission and distribution system can be sustained within the acceptable range by exchanging the required power with the electrical grid and performing active and reactive power control. Voltage regulation ensures reliable and continuous electricity flow across the power grid and ensures that both active and reactive power production are matched with demand.

5-Black Start: In the event of a grid outage, black start is the process of restoring power stations to operation in order to bring the regional grid back online. Some large power stations are themselves black start capable where the electric power required within the plant is provided from the station's own generators or black start generation assets rather than the external transmission network.

6-Resource Adequacy: Energy storage can provide adequate supply during peak load and/or generation outage events, and incrementally defer or reduce the need for new generation capacity. To this end, energy storage can be procured by grid operators and utilities instead of investing in new natural gas combustion turbines in order to minimize the risk of overinvestment in that area

7-Distribution Deferral: Energy storage can be deployed to delay, reduce, or entirely avoid utility investments in distribution system upgrades necessary to supply projected load growth on particular nodes in the power system.

8-Transmission Congestion Relief: When electricity demand exceeds the transmission capacity, transmission congestion occurs. Normally, utilities are charged extra by ISOs using congested transmission corridors. One solution is to upgrade the Transmission and Distribution (T&D) system. However, Energy storage systems can defer such investments by providing an alternative for solving this issue. Energy storage systems deployed downstream of congested transmission corridors can be discharged during congested periods to reduce the load burden on the transmission system.

9-Transmission Deferral: Energy storage can be deployed to delay, reduce, or entirely avoid utility investments in transmission system upgrades necessary to supply projected load growth on particular nodes in the power system.

10- Bill Management using time of use pricing: Energy storage can be deployed by behind-the-meter customers to reduce their electricity bill. Energy storage by shifting the load from the periods that time-of-use (TOU) rates are high to periods of lower rates can minimize electricity bill.

11- Solar PV self-consumption: When utility rate structures such as non-export tariffs do not incentivize distributed PV penetration. Energy storage by maximizing the local utilization of electricity generated by behind-the-meter PV systems can minimize export of solar power and maximize the financial benefit of solar PV.

12- Demand charge reduction: For commercial customers, electricity bill is composed of two components: 1- energy consumption and demand charge. Demand charge is a fee proportional to the peak power. Demand charges can constitute more than 50 percent of monthly electricity bill. Energy storage can help with peak demand reduction and consequently reducing the demand charge by performing load leveling and peak shaving.

13-Backup power: In the event of power outage, energy storage integrated with a local generator can provide backup power for industrial operations and residential customers.

The services and values created by energy storage highly depend on where this technology is deployed on the electricity system. The battery can be integrated at three different levels: transmission level, distribution level, or behind the meter, and generally benefit three groups of stakeholder including utilities, independent system operators/regional transmission organizations (ISO/RTOs), and electricity customers. Figure 15 illustrates thirteen different services provided by storage as well as benefits flow to each of stakeholder groups based on the integration location. In brief, the further downstream battery energy storage systems are located on the power system, the more services they can offer to the system at large.

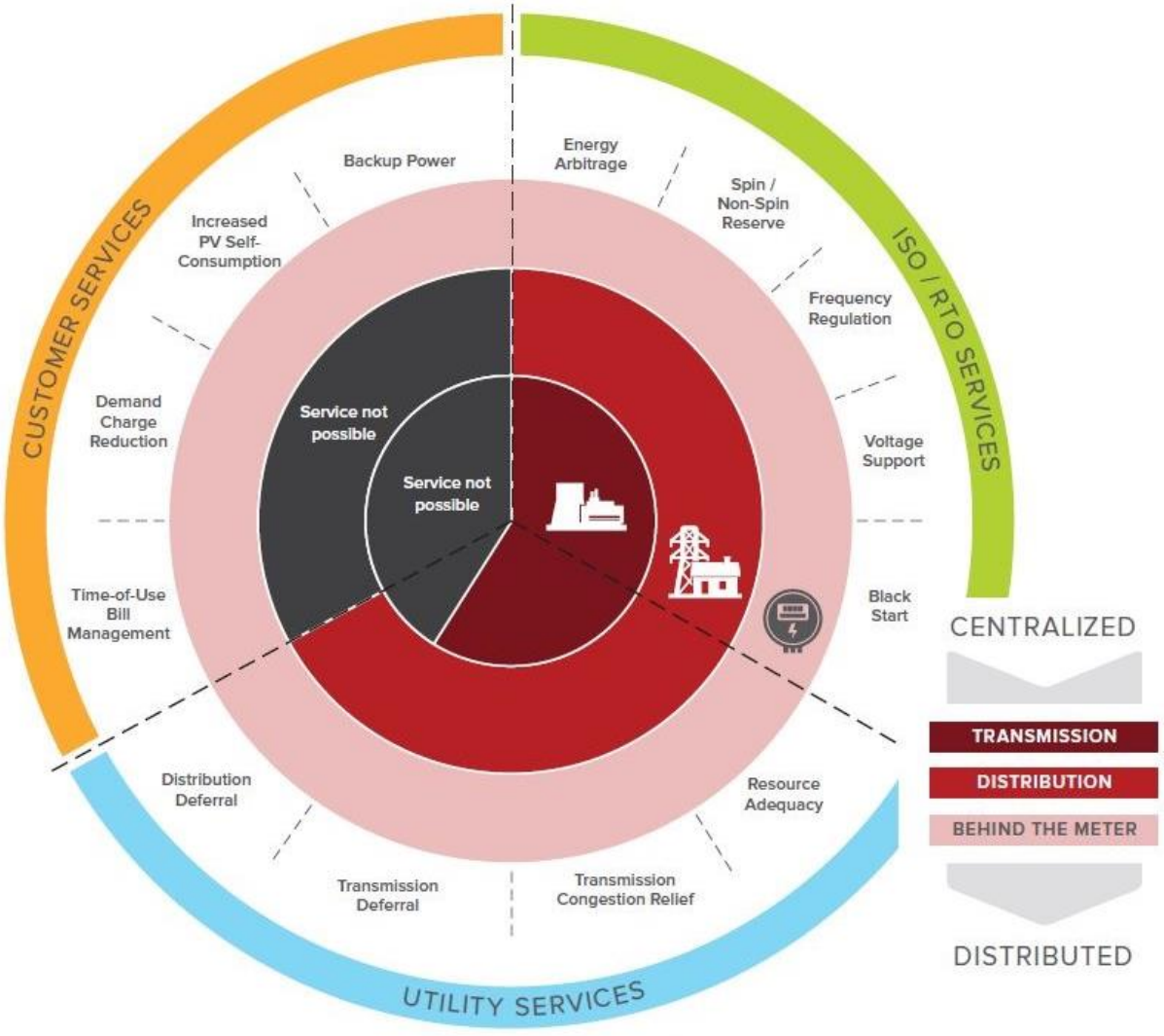

Figure 15 Services provided by battery storage to three stakeholder groups

Recently, in order to support investment in storage and storage related activities, Congress debated two bills that would help codify the cost structure for storage-related partnership taxation structures and subsidies. Furthermore, several projects that were funded under ARRA through the Smart- Grid Demonstration Grant program came online in 2013, while it is expected that their performance will conduct future investment decisions and policy initiatives. In total, an estimated 59 MW of storage capacity was scheduled to come online in 2013, constituting 7 of the 16 ARRA-

funded projects. Also, hydrogen fuel cells are being utilized as backup power in more than 800 units associated with telecom towers in the U.S., as a result of ARRA funding [66].

Besides these national developments, California, Texas, Washington, New York, and Hawaii have proposed substantial policies on storage. The California legislature have passed laws that make energy storage more feasible in terms of cost and regulatory perspective, and give power to the California Public Utilities Commission (CPUC) to authorize certain regional storage penetration levels. The CPUC recently mandated that 50 MW of storage be installed in the Los Angeles Basin by 2020, in addition to a top-line mandate of 1.3 GW of storage for the entire state. Texas has legislated SB 943 that classifies energy storage technologies along with generation equipment. Moreover, the Texas Public Utility Commission enacted key aspects of the bill as well as clarified rules, requirements, and definitions for energy storage. New York State established the NY Battery and Energy Storage Technology Consortium (NY-BEST) in 2010, a public-private partnership that investigates storage technology and manufacturing, supports potential stakeholders and energy storage organizations, and favors policies and programs that improve energy storage. Finally, Washington State enacted two laws related to energy storage: the first enables qualifying utilities to credit energy storage output of renewable sourced energy at 2.5 times the normal value; the second requires electric utilities to involve energy storage in all integrated resource plans [66].

Internationally, Japan has followed the development and deployment of energy storage to balance the variability of load on its nuclear power plants. Japan completed an initial phase of building pumped hydro storage plants and at the same time pursued development of other types of storage technologies. Its most noticeable accomplishment was the commercial development of high temperature sodium-sulfur batteries through a nonstop research and development program that

lasted two decades. Today, Japan-based NGK is the only source of sodium-sulfur batteries and, as of 2012, NGK had over 450 MW of sodium sulfur storage systems installed.

India and China are also pursuing energy storage programs to support the fast growth in their electric energy demand. Energy storage could serve many grid needs in both India and China to compensate the gap between available generation and customer loads during system peaks and as distributed resources on the customer-side of the meter. In one example, India is aggressively pursuing energy storage as a secure power resource for more than 300,000 telecom towers, and announced a $40 million contract in July 2013 for Li-ion battery energy storage systems to meet that need. This example clearly introduces telecom towers as a "first market" of storage technologies, which is developed and manufactured in the U.S. [66].

Table 1 describes some of the country-specific highlights of international grid storage.

Table 2 International status of grid storage [66]

Country	Storage Targets	Projects	Other Issues	Technology & Applications
Italy	75 MW	• 51 MW of Storage Commissioned by 2015 • Additional 24 MW funded	Italy has substantial renewables capacity relative to grid size, and the grid is currently struggling with reliability issues; additional renewables capacity will only exacerbate this problem	• 35 MW to be Sodium-Sulfur Batteries for long-duration discharge • Additional capacity is focused on reliability issues and frequency regulation
Japan	30 MW	• Approved 30 MW of Lithium-ion battery installations	• Potential decommissioning of nuclear fleet • Large installation of intermittent	• Primarily Lithium ion batteries • Recently increased

			sources - est. 9.4 GW of solar PV installed in 2013 alone • Several isolated grids with insufficient transmission infrastructure during peak demand periods	regulatory approved storage devices from 31 to 55
South Korea	154 MW	• 54 MW lithium-ion batteries •100 MW CAES	Significant regulatory/performance issues with nuclear fleet	Reliability & UPS
Germany	$260m for grid storage	$172m already apportioned to announced projects	• Decommissioning entire nuclear fleet; Large (and expanding) intermittent renewable generation capabilities • Over 160 energy storage pilot projects • Awaiting information on energy storage mandates	Hydrogen; CAES & Geological; Frequency Regulation
Canada	-	Announced 1st frequency regulation plant	-	-
UK	-	6 MW multi-use battery	• Other small R&D and Demonstration projects	Battery will perform both load shifting and frequency regulation applications

5 Testbed Implementation

Design and setup the experimental testbed in order to implement and test the proposed research concept is the primary step in this dissertation. In this context, a testbed platform consists of battery storage system, inverters, solar PV panels, dynamic loads (electric vehicles) is proposed. This system is designed to be controlled from control center and/or local controller through power electronics devices and switches. To this end, the electrical infrastructure including electrical panels, protection devices, power electronic devices, control devices, switches, and measurement units has been installed. On the other hand, communication infrastructure has been established in order to exchange control signals and data among control units, measurement units, and equipment. The deployed infrastructures as well as real system implementation helps to collect a variety of real data as the basis of this research. This research project involves several uncontrollable and unpredictable elements including intermittent energy sources and stochastic loads. Therefore, gathering data from real systems helps to better understand the problems and consequently propose a better solution. Moreover, designing the BESS control approach based on the real system and data increases the reliability and credibility of the proposed solution. Finally, the proposed control solution can be applied to the testbed platform while its performance is evaluated within an experimental implementation besides the simulation studies. To this end, this research project considers and deals with both practical and theoretical challenges.

This chapter explains the steps toward design and impletion of the developed testbed as well as the specification of the platform.

5.1 Testbed Topology

In order to integrate the battery storage system and solar panels into the UCLA distribution circuit, the first step was designing the configuration of the system with desired features. To this end, the topology of the integrated system is designed with the following features: 1) operate in grid-connected mode; 2) operate in islanding mode; 3) interact with electric vehicles charger; 4) Interact with solar PV panels 5) measure and report all required information on the AC and DC sides; 6) operate safe and protected.

Figure 16 shows the main components of the testbed platform including 74kWh/129kW battery energy storage system, 36kW grid-tie inverter, and 36kW off-grid inverter interacting with 30kW solar PV and 50kW DC fast charger.

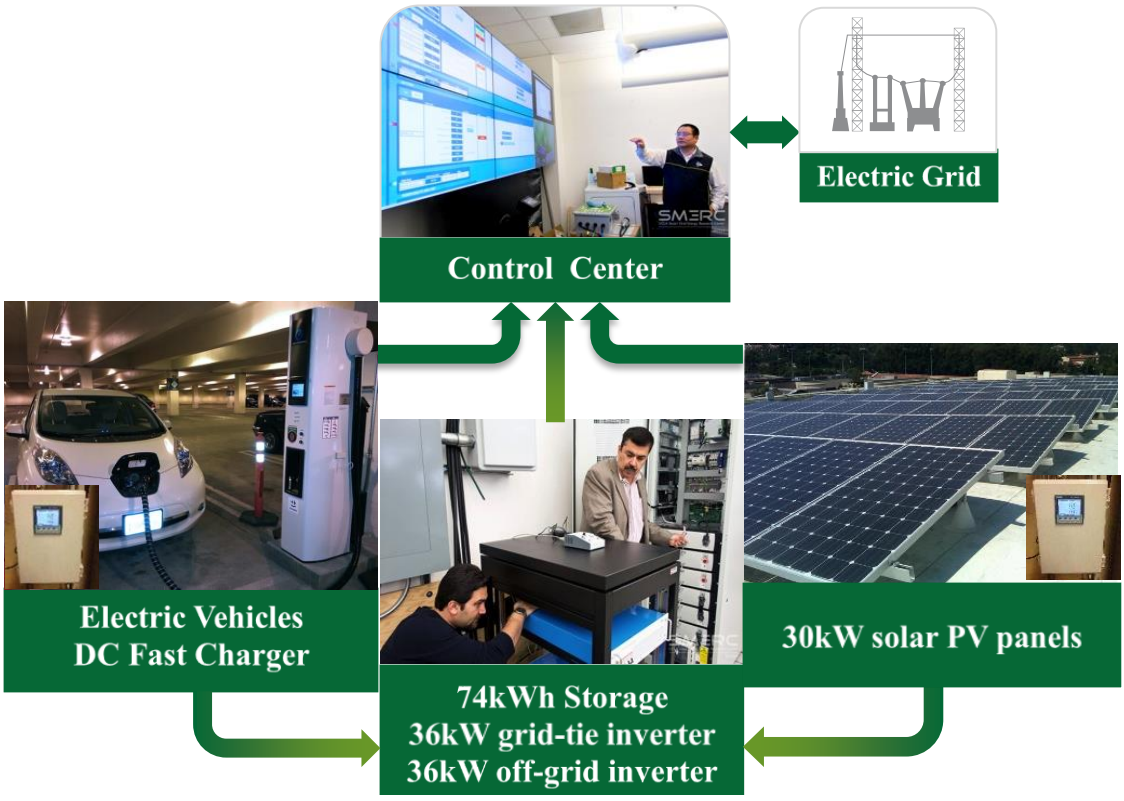

Figure 16 Main components of the testbed platform

Schematic of the system topology is illustrated in Figure 17. The protection devices are considered in the design and cable sizes are chosen based on the existing standards and designed capacity of the system. Measurement units are placed in both AC and Dc sides for data gathering.

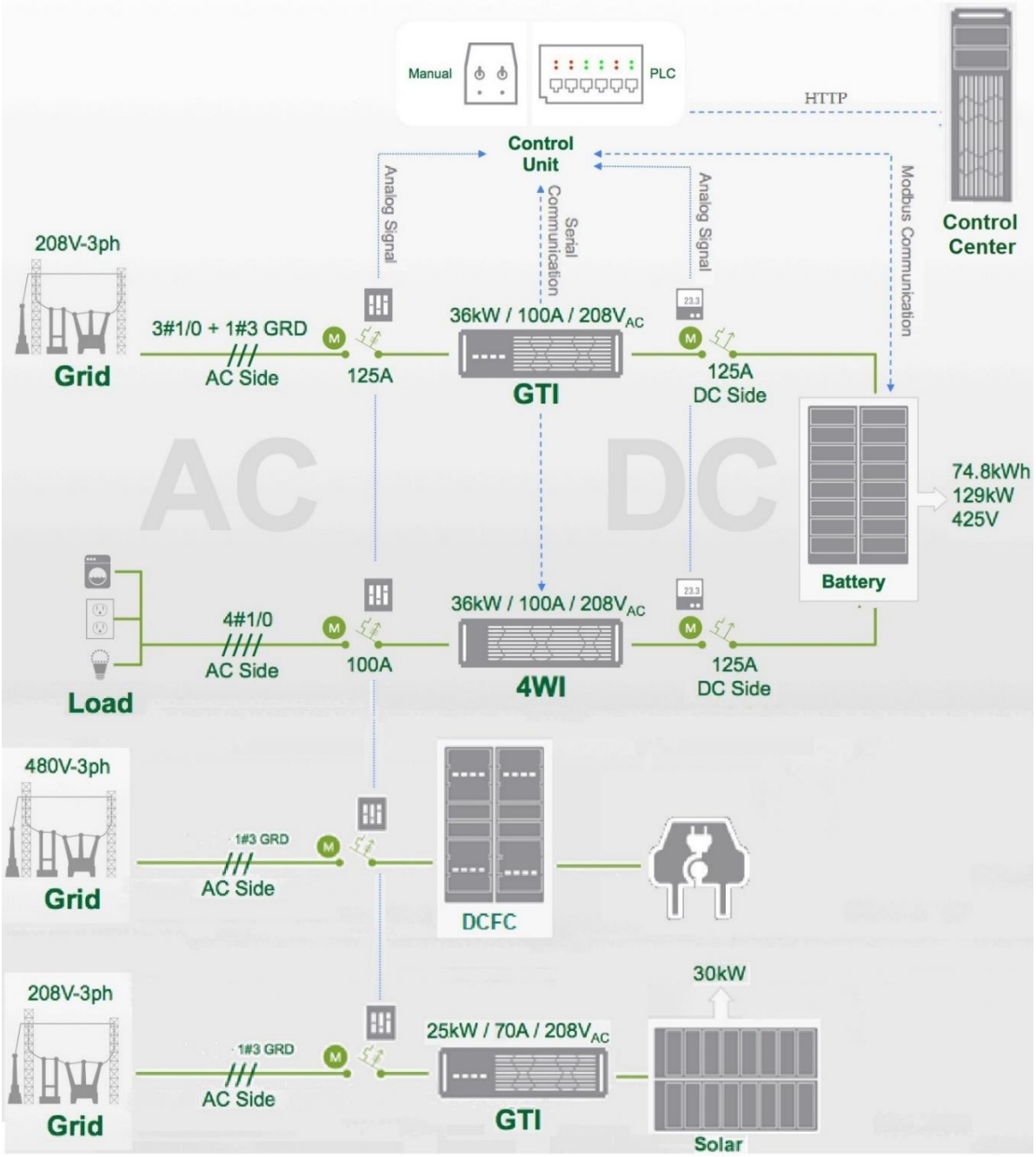

Figure 17 Circuit topology of solar, DCFC, and battery integration

5.2 Battery Energy Storage System

Figure 18 depicts the 74kWh/129kW grid integrated battery storage system including battery cabinet, AC panel, DC panel, grid-tie inverter, off-grid inverter, and controller. The battery cabinet is connected to the grid through 36kW grid-tie inverter and is also connected to the 36kW 4-wire off-grid inverter to supply the local loads. AC and DC panels include protection devices for system safety. The system currently is in operation and data gathering and analysis are being performed.

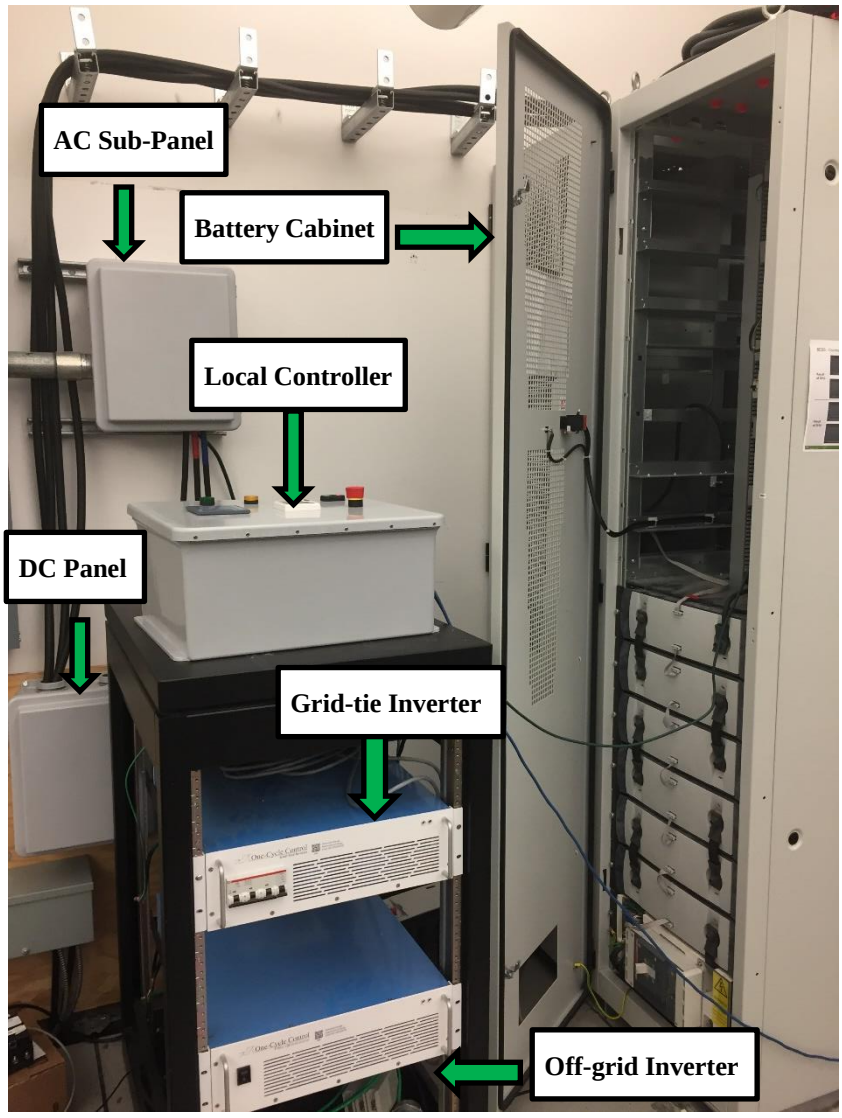

Figure 18 The grid integrated battery energy stroage system

One of the main practices in implementing the battery energy storage system was designing the top level control. In this system, the power does not flow, unless the battery storage system and inverters communicate and handshake with each other through the top-level controller. The top level control has several responsibility including:

1) Communication with the Battery Management System (BMS), grid-tie inverter, 4-wire inverter, measurement units, and control center

2) Collecting data from the measurement units, inverts and BMS for system monitoring

3) Controlling the entire system to operate in a safe and efficient manner.

A Programmable Logic Controller (PLC) is employed as the top level controller and is programmed to communicate with battery energy management system, inverters, and measurement units using the communication protocols associated with these components. In addition, the controller monitors and controls the criteria for safe operation of battery storage system and power electronic devices, These criteria includes over-temperature of battery modules, overcurrent of charging and discharging, under voltage, overvoltage, ventilation problem, cell imbalance, state of the health degradation, short circuit, and ground fault. If any violation from these criteria happens in the system the controller performs the require actions to solve the problem, otherwise cease the operation of the system immediately. The top-level control is configured to remotely control devices through the local network and Internet and also communicate with control center to exchange the control signals and data. Figure 19 shows the software used to monitor the status of battery energy storage system, and Figure 20 depicts the software interface employed to program the local controller.

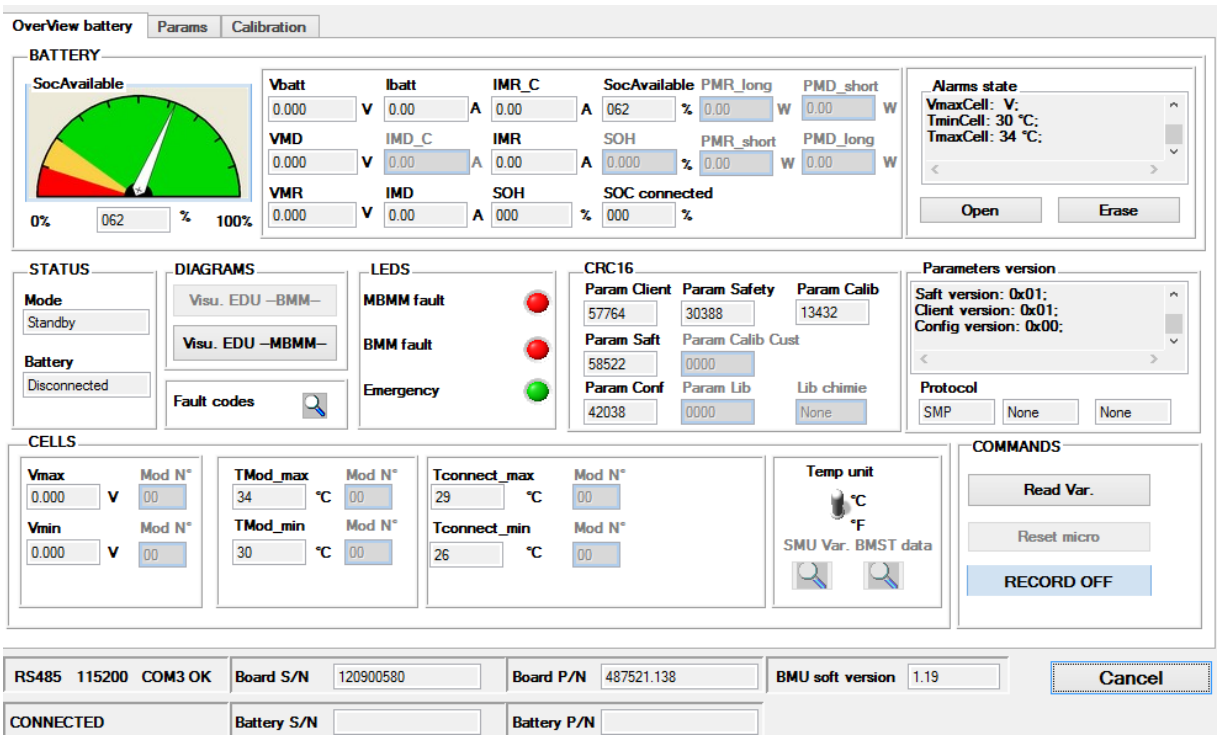

Figure 19 Monitoring software of battery energy storage status

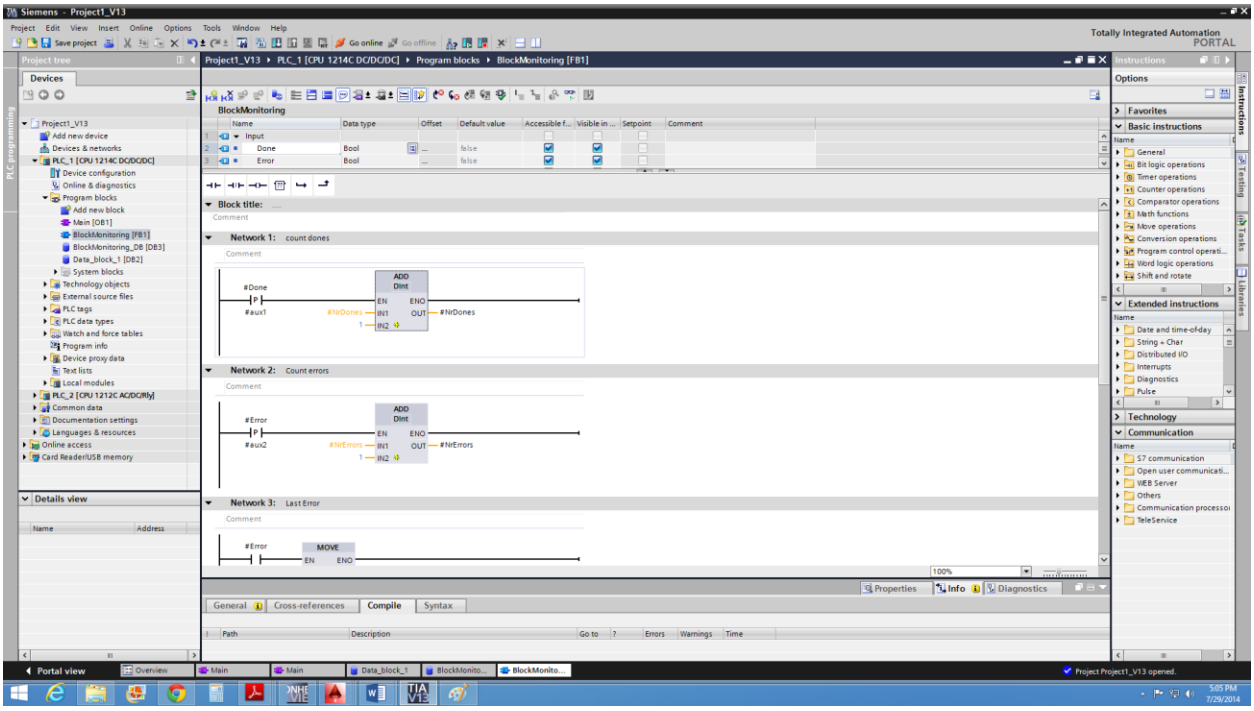

Figure 20 Software interface for programming the controller

This system is able to inject and absorb active and reactive power based on the policy that the controller determines for the system. The system operates in four quadrants, which provides the capability to control both active and reactive power. The obtained results from the four modes of operation, seen in Figure 21, illustrate the voltage and current curves during: 1) charging mode, 2) discharging mode, 3) leading mode, and 4) lagging mode.

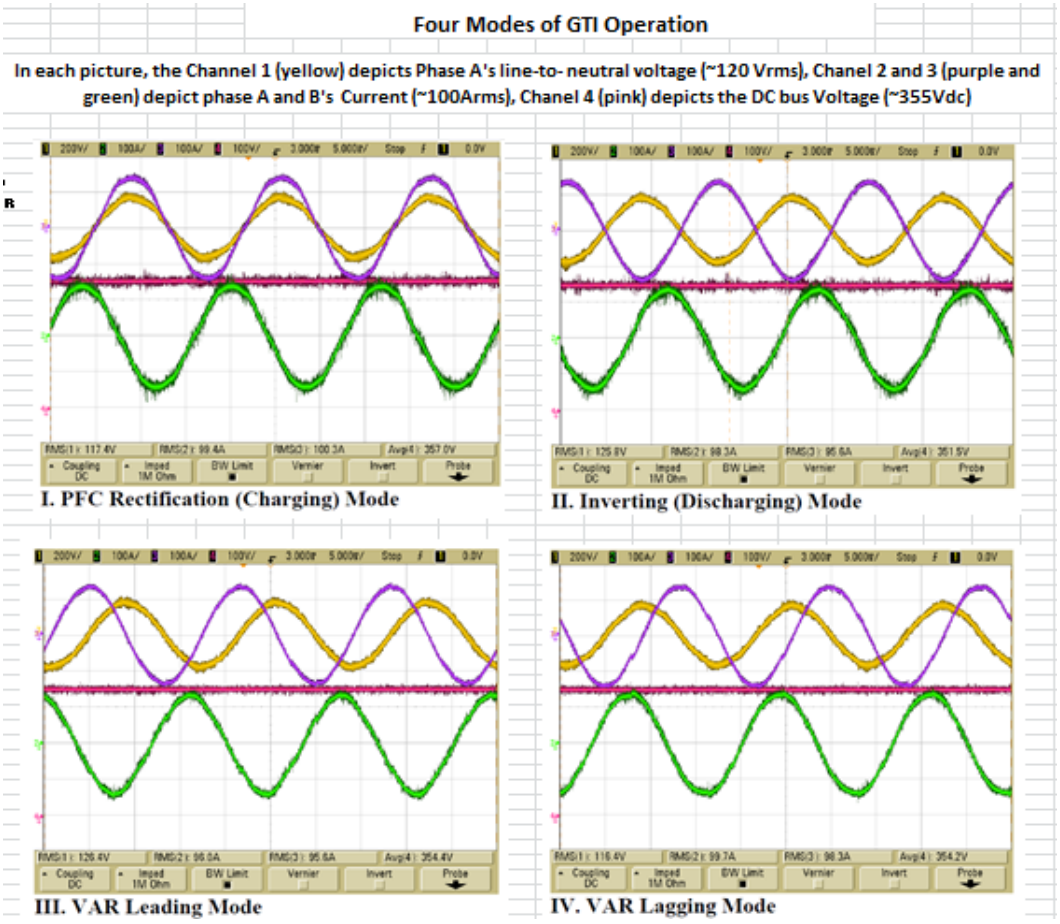

Figure 21 Four mode of GTI operation

5.3 Solar PV panels

UCLA has already installed solar PV panels on the roof of UCLA Ackerman Union, as shown in Figure 22. Interacting with battery energy storage system, a measurement and communication

infrastructure is added to this platform in order to send the data to the control center. To this end, three-phased, level-3 ZigBee smart meters is installed at Ackerman Union. The smart meters connect to the output channel of the solar panels to measure power, voltage, current, power factor, etc. The smart meters communicate via ZigBee protocol with a Billion gateway that includes a 3G dongle with a static IP address. For the purpose of security, the gateway can only be accessed by a set of predefined IP addresses, as well as those for the SMERC servers. The SMERC server can retrieve power data as measured by the smart meters, using a set of JSON APIs from the gateway. The remote server receives data every minute via a CRON job and stores these power data into its local database; only local or a predefined range of IPs can access the database. The monitoring framework block diagram is shown in

Figure 22 Solar panels on Ackerman Union's roof

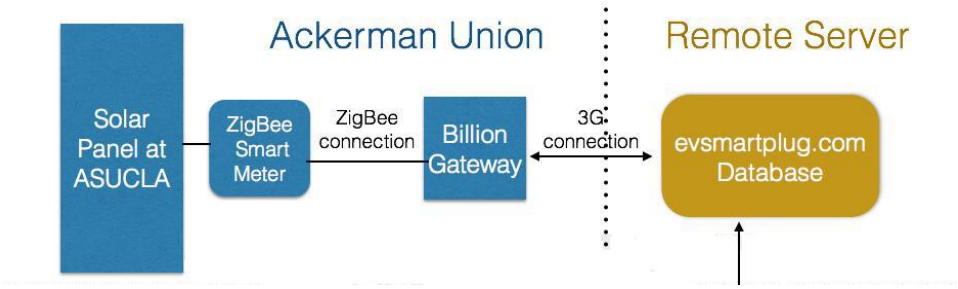

Figure 23 Block diagram of the monitoring framework for the solar panels

5.4 Electric Vehicle DC Fast Charger

The DC Fast Charging (DCFC) charger employed in this study is CHAdeMO charger designed by Nissan Motor [68]. Different from the level I and level II charging, this charger operates at 480 Volts and delivers Direct Current (DC) into EV's battery pack. This charger along with a power meter and a smart sub-meter has already been installed and integrated to the UCLA distribution circuit as shown in Figure 24. The charging data is retrieve and reported to the control center with the similar measurement and communication structure used for solar system.

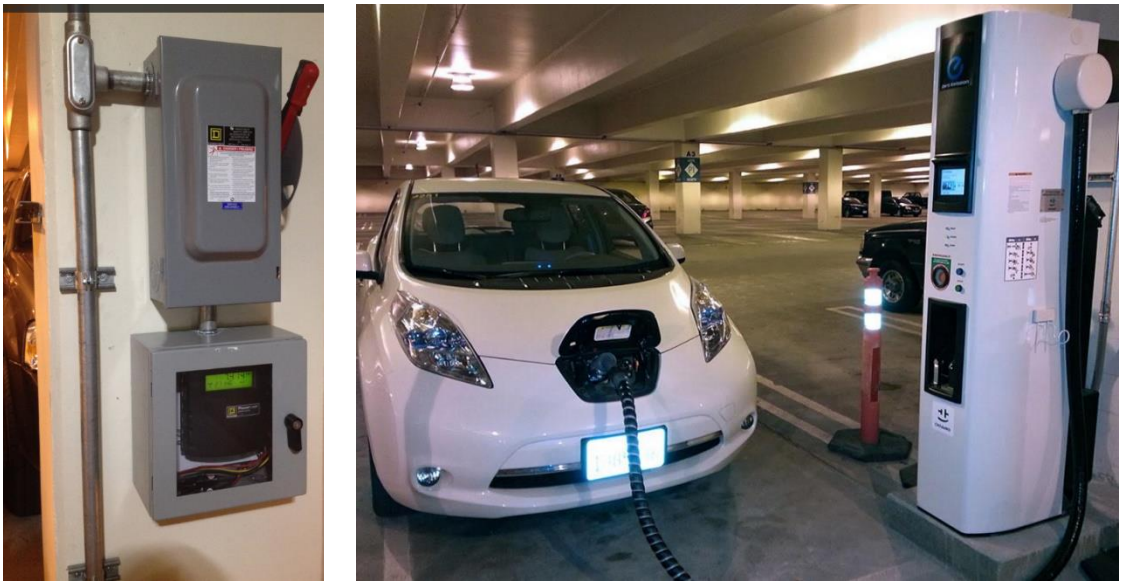

Figure 24 Nissan DC Fast Charger Installation at UCLA Parking Structure # 4 P1 level

6 Solar Power Prediction

This chapter proposes a new hybrid method for super short-term solar power prediction. Solar output power usually has a complex, nonstationary, and nonlinear characteristic due to intermittent and time varying behavior of solar radiance. In addition, solar power dynamics is fast and is inertia less. An accurate super short-time prediction is required to compensate for the fluctuations and reduce the impact of solar power penetration on the power system. The objective is to predict one step-ahead solar power generation based only on historical solar power time series data. The proposed method incorporates discrete wavelet transform (DWT), Auto-Regressive Moving Average (ARMA) models, and Recurrent Neural Networks (RNN), while the RNN architecture is based on Nonlinear Auto-Regressive models with eXogenous inputs (NARX). The wavelet transform is utilized to decompose the solar power time series into a set of richer-behaved forming series for prediction. ARMA model is employed as a linear predictor while NARX is used as a nonlinear pattern recognition tool to estimate and compensate the error of wavelet-ARMA prediction. The proposed method is applied to the data captured from UCLA solar PV panels and the results are compared with some of the common and most recent solar power prediction methods. The results validate the effectiveness of the proposed approach and show a considerable improvement in the prediction precision

6.1 Introduction

Extensive propagation of intermittent renewable energy sources to address the electricity power demand and the environmental concerns raises new challenges for power system operation due to the stochastic nature of these resources [69]. There is no doubt that renewable energy

resources are necessary to meet our current energy demand. Reliable prediction of renewable energy is essential for its efficient utilization to address that demand. Embedding renewable energy prediction techniques in grid operation procedure facilitates the massive integration of renewables. Real time control and compensating of renewables would be more practical and efficient if super short-time prediction is available. Reliable super short-term prediction methods may also improve the power quality and reliability of the power grid by enabling prompt compensation of negative consequences of renewable dynamics and fluctuations [70]. By evolving smart grids technology which expands hybrid renewables integration, the operation of distribution networks will also benefit from state-of-the-art renewables outputs prediction [71], [72].

The necessity of renewables prediction from one side and its complexity from other side have motivated many researchers in this area to find a practical solution. Renewables power predication methods are mostly based on multivariate-models. These prediction methods are normally based on physical and atmospheric parameters which influence renewables generation such as temperature, irradiance, wind speed, relative humidity, etc., [73], [74]. For solar power prediction which is the focus of this chapter, multivariate model-based methods estimate the solar power, solar irradiance, cloudiness and clearness indices based on spatial, temporal and climatic conditions. Authors in [75] use measured air temperature, relative humidity and sunshine hours to predict daily global solar radiation. In [76], prediction inputs to generalized fuzzy model are the day of the year, sun shine hour, ambient temperature, relative humidity and atmospheric pressure. Assi et al. [77] use air temperature, wind speed, sun duration, and relative humidity as the inputs of an ANN to predict solar radiation. Aerosol index which indicates the particulate matter in the atmosphere is proposed besides the other meteorological data to get more accurate forecasting results [78]. Mathematically, different statistical models are adopted in these prediction methods. Among the

linear models, Auto-Regressive (AR) and ARMA are commonly used for wind and solar power prediction [79], [80]. However, linear time series models are addressed notably in the literature, behavior of renewable power generation series may not be entirely captured by the linear techniques due to time varying and inherent nonlinear characteristic of renewables generation [81]. Thus, nonlinear methods have been proposed by many scientists. Takagi Sugeno (TS) fuzzy model [82], wavelet-based methods [83], Neural Networks (NNs) [84], [85], support vector machine [81], echo state network [86], k-nearest neighbors (kNN) [87], [88], and adaptive neural fuzzy inference systems (ANFIS) [89], are some of the examples of the prediction methods. Although the superiority of nonlinear statistical models over linear models has been shown before, researchers are not still satisfied with the prediction precision and generalization capability of the existing advanced methods [90].

Intermittent characteristics of generated power by solar, outliers, and inconsistent mean and variance, turn the solar prediction problem into a complicated problem. To solve this problem, a variety of complex solutions with multivariate inputs are applied so far. However, for super short–time prediction horizons, the cost of acquiring and maintaining a weather station which is able to collect and store solar radiation, sun duration, temperature, wind speed, and relative humidity data is exorbitant. Satellite imagery and numerical weather prediction are also restricted [91]. Moreover, the effectiveness of employing individual meteorological variable has not been studied yet [92]. The focus of this chapter is on a univariate model based method which is economic and realistic for super short-time prediction. In this method a prediction model is a function of the current or past values of the power time series but not of any other time series such as temperature, wind speed, and relative humidity.

In this chapter, a new univariate hybrid methodology is presented. This method uses linear and nonlinear models including DWT, ARMA models and NARX architecture of RNN to predict solar power. The wavelet transform is used to decompose the historical power series into the better-behaved series for prediction. ARMA model is applied as a linear predictor and NARX is utilized as a nonlinear pattern recognition tool to estimate and compensate the error of wavelet-ARMA prediction. The proposed method is applied to the UCLA solar power dataset for nearly two hundred thousand observations, sampled at a rate of once per minute. This dataset is large enough to implement the proposed prediction algorithms.

The rest of the chapter is organized as follows. In Section 6.2, the principles of the proposed algorithm are described. Then, simulation results obtained from applying the proposed algorithm on real solar data are presented in Sections 6.3. Finally, concluding remarks are in Section 6.4.

6.2 Methodology

The majority of the prediction methods require a wide range of input data (multivariate). The drawback of these approaches is that the limited availability of input data causes loss in accuracy. In addition, inaccuracy in input data propagates to the output and those errors are accumulated. There is a need for prediction methods that are reasonably accurate and work with limited input data. In the prediction literature, it is well-known that a single method cannot provide the best solution for all different situations. Both experimental and theoretical analysis show that combining different methods can increase prediction accuracy [93]. In this Section, a RNN is integrated with an ARMA model and the wavelet method is employed to decompose the input data to a series with better feature for prediction. The proposed hybrid method includes the following prediction stages:

Stage 1) Decomposition of historical power series into the constitutive series through the wavelet transforms.

Stage 2) Modeling each of the constitutive series by ARMA model for recognition of their linear pattern.

Stage 3) Recomposition of estimated series obtained from ARMA model for each constitutive series through the inverse wavelet transform.

Stage 4) Compensating the error of the wavelet-ARMA model prediction by recurrent neural networks through capturing the nonlinear patterns buried in residual part.

6.2.1 Wavelet Transform

When the time series like solar power series is non-stationary [94], the identification of an appropriate global model is very difficult if not impossible [95]. In order to cope with this challenge, wavelet transform technique has been introduced as an effective way for better analysis and prediction in the preprocessing step. The Wavelet Transform (WT) is a time–frequency decomposition that provides useful basis of time series in both time and frequency. This approach allows the collected measurements be smoothed until some hidden trend is identified. This capability is performed by diagnostic the main frequency component from the time series and mining abstract local information. Recently, WT has been frequently utilized for analysis and forecasting time series [96], [97].

In discrete wavelet series the so-called "approximated series" (A_i) and the "detail series" (D_i) are calculated as [98]:

$$A_{i+1}(k) = \sum_{l} H(l).A_i(2k + l) \quad (1)$$

$$D_{i+1}(k) = \sum_{l} G(l).A_i(2k + l) \tag{2}$$

where *i=0,1,2,.....M* are the wavelet decomposition levels. The functions *G* and *H* are the high-pass and low-pass filters' finite impulse responses, respectively. These two filters are related to each other and they are known as quadrature mirror filter. A_0, is equal to the original finite-length sequence *S(n)*. Figure 25 depicts the decomposition structure of wavelet transforms for level 3.

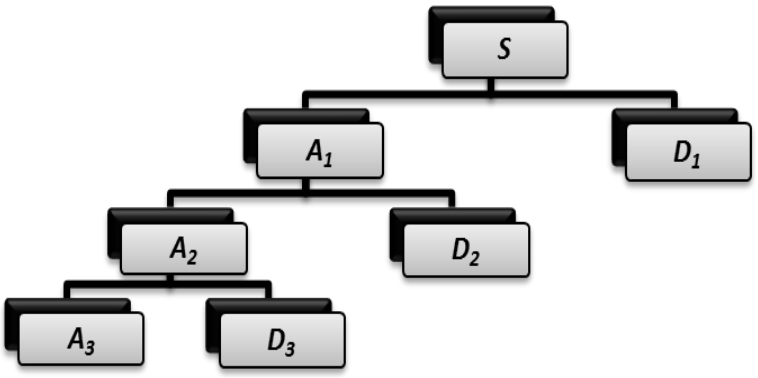

Figure 25 Wavelet decomposition tree at level 3

The inverse discrete wavelet transform can be obtained from (3).

$$A_i(k) = \sum_{l} H(l).A_{i+1}(2k + l) + \sum_{l} G(l).D_{i+1}(2k + l) \tag{3}$$

In this transformation the data series is broken down by the transformation into its wavelets that are scaled and shifted version of the mother wavelet which is the main function of transformation. Figure 26 depicts the signal and corresponding wavelet including low scale and high scale concept of the signal decomposition. Wavelet transform projects a signal into different scale components. Multiplying each wavelet coefficient by the appropriately scaled and shifted wavelet yields the constituent wavelets of the original signal.

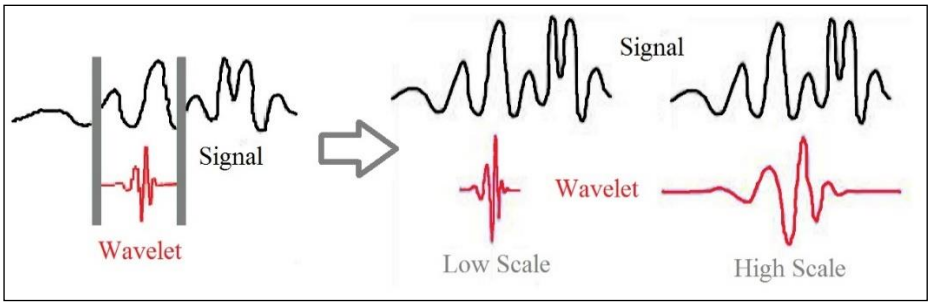

Figure 26 Signal and wavelet representation

6.2.2 ARMA

ARMA model is a simple and cost effective method to extract useful statistical properties of the data which is based on the well-known Box–Jenkins methodology [94]. The ARMA model is a stochastic process coupling AR to a Moving Average (MA) component. The AR component computes the current value of series as a function of past samples, while the MA component integrates a random process representing noise in the data. This kind of model is called ARMA *(p, q)* and is expressed with *p* and *q* parameter as:

$$x(t) - \sum_{k=1}^{p} \varphi_t(k) x(t-k) = \varepsilon_t + \sum_{i=1}^{q} \theta_t(k) \varepsilon(t-i) \tag{4}$$

where, x_t is a time series, ε is an error term distributed as a Gaussian white noise, and φ_t and θ_t.are the parameters of the autoregressive and moving average part respectively.

6.2.3 RNN-NARX

There are two major types of neural networks, feed-forward and recurrent. Unlike feed-forward neural networks, RNNs can use their internal memory to process arbitrary sequences of inputs. In this document, in order to deal with nonlinearity of time series the proposed RNN architecture used

here is one based on Nonlinear Autoregressive models with eXogenous input (NARX model). Since ARMA models are linear, here NARX is employed to model the nonlinear part of the time series which is not parametric.

As opposed to other recurrent network architecture, NARX networks have a limited feedback and it comes from only the output neuron rather than from hidden states. NARX models are formalized by [99]:

$$y(t) = f(u(t-n_u), \dots, u(t-1), u(t), y(t-n_y), \dots, y(t-1)) \quad (5)$$

where function *f* is a nonlinear function, $u(t)$ and $y(t)$ represent input and output of the network respectively at time *t*, n_u and n_y are order of input and output. Figure 27 shows the dynamic structure of NARX.

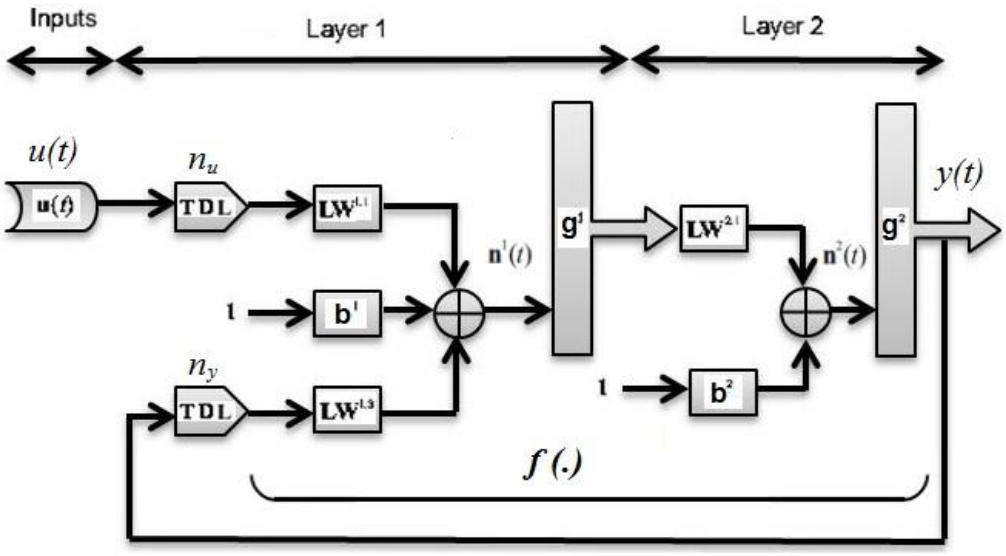

Figure 27 NARX dynamic architecture of two layers

6.2.4 Hybrid Algorithm

With the aim of improving the prediction accuracy this Section proposes the idea of considering the time series as the composition of a linear stationary and autocorrelation component (S_L), and a nonlinear structure (S_N).

$$S(t) = S_L(t) + S_N(t) \tag{6}$$

Thus the linear (S_L) and nonlinear (S_N) components have to be predicted according to the current and past data separately. The idea is that the decomposed time series by wavelet, first is modeled through ARMA. That is the wavelet-ARMA method models the linear component of the time-series. Then referring to (6), the residual of the wavelet-ARMA model (linear model) contains only the nonlinear part of time series. That means after estimation of predicted value of linear component from time series ($\hat{S}_L$), the error of prediction (e_t) is calculated from (7).

$$e(t) = S(t) - \hat{S}_L(t) \tag{7}$$

The next step is the residual analysis for mining nonlinear pattern in the error. Extracting any meaningful nonlinear pattern in the error compensates for the wavelet-ARMA limitation and leads to improvement of the prediction algorithm. In this work the NARX is proposed to capture the nonlinearity in the error. Therefore the NARX model of error at each time can be expressed by a nonlinear function of past errors as a feedback target and power times series changes as non-feedback inputs.

$$e(t) = f\left(S(t-n_u), \dots, S(t-1), S(t), e\left(t-n_y\right), \dots, e(t-1)\right) + \varepsilon(t) \tag{8}$$

where function $f(.)$ is a nonlinear function defined by NARX and $\varepsilon(t)$ is the random remaining error, $S(t)$ is power time series and $e(t)$ is wavelet-ARMA error. In fact, the $f(.)$ is modeling the prediction of nonlinear component of time series ($\hat{S}_N$). Therefore, the proposed method is benefiting

from the privilege of wavelet-ARMA model for extracting linear feature of data, and it is taking advantage from NARX model for exploring nonlinear characteristic of the error. The flowchart of the proposed algorithm is shown in Figure 28.

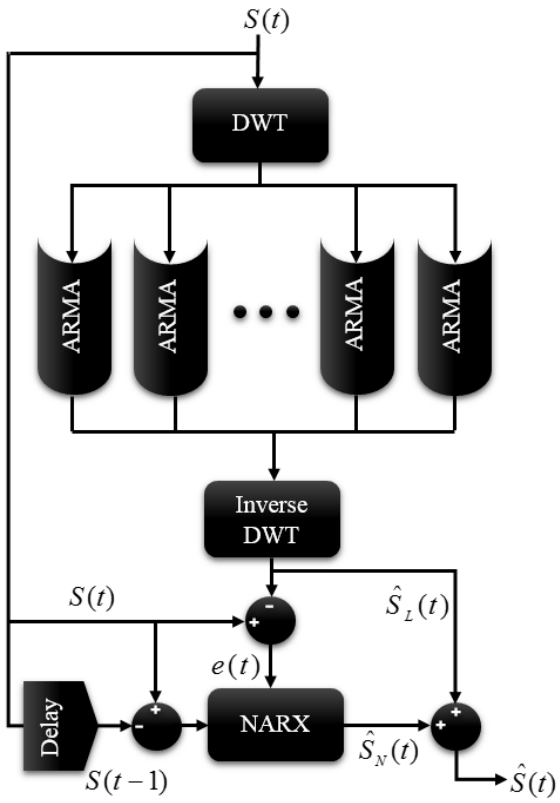

Figure 28 Proposed hybrid prediction algorithm

6.2.5 Prediction Accuracy

In order to evaluate the prediction accuracy of the proposed method and assess its prediction capability the Mean Absolute Normalized Error (MAE), Mean Squared Normalized Error (MSE), and Maximum of Normalized Error (MAXE) are introduced as the performance indices. Normalized error is calculated from (9).

$$E_{norm} = \left(S(t) - \hat{S}(t)\right)/\bar{S}\,(t) \tag{9}$$

where $\bar{S}(t)$ is the mean value of $S(t)$.

6.3 Simulation Results

The solar power data captured every minute from the solar panels at UCLA Student Union is considered as the case study for the proposed prediction method. The algorithm is applied to both cloudy day and sunny day. The proposed hybrid method is compared with some common prediction algorithms.

The implemented prediction method is developed based on flow chart in Figure 28. It uses a wavelet function of type Daubechies, order 20 and 3 level of decomposition. Figure 29 shows three level wavelet decomposition of solar power time series in a cloudy day. The ARMA model orders are p=8, and q=8. Finally NARX includes 45 hidden layers and one output layers. The following parameters are tuned by running several experiments to reach the acceptable accuracy. There exist different systematic approaches for designing the NARX such as particle swarm optimization but that is outside of scope of this work.

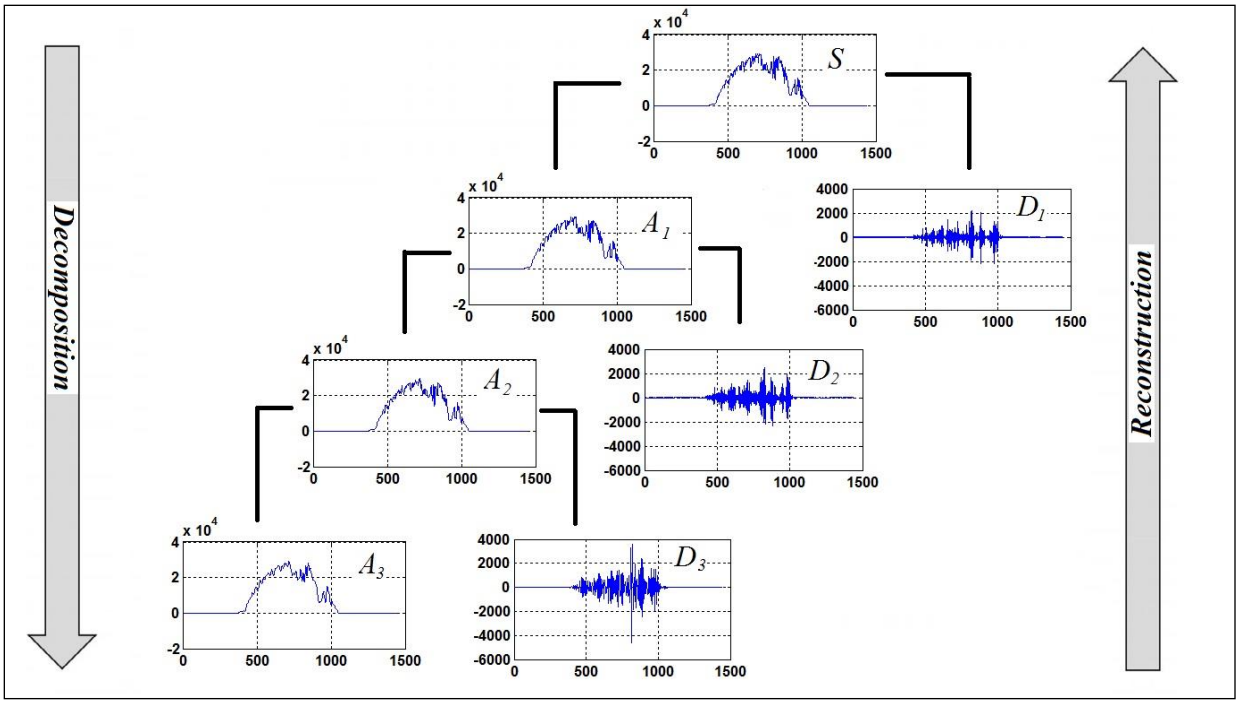

Figure 29 Three level wavelet decomposition of solar power time series

Figure 29 shows the decomposition of the signal achieved using wavelet transformation. The level three A-series (D-series) data has mostly low frequency (high frequency) content that can be used for accurate prediction.

Figure 30 depicts the solar power captured in a sunny and a cloudy day. It can be seen that power fluctuates is more in cloudy day compared to sunny day and the peak of solar power generated is less.

Figure 31 shows the actual solar power and predicted curves for a sunny day, and Figure 32 plots the percentage of prediction error over the maximum capacity of solar. Figure 33, and Figure 34 also show the solar power prediction and prediction error percentage for a cloudy day. Figure 32 and Figure 34 compare the error of wavelet-ARMA approach and wavelet-ARMA-NARX to

show the improvement provided by employing the neural network for nonlinear pattern recognition of residuals.

The correlation analysis depicts that the correlation of the NARX final error at each point is less than 0.1 with previous data which reflects no correlation between data to improve the prediction.

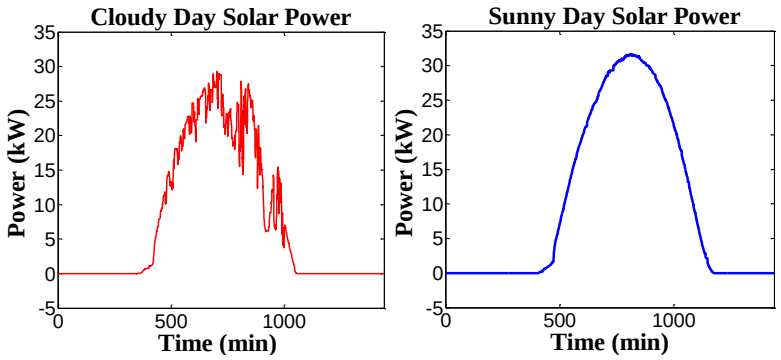

Figure 30 Solar power in a sunny and a cloudy day

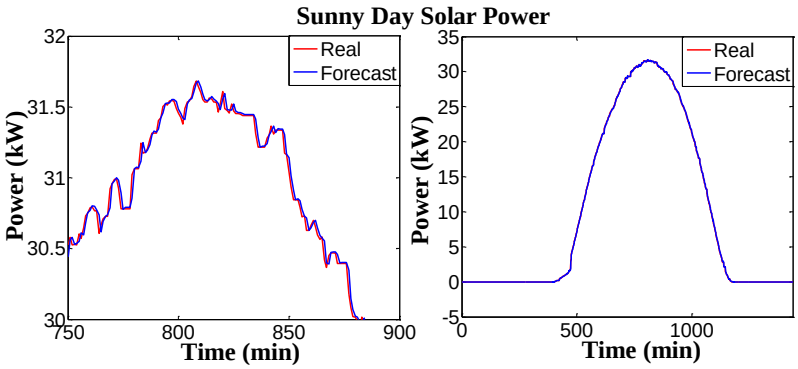

Figure 31 Actual solar power and predicted curves for a sunny day

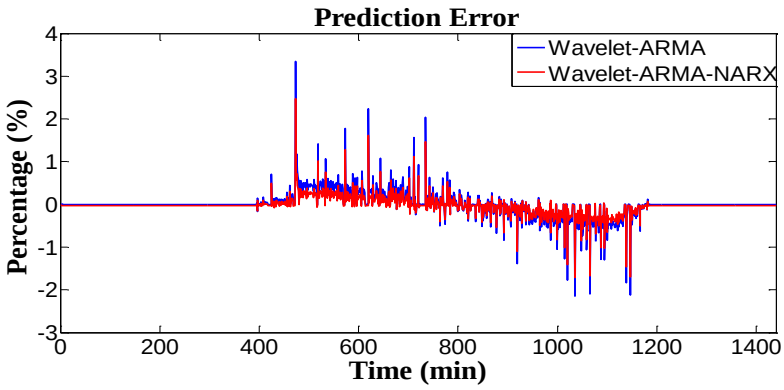

Figure 32 Prediction error for sunny day

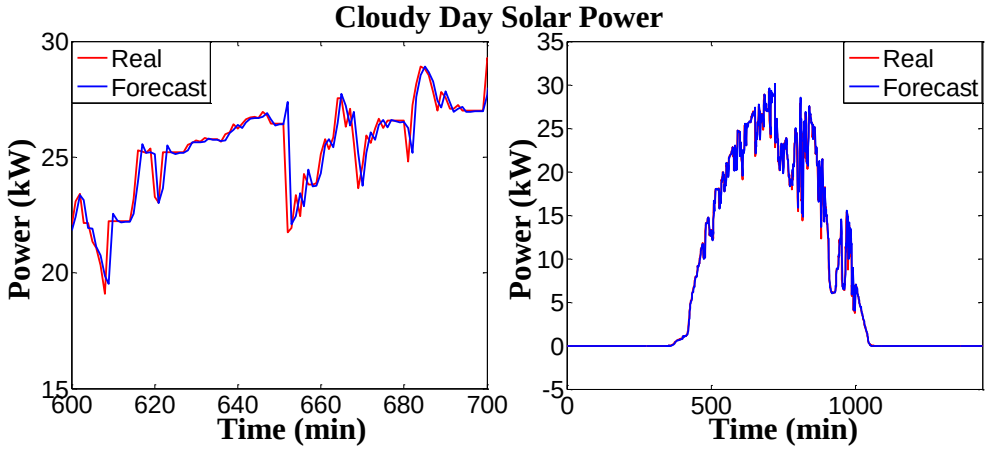

Figure 33 Actual solar power and predicted curves for a cloudy day

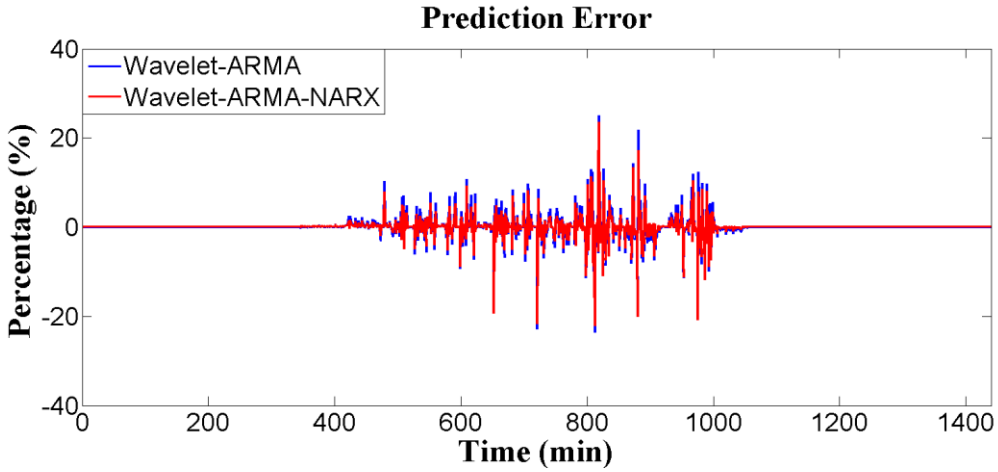

Figure 34 Prediction error for cloudy day

Table 3 and Table 4 depict the comparison results between the performance of the proposed hybrid approach and some other common approaches for a sunny and a cloudy day. The comparison is based on calculated error through MAE, MSE and MAXE criteria. The obtained results validate the effectiveness and performance of wavelet-ARMA-NARX compared with ARMA, wavelet-ARMA, and NN methods.

Table 3 Comparison of different prediction method for sunny day

	MAE	**MSE**	**MAXE**
ARMA	0.9303	0.0251	0.1087
Wavelet-ARMA	0.4703	0.0095	0.1061
NN	1.0329	0.0247	0.1321
Wavelet-ARMA-NRX	0.3668	0.0050	0.0783

Table 4 Comparison of different prediction method for cloudy day

	MAE	**MSE**	**MAXE**
ARMA	4.7791	1.1514	0.9887
Wavelet-ARMA	3.7517	1.0289	0.9907
NN	4.8410	1.0687	1.0088
Wavelet-ARMA-NRX	3.3742	0.8971	0.9603

6.4 Conclusion

In this chapter, a new univariate hybrid method is developed to predict the solar output power and model the intermittent characteristic of solar power generation. This method incorporates wavelet, ARMA and RNN to predict one minute ahead solar power. The wavelet algorithm is used to decompose the time series to better behaved components for prediction, ARMA is employed for modeling the linear features of the data, and finally NARX has been included to compensate the error of wavelet-ARMA and capture the nonlinear pattern in the residual. One of the attractions of

this method is that it requires only the historical output solar power time series. This method is simple, affordable, and practical for super short-time prediction. The numerical results validate the accuracy and effectiveness of this method

7 Solar Smoothing

A new method for the control of a battery energy storage system, and its implementation on a 25kW solar system to compensate solar power intermittency and improve distribution grid power quality is presented in this chapter. The novelty of the proposed method is to provide a systematic way to optimize the size of the battery capacity for the desired level of solar power smoothing. This goal is achieved by designing a two-stage filter solution. The first stage is a fast response digital Finite Impulse Response (FIR) filter that makes a trade-off between smoothing of the solar output and battery capacity. This chapter proposes an optimal design of minimum-length, low-group-delay FIR filter by employing convex optimization, Discrete Signal Processing (DSP), and polynomial stabilization techniques. The new method proposed in this chapter formulates the design of a length-N low-group-delay FIR filter as a convex SOCP which guarantees that all the filter zeros are inside the unit circle (minimum-phase). A quasi-convex optimization problem is formulated to minimize the length of low-group-delay FIR filter. The second stage filter is designed to level the battery charging load. The effectiveness and performance of the proposed approach is demonstrated by simulation results and also over a real case implementation.

7.1 Introduction

Environmental concerns and the need to find cleaner energy sources has resulted in the rapidly increasing penetration of distributed generation from intermittent renewable resources like solar [24]. For low level penetration of the PV systems (less than 5 percent), the fluctuations in the PV power is relatively insignificant and does not present much problem to the operation or control of power systems [100]. For higher PV penetration, the fluctuations of PV power may adversely affect

the operation of power systems. Technical concerns associated with higher penetrations of PV include voltage regulation, grid stability, power quality (voltage sags, rise, flicker, and frequency fluctuations), and protection issues [24], [101]. This is especially critical in low voltage networks with a high penetration of distributed renewables. The absence of buffering through either demand response or storage can result in large voltage variations, uncertainty of power flows, and possibly even reversed power flow to the transmission network which may impact local operation of the grid [24]. Some countries are currently working on grid codes that take this problem into account [102]. For example, the Puerto Rico Electric Power Authority requires the PV plant fluctuations to be less than ten percent of the maximum AC active power capacity per minute [103]. In other countries, such as Mexico, the regulations target tighter restrictions, of around one to five percent per minute [104].

Several approaches have been proposed to solve or alleviate the intermittency problem [105]. Some approaches are: reducing the PV power output, providing sufficient load-following capacity by changing the generation mix of the system, and dispersing the solar array fields to reduce their energy density. More examples include forcing the economic dispatch to provide a higher spinning reserve, improving the design of power plants to provide faster response rate and wider regulating range, and accurate prediction of solar power generation. Another approach is to smooth out the variations of PV output with an integrated energy storage system. Recent advances in electric energy storage technology provide an opportunity for using BESS to address the intermittent behavior problem of renewable energy sources and making solar a much more deployable resource [106]. Energy storage systems with rapid response can be exploited to handle the solar intermittency that results from cloud cover [107]. When a cloud casts a shadow on the solar array, the storage

unit automatically smooths the output of the solar panels by instantaneously dispatching energy to fill in the drop created by the cloud. This increases the reliability of power from solar.

When using BESS to control PV power fluctuations, there is a trade-off between battery capacity and the level of smoothness. That is, a smoother output requires a higher battery capacity.

So far, several energy storage-based control strategies have been proposed to mitigate the effect of the solar power fluctuation [106], [108], [109]. The most ubiquitous strategies in the literature are ramp-rate control [110], [111] and the moving average technique [112], [113], [114].

In [111] a new method for ramp-rate control of solar using energy storage is proposed. In this method during a ramp-down or ramp-up event, the energy storage system is controlled based on an inverse characteristic of the desired ramp-rate of PV inverter with respect to the ramp-rate of the PV panel output. However, this method only smooths steep change in PV power by ramps up or down, but cannot capture the slow variations in the PV power.

The moving average filtering approach is employed by authors in [112], [113], [114]. However, in this approach, the high delay of the filter causes a large gap between the input and output of the filter and that needs a considerable battery capacity for compensation.

The authors in [102] proposed a new control strategy called “step-control” to smooth short-term power fluctuation of PVs using battery storage systems. However, the results presented by the authors show that the moving-average strategy requires a smaller battery capacity compared with the step-control method.

As a secondary control, a variety of scheduling and sizing algorithms are proposed in the literature that optimize the dispatch of PV, wind, energy storage, and diesel generator to obtain a smoothed output power [115], [116], [117]. The real-time smoothing of solar power fluctuations with high dynamics is beyond the scope of these approaches.

Thus far, although various effective BESS-based methods for smoothing power fluctuations in renewable power generation systems have been proposed, smoothing targets for grid-connected PVs through fast acting controller generally have not been formulated.

This chapter proposes a novel real-time fast acting BESS-based control approach to smooth the solar power by making optimal use of the BESS capacity. The goal is achieved by developing a novel fast response digital FIR filter.

A fundamental issue in the design of an FIR filter for solar power smoothing applications is the delay of the filter. If the filter delay is small, the lag between the output of the filter (smoothed solar power) and the input of the filter (actual solar power) would be less. That means less battery is required to compensate the difference between input and output of the filter. However, the low delay filter offers less level of smoothness. A large delay gives a good smoothing but it increases the required battery capacity. The method proposed in this chapter is a compromise between these two conflicting requirements. To this end, there are several factors that should be considered in designing an FIR filter for this application, rather than satisfying the low-pass filter cut-off frequency criterion. These factors include: 1) length of the filter: minimizing the filter length reduces the complexity and cost of the controller and reduces the filter delay; 2) filter group delay: the filter with a small group delay uses less battery capacity for smoothing purpose; 3) stopband attenuation: a higher stopband attenuation for specific filter length means a smoother output curve due to higher damping at high frequencies.

This chapter presents an approach for an optimal design of minimum-length, low-group-delay FIR filter with maximum stopband attenuation for a given cut-off frequency. The user specifies the level of smoothness by only defining the filter cut-off frequency and then the proposed algorithm automatically optimizes the rest of the low-pass filter design parameters to find the low delay, high

performance FIR filter. The obtained FIR filter, as a real-time primary controller of BESS, minimizes the deployed battery capacity and maximizes the solar power smoothness. This capability reflects the excellence of the proposed approach over traditional approaches.

This chapter also proposes a second stage filter which is activated only when there is no solar generation for charging the battery. In a 24-hour cycle, the battery charging load is distributed over time, when the solar output is zero, to reduce the burden of demand on the grid. The designed filter maintains the area under the normal charging curve of battery and the distributed charging curve unchanged as this area represents the required energy to charge the battery.

The outline of the chapter is organized as follows: in Section 7.2, the background and the problem statement is presented. In Section 7.3, the proposed design algorithm for the first stage filter including convex optimization, discrete signal processing, and polynomial root placement methods are introduced. Section 7.4 studies the design methodology for the second stage filter. Design examples, simulation and implementation of the proposed method over real solar data, and a comparison of results with the common approaches are provided in Section 7.5. Finally, the concluding remarks are given in Section 7.6.

7.2 Problem Description

A length-*N* FIR filter can be represented by its frequency response as [118]:

$$H\left(e^{j\omega}\right) = \sum_{n=0}^{N-1} h[n]e^{-j\omega n} \tag{10}$$

where $h[n],\ n = 0,1,\dots,N-1$, are real filter coefficients. The frequency response $H\left(e^{j\omega}\right)$ can be characterized by magnitude and phase as:

$$H\left(e^{j\omega}\right) = A(\omega)e^{j\varphi(\omega)} \tag{11}$$

where $A(\omega) = \left|H\left(e^{j\omega}\right)\right|$ represents the magnitude of $H\left(e^{j\omega}\right)$, and $\varphi(\omega)$ is the phase. The group delay of the system is defined as:

$$\tau(\omega) = \text{grd}\left[H\left(e^{j\omega}\right)\right] = -\frac{d}{d\omega}\left(\arg\left[H\left(e^{j\omega}\right)\right]\right) = -\frac{d\varphi(\omega)}{d\omega} \tag{12}$$

As opposed to the phase delay, the group delay is a measure of the time delay of the amplitude envelopes of the various sinusoidal components of the signal. That is, the group delay reflects the time difference from the input pulse envelope peak to the output pulse envelope peak. The idea of designing a filter with low-group-delay for the real-time applications like solar smoothing is to minimize the time-delay induced by the filter.

In view of the above definitions the first problem is defined as:

Problem 1: Design a minimum-phase low-pass filter which has the following specification: 1) the maximum attenuation at the stopband; 2) minimum-group-delay in the passband; and 3) minimum length. This problem can be expressed as (13):

$$\begin{aligned} &\min_{h[n]} \ \alpha_1 N + \alpha_2\varepsilon_1 + \ \alpha_3\varepsilon_2 \\ &\text{s.t.} \ \ \left\|H(e^{j\omega})\right\|_2 \le \varepsilon_1 \ for \ \ \omega \ge \omega_c \\ &\text{grd}\left[H(e^{j\omega})\right] \le \varepsilon_2 \ for \ \omega \le \omega_c \end{aligned} \tag{13}$$

where N is the length of FIR filter, ε_1 and ε_2 are the upper limits for filter magnitude response at the stopband, and group delay of the passband, respectively, ω_c represents the cutoff frequency, $\text{grd}\left[H\left(e^{j\omega}\right)\right]$ is group delay of the $H\left(e^{j\omega}\right)$ filter, and α_1, α_2 and α_3 are weighting factors.

Considering the fact that $H(e^{j\omega})$ should be also a minimum-phase filter, the optimization problem in (13) is not a convex optimization problem. Also because of the nonlinearity of

$\mathrm{grd}\left[H\left(e^{j\omega}\right)\right]$ with respect to $h[n]$, the optimization problem defined in (13) may not be solvable directly [119]. Therefore, the original problem should be transformed so that it can be solved.

Moreover, in the process of smoothing the solar power by battery energy storage systems, the controller should automatically recover the State of the Charge (SOC) of the battery at the end of each cycle (24-hour) such that the battery would be ready for the next cycle. Therefore, after the sunset, when the solar generation is zero, the battery storage system is charged by grid such that the battery SOC remains unchanged over a day of operation. However, sudden charging of the battery at the evening (peak time), when there is no solar generation, is not desirable for the grid. Therefore, the required energy which brings back the SOC to the primary level should be distributed over the entire night. Thus, the second problem is defined as:

Problem 2: Design a filter to automatically recover the battery SOC at the end of each cycle, and distribute the energy mismatch, exchanged by the battery, over time to reduce its impact on the grid.

7.3 Theory for the First Stage Filter

Three separate techniques are employed to transform the optimization problem (13) into a solvable form composed of two optimization loops. These techniques include 1) discrete signal processing theorems 2) optimization techniques, and 3) polynomial root analysis. The DSP theory is utilized to structure and formulate an FIR filter design problem, in discrete time domain which filters the solar output power in real-time. The optimization techniques are used to optimize the filter coefficient in an inner loop for a given filter length such that minimizes the filter delay (battery capacity) and maximizes the stopband attenuation (level of smoothness). It also minimizes the filter length in the outer loop to meet the cut-off frequency requirement. Finally, the polynomial theorem helps to define the FIR filter design problem in the domain of minimum-phase FIR filters which

has minimum possible group-delay. The smoothness performance of the filter is adjusted by choosing an appropriate cut-off frequency, ω_c. The selection method for the application of smoothing the output of the solar power with the battery system is discussed later in the chapter.

7.3.1 Discrete signal processing

This Section is concerned with designing a filter that is able to smooth the solar generation. The focus of this Section is on designing the "minimum-phase" FIR filter. The motivation for designing the minimum-phase filter is related to the properties that these types of filters offer including minimum-phase-lag, minimum-group-delay, and minimum-energy-delay. The following three theorems provide a justification for restricting the domain of the filters to minimum-phase FIR filters.

Theorem 1 [118]: The causal, stable system that has $\left|H_{min}\left(e^{j\omega}\right)\right|$ as its magnitude response and also has all its zeros and poles inside the unit circle has the minimum-phase-lag function (for $0 \leq \omega \leq \pi$) of all the systems having that same magnitude response.

Theorem 2 [118]: Among all the systems that have a given magnitude response $\left|H_{min}\left(e^{j\omega}\right)\right|$, the one that has all its poles and zeros inside the unit circle has the minimum-group-delay.

Theorem 3 [118]: For any causal, stable sequence $h[n]$ for which $\left|H\left(e^{j\omega}\right)\right| = \left|H_{min}\left(e^{j\omega}\right)\right|$, then $|h[0]| \leq |h_{min}[0]|$.

If the partial energy of the impulse response is defined as $E[n] = \sum_{m=0}^{n}|h[m]|^2$, then for all $h[n]$ belonging to the family of systems that have the magnitude response $\left|H\left(e^{j\omega}\right)\right| = \left|H_{min}\left(e^{j\omega}\right)\right|$, it can be shown that [118]:

$$\sum_{m=0}^{n} |h[m]|^2 \leq \sum_{m=0}^{n} |h_{min}[m]|^2 \tag{14}$$

According to (14), the partial energy of the minimum-phase system is mostly concentrated around $m = 0$; i.e., the energy of the minimum-phase system is delayed the least of all systems having the same magnitude response function.

The proposed method in this chapter utilizes the above theorems to transform the problem in (13) to minimize the delay in real-time application. The next Section will describe how the optimization algorithm and polynomial root theorem are employed to design the optimal minimum-phase filter.

7.3.2 Optimization

This Section describes how the minimum-phase filter is designed by employing optimization algorithm and solving convex and quasi-convex optimization problems.

Typically, it is hard to infer much from a phase plot, while a group delay plot gives more useful information.

Differentiating both sides of the amplitude/phase representation (11):

$$H'\left(e^{j\omega}\right) = A'(\omega)e^{j\varphi(\omega)} + A(\omega)e^{j\varphi(\omega)}\left(j\varphi'(\omega)\right) \tag{15}$$

and dividing them by (11), since both $A'(\omega)/A(\omega)$ and $\varphi'(\omega)$ are real, the group delay in (12) can be restated as:

$$\tau(\omega) = Im\left(\frac{H'\left(e^{j\omega}\right)}{H(e^{j\omega})}\right) \tag{16}$$

If $h[n]$ represents the filter coefficients of $H\left(e^{j\omega}\right)$, one can apply the frequency differentiation property of the Fourier transform and get, $-jnh[n]$ as the filter coefficients of $H'\left(e^{j\omega}\right)$.

Denoting Fourier transform of $h[n]$ as $F.T.(h[n])$:

$$\tau(\omega) = Real\left(\frac{F.T.(nh[n])}{F.T.(h[n])}\right) \tag{17}$$

It is desired to design the filter with minimum possible group delay in the passband in order to have a fast response and minimize the gap between input and output signals of the filter. For this purpose, the idea is to force the group delay at ω=0 equal to zero. One can have:

$$\tau(0) = Real\left(\frac{F.T.(nh[n])}{F.T.(h[n])}\right)\Big|_{\omega=0} = 0 \Leftrightarrow \sum_{n=0}^{N-1} nh[n] = 0 \tag{18}$$

Constraint (18) ($\sum_{n=0}^{N-1} nh[n] = 0$) can satisfy the zero group delay for the DC component of the signal. By making the derivation from (17) and substituting constraint (18) into it, one can show $\tau'(0) = 0$. That is, the condition (18) also provides the zero slope for group delay at $\omega = 0$ ($\tau'(0) = 0$), which can further lower the group delay in the passband.

Although constraint (18) reduces the low frequency group delay significantly, another condition is required for having a minimum-phase FIR filter. Minimum-phase characteristic can guarantee the minimum-group-delay among all the systems that have the same magnitude response. Here is a helpful theorem to define the optimization problem for designing minimum-phase filter.

Theorem 4 [120]: Let $B_0, B_1, \dots, B_n$ be real scalars (with $B_1, \dots, B_n$ not all zero) and consider the affine family of monic polynomials:

$$P = \left\{ z^n + a_1 z^{n-1} + \cdots + a_{n-1} z + a_n \mid B_0 + \sum_{j=1}^{n} B_j a_j = 0, a_i \in \mathbb{R} \right\} \tag{19}$$

The optimization problem:

$$\rho^* \coloneqq \inf_{p \in P} \rho(p) \tag{20}$$

where $\rho(p)$ denotes the root radius of a polynomial p and is defined as (21):

$$\rho(p) = max\{|z| \mid p(z) = 0, z \in \mathbb{C}\} \quad (21)$$

has a globally optimal solution of the form:

$$p^*(z) = (z-\gamma)^{n-k}(z+\gamma)^k \in P \quad (22)$$

for some integer k with $0 \leq k \leq n$, where $\rho^* = \gamma$.

The theorem describes that when the maximum root radius (γ) is equal to zero, all the coefficient of the polynomial need to be equal to zero ($a_1 = \cdots = a_{n-1} = a_n = 0$) which leads to $p(z) = z^n$. Therefore, since problem in Theorem 4 is a convex optimization problem, by minimizing the coefficients of the polynomial one can move towards the zero root radius. In other words, the radius of polynomials roots will be reduced by minimizing the polynomial coefficient $(a_1, \dots, a_{n-1}, a_n)$ while $B_0 + \sum_{j=1}^{n} B_j a_j = 0$. This approach will help to push polynomial roots inside the unit circle which is the requirement of the minimum-phase filter.

The equation (23) represents the group delay contribution of a zero ($1 - re^{j\theta}e^{-j\omega}$) in the filter transfer function where r is the radius and θ is the angle of the zero in the z-plane:

$$\text{grd}\left[1 - re^{j\theta}e^{-j\omega}\right] = \frac{r^2 - r\cos(\omega-\theta)}{1 + r^2 - 2r\cos(\omega-\theta)} \quad (23)$$

The maximum amount of group delay for each zero happens when $\omega - \theta = \pi$ thus:

$$max(\text{grd}\left[1 - re^{j\theta}e^{-j\omega}\right]) = r/(1+r) \quad (24)$$

Therefore, minimizing the polynomial coefficient and consequently reducing the radius of the polynomial roots (r), the group delay eventually decreases which is desirable.

As a result, by considering the FIR filter described with $H\left(e^{j\omega}\right) = \sum_{n=0}^{N-1} h[n]e^{-j\omega n}$ and the design variables being filter coefficients $h[n]$, the design problem of a low-pass filter can be structured which includes the following specifications:

1) For low-pass filter the magnitude at $\omega = 0$ needs to be equal to one, thus, the term $H(e^{j0}) = \sum_{n=0}^{N-1} h[n] = 1$ is added as a constraint

2) For $\omega_c \leq \omega \leq \pi$ the magnitude of the filter should be minimized, thus the following term for $\omega_c \leq \omega \leq \pi$ is added in the objective function:

$$\min_{h[n]} \left|H(e^{j\omega})\right| = \min_{h[n]} \left\|\sum_{n=0}^{N-1} h[n]e^{-j\omega n}\right\|$$

3) For ω=0 the group delay should be zero to have no delay for DC component and minimum delay in low frequency, therefore, the term $\sum_{n=0}^{N-1} nh[n] = 0$ is added in constrain

4) The coefficient of the filter should be minimized to guarantee the minimum-phase filter with minimum-group-delay $(\min h[n]\ for\ n = 1, \dots, (N-1))$. Thus, the term $\alpha\|\sum_{n=1}^{N-1} h[n]\|$ is included in objective function for $\omega_c \leq \omega \leq \pi$.

Finally, the optimization problem can be expressed as:

Optimization Problem

Optimization Variable: $h[n]$

$$\min_{h[n]} \left\|\sum_{n=0}^{N-1} h[n]e^{-j\omega n}\right\| + \alpha \left\|\sum_{n=1}^{N-1} h[n]\right\| \qquad \omega_c \leq \omega \leq \pi$$

subject to:

$$\sum_{n=0}^{N-1} h[n] = 1 \quad and \quad \sum_{n=0}^{N-1} nh[n] = 0 \qquad (25)$$

where α is a weighting factor which is changed in a loop to make sure that for the minimum amount all the roots are placed inside the unit circle for a minimum-phase filter.

Problem (25) can be expressed as the second-order cone programming (SOCP) by defining some new parameters:

$$\min_{h[n]} (t_1 + \alpha t_2)$$

$$\text{Subject to} \quad \|A_k x\|_2 \le t_1, \quad \|Bx\|_2 \le t_2, \; Cx = d \tag{26}$$

where $x = [h[0] \quad h[1] \quad \dots \quad h[N-1]]^T$

$A_k = [e^{-j\omega_k \cdot 0} \quad e^{-j\omega_k \cdot 1} \quad \dots \quad e^{-j\omega_k \cdot (N-1)}]$

$\omega_c \le \omega_1 \le \omega_2 \le \cdots \le \omega_k \le \pi, \; k = 1, \dots, M, \; M \approx 15N$

$B = [0 \quad 1 \quad 1 \quad \dots \quad 1]_{1\times N}$

$C = \begin{bmatrix} 0 & 1 & 2 & \cdots & N-1 \\ 1 & 1 & 1 & \cdots & 1 \end{bmatrix}_{2\times N}$ and $d = [0 \quad 1]^T$

As it was shown in (26), a very special form of the semi-infinite constraints appears in the filter design problems.

Lemma 1: The semi-infinite inequality constraint:

$$g_i(x, \omega) \le t_i \text{ for all } \omega \in [\omega_c, \pi] \tag{27}$$

can be expressed as the ordinary inequality constraint:

$$h_i(x) = \sup_{\omega \in [\omega_c \; \pi]} g_i(x, \omega) \le t_i \tag{28}$$

It is easily verified that h_i is a convex function of *x*, since for each *ω*, $g_i(x, \omega)$ is convex in *x*. On the other hand, h_i is often nondifferentiable, even if the functions g_i are differentiable. Several methods such as bundle methods, ellipsoid methods, or cutting plane methods for general (non-differentiable) convex optimization are proposed that can be used to solve the semi-infinite constraints in (26). One of the requirements for these methods is an efficient method to evaluate h_i and a subgradient at any *x*. This involves computing a frequency υ for which $g_i(x, \upsilon) = h_i(x)$. It

is also possible to solve some magnitude filter design problems exactly, by transforming the semi-infinite constraints into (finite-dimensional) constraints that involve linear matrix inequalities. The semi-infinite constraints can also be approximated in a very straightforward way by sampling or discretizing frequency. We choose a set of frequencies $\omega_c \leq \omega_1 \leq \omega_2 \leq \cdots \leq \omega_M \leq \pi$ often uniformly or logarithmically spaced, and replace the semi-infinite inequality constraint:

$$g_i(x, \omega) \leq t_i \text{ for all } \omega \in [\omega_c, \pi] \tag{29}$$

with the set of *M* ordinary inequality constraints:

$$g_i(x, \omega_k) \leq t_i \text{ for all } k = 1, \ldots, M \tag{30}$$

Note that sampling preserves convexity. When *M* is sufficiently large, discretization yields a good approximation of the semi-infinite programming (SIP). A standard rule of thumb is to choose $M \approx 15N$ [121].

There are still two more parameters, *N* and ω_c, that need to be designed in order to have a desired low pass FIR filter, where *N* is the length of the FIR filter and ω_c is the cut-off frequency.

Theorem 5*:* The length of an FIR filter (*N*) is a quasi-convex function of its coefficients (x) [122].

Lemma 2: By defining $f(a) = min\{k \mid a_{k+1} = \cdots = a_N = 0\}$, the sublevel sets of *f* are affine sets and convex: $\{a \mid f(a) \leq k\} = \{a \mid a_{k+1} = \cdots = a_N = 0\}$. This means that *f* is a quasi-convex function, and optimization problem is a quasi-convex optimization problem.

The problem of finding the minimum-length FIR filter given cut-off frequency ω_c is expressed in (31). This problem can be solved using bisection on *N*. Each iteration of the bisection involves solving an SOCP feasibility problem:

Optimization Problem

minimize N

subject to

$$\|A_k x(N)\|_2 \leq 0.7079\ (-3\ dB) \qquad k \in I\ , \tag{31}$$

where $I = \{k|\omega_k \geq \omega_c\}$

In summary, the proposed algorithm performs an iterative scheme through two loops: 1) the outer quasi-convex optimization problem loop shown in (31) which adjusts N using bisection and 2) the inner SOCP convex optimization problem loop presented in (26) which adjusts α. Once the minimum-phase and cut-off frequency criteria are met, the proposed FIR filter is obtained.

7.4 Theory for the Second Stage Filter

This Section proposes a second stage filter cascaded with the primary one to gradually restore the SOC of the battery to the initial value at each cycle. At the time of sunset, when the solar generation is zero, the output signal of the primary filter is negative which means the battery storage system is charged by grid such that the battery SOC remains unchanged over a day. The role of the second filter is to distribute the energy mismatch, exchanged by the battery, in the time horizon to reduce the impact on the grid. Therefore, when the output signal of the primary filter becomes negative, the second filter is activated and distributes the battery storage load over time. Figure 35 depicts the structure of two-filter cascading.

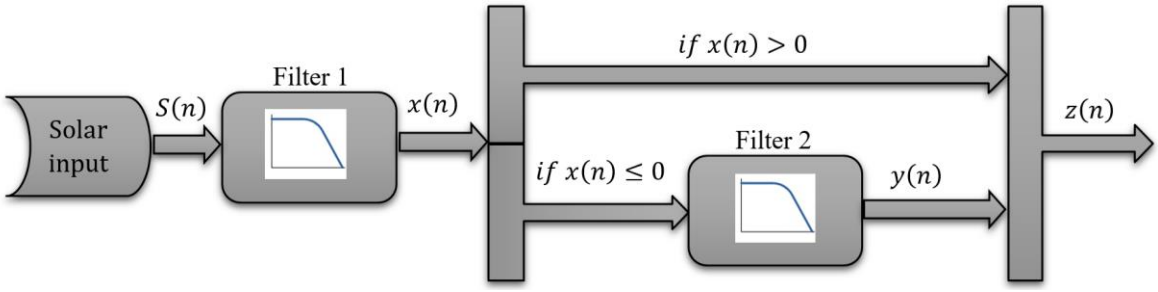

Figure 35 Filter cascading structure

The main criterion for designing the second filter is that the area under the input and output signal of the filter remains the same, as this area represents the required energy to charge the battery (filtering should not change the area under the signal). This criterion is shown in Figure 36.

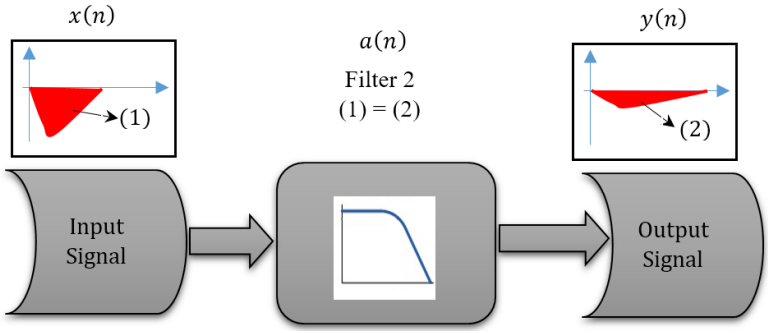

Figure 36 Second Filter, input signal, and output signal

Lemma 3: Let a Linear Time-invariant (LTI) filter with length N have its impulse response $a[n]$. The output $y[n]$ due to a given input $x[n]$ with length M while $N < M$ can be specified through the convolution sum:

$$y[n] = x[n] \circledast a[n] = \sum_{k=-\infty}^{\infty} x[k]a[n-k] \tag{32}$$

If the following two conditions are satisfied, then the area under the input signal and output signal unchanged:

1) $\sum_{n=1}^{N} a[n] = 1$

2) $x[k] = 0 \quad for \quad M - N + 1 \leq k \leq M$

From (32), the area under the output can be defined as:

$$\sum_{n=1}^{M} y[n] = \sum_{n=1}^{M}\sum_{k=1}^{M} x[k]a[n-k] = \sum_{k=1}^{M}\left(x[k]\sum_{n=1}^{M} a[n-k]\right)$$

$$\Rightarrow \sum_{n=1}^{M} y[n] = \sum_{k=1}^{M-N} x[k] \times \sum_{n=1}^{N} a[n] + \sum_{k=M-N+1}^{M}\left(x[k]\sum_{n=1}^{M} a[n-k]\right) \tag{33}$$

where $a[n] = 0$ for $n < 0$.

Condition 1) guarantees that the first term on the right-hand-side of (33) is the area under the input signal and Condition 2) makes the second term zero.

The second condition can be interpreted as follows. The input signal should be zero outside of the filter window. That is, *N* should be defined such that the length of filter (filter window) covers the entire non-zero part of input signal $x[n]$. To this end, the filter is able to deliver the entire energy of the input signal. The first and second conditions can be easily satisfied by adjusting the length of LTI filter (*N*), and the filter coefficients ($a[n]$).

7.5 Case Studies

7.5.1 Simulation Results

The performance of the purposed approached is first demonstrated over simulation results in MATLAB. The numerical calculation and simulations are performed on an Intel Core i7 4.00 GHz windows based PC. In the simulation, the minimum-length-low-group-delay FIR filter is designed

by solving the optimization problems (25) and (31). For that purpose, the cut-off frequency is selected as $\omega_c = 0.006\,\pi\ rad/sample$.

In this document, the cut-off frequency is selected based on a pre-study and analysis of the historical power data captured from the UCLA Ackerman Union solar panels during both cloudy and clear days. In this context, a spectrum analysis is performed and the harmonics of the solar power is found. This information helps finding the best cut-off frequency to reach a smooth curve. Figure 37 shows the output power of the solar PV at UCLA Ackerman Union and the frequency spectrum of the signals over a couple of weeks. It is observed that for a wide range of frequencies the magnitude of the harmonics is below 30. Therefore, it is decided to filter the harmonics with magnitude less than 30 which corresponds to the cut-off frequency of around $\omega_c = 0.006\,\pi\ rad/sample$. For different scenarios in different locations the spectrum analysis of the historical solar power would be different, and consequently the selection of cut-off frequency and also the designed filter is different.

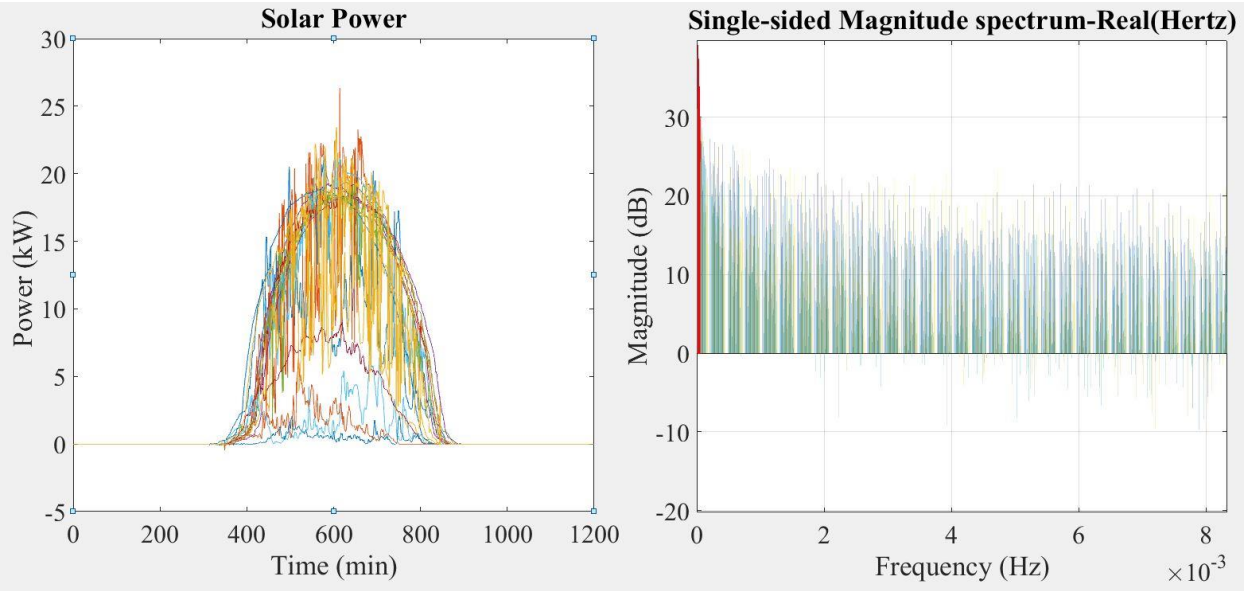

Figure 37 The output power of solar panel and the power spectrum

In these case studies, without loss of generality, the solar PV data are captured every 30 seconds. Thus, the length of the data for entire day would be 2880 samples. Since the length of FIR filter represents the depth and number of previous data used by the filter, therefore, it is expected that the length of the filter does not exceed 2880. The design process, including solving the convex and quasi-convex optimization problems, takes 28 minutes and 58 seconds to converge to the solution. The minimum length of the filter obtained from quasi-convex optimization problem that meets the selected cut-off frequency is 433. The obtained cut-off frequency ($0.00609\,\pi\ rad/sample$) is matched with the design parameter and the small deviation is due to discretizing the convex optimization problem. Although the length of the filter is 433, the max delay reaches to 191.8 samples. In addition, all poles and zeros are inside the unit circle as it is ilustrated in Figure 38.

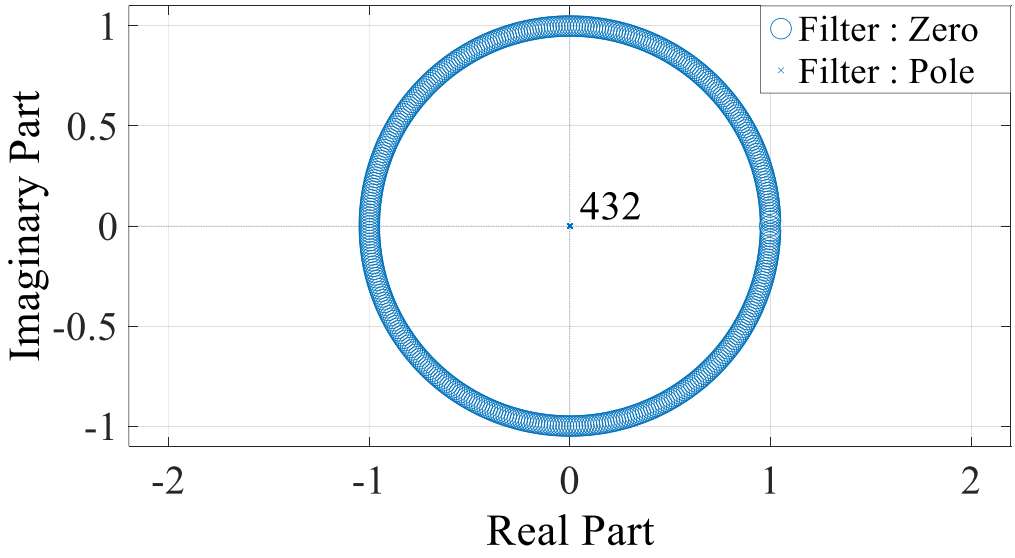

a)

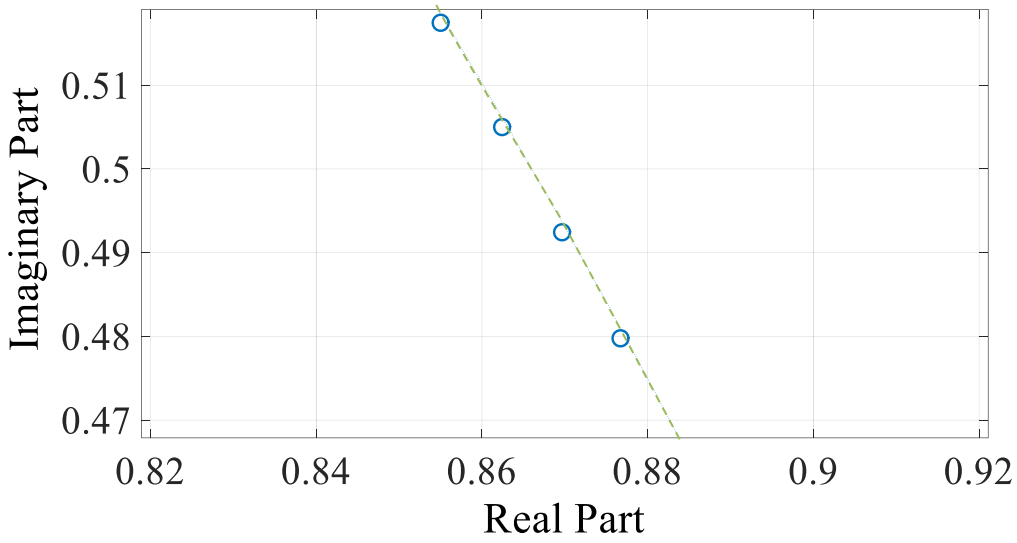

b)

Figure 38 Zero/pole placement of the proposed filter with 432 poles a) the zero/pole placement b) zoom-in of the zero/pole placement

In order to demonstrate the effectiveness of the proposed approach the same length filter is designed using two other popular approaches. The first is using the method proposed by Herrmann and Schuessler for minimum phase design [123], and the second is designed with the moving average approach which is the common solar smoothing method in the literature [114].

The proposed filter, moving average filter, and Herrmann and Schuessler filter (with the same filter length) are applied to the solar PV power output of the UCLA Ackerman union, recorded every 30 seconds for a typical day. Figure 39 depicts the performance of each filter in generating the reference signal to control the battery storage system power flow for smoothing the PV power curve. The output signal generated by proposed approach has the minimum delay from the original solar signal which reduces the share of battery storage system for compensation. The results in Figure 39 demonstrate how decreasing the passband group delay reduces the lag of filter output (red curve) compared with solar generation curve (blue curve) and consequently reduces the gap.

That means, with the new approach less battery capacity is required to compensate the gap between input and output signal as blue and red curve are close to each other.

Figure 40 shows the passband group delay of the proposed filter, moving average filter, and Herrmann and Schuessler filter with the same filter length. It is shown that in the proposed approach the group delay is significantly lower in the passband compared with the two other approaches.

The battery capacity (kWh) deployed for smoothing process can be calculated based on the actual battery charging /discharging response. The required size of storage for smoothing the solar power highly depends on the solar generation profile. That is, the more the fluctuations occur in the solar power the more the battery capacity is used for compensation. To this end, the capacity of the battery is calculated based on the maximum exchanged energy through smoothing process. The maximum exchanged energy is multiplied by the factor of 1.2 considering a 20 percent margin for battery capacity. It is assumed that the initial SOC of the battery at the beginning of the cycle is 50 percent. Therefore, the capacity of battery is obtained from:

$$C_{battery} = 2 \times \max(|E_{battery}|) \times 1.2 \tag{34}$$

where $C_{battery}$ is the energy capacity of battery in kWh, and $E_{battery}(k)$ is the battery energy level at step k which is calculated as:

$$E_{battery}(k) = \frac{T}{60} \times \sum_{i=1}^{k} [P_{battery}(i)] \tag{35}$$

where T is the sampling time in minute, and $P_{battery}(i)$ is the exchanged power by battery at step i in kW.

The capacity of the inverter can also be calculated by multiplying the maximum exchanged power of the battery by the factor of 1.2 as:

$$C_{inverter} = \max(|P_{battery}|) \times 1.2 \quad (36)$$

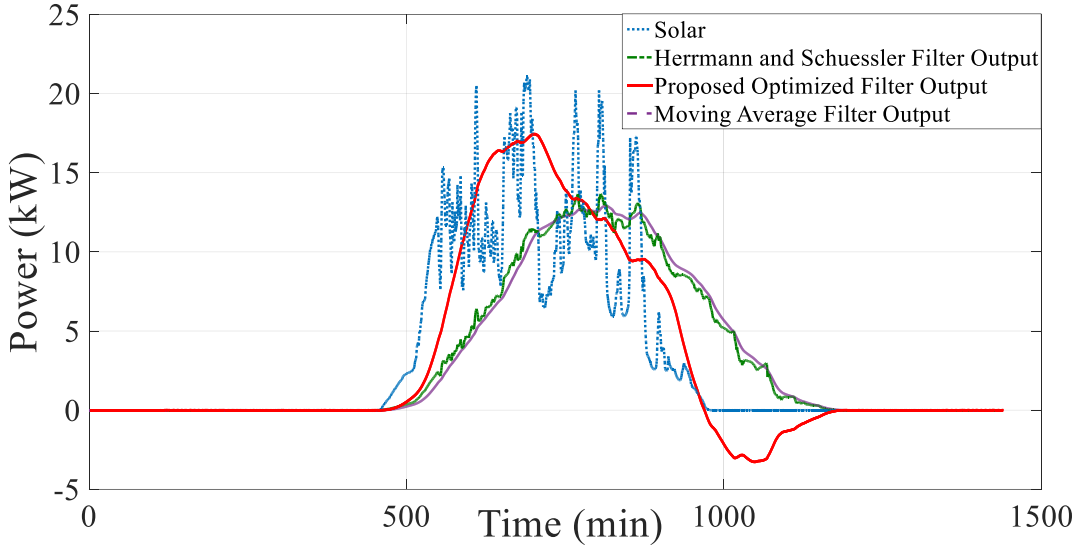

Figure 39 Solar output power, and the reference signal obtained from proposed approach with $\omega_c = 0.006\,\pi\ rad/sample$ compared with two filter designed approaches

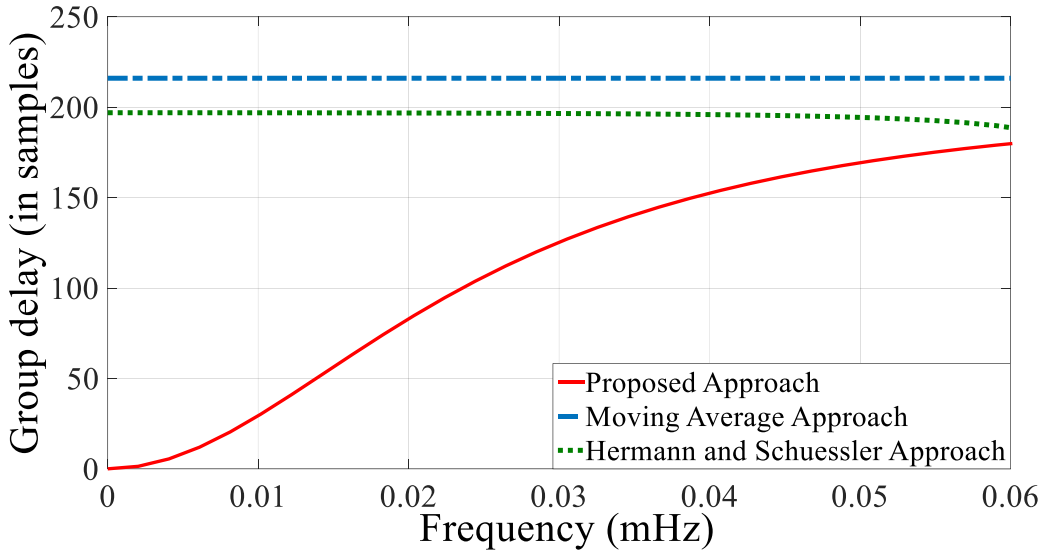

Figure 40 Group delay comparison of the proposed filter, Moving average filter, and Herrmann and Schuessler filter with the same filter length.

The simulation results show that the required battery capacity with the proposed control method is 16kWh while this number for Herrmann and Schuessler FIR filter with the same length

is 26.9kWh, almost 170 percent of the one for the proposed approach. For moving average filter the battery storage demand is 29.3kWh.

The proposed filter, a moving average filter, and the Herrmann and Schuessler filter with the same length are also applied to a randomly selected solar power profile over a month shown in Figure 41. The required power capacity and energy capacity by each are summarized in Table 5.

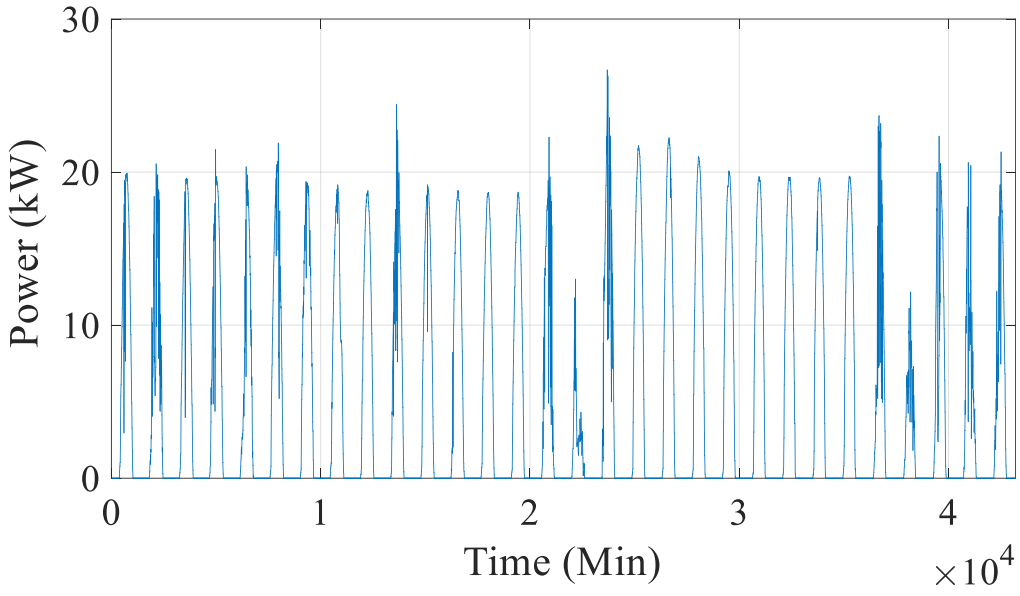

Figure 41 Solar power profile for 30 subsequent days

Table 5 Power rating and capacity of BESS for solar smoothing applying different filters

Filter Type	***Filter Length***	***BESS Power rating (kW)***	***Battery Capacity usage (kWh)***
Proposed approach	433	23.2	31.1
Moving Average approach	433	25	83.5
Herrmann and Schuessler Filter	433	23.9	76.8

Although the proposed approach offers better power rating compared with two other approaches, unlike the energy rating the power rating results are very close.

In the second analysis, the FIR filter designed by the proposed approach with $\omega_c = 0.006\,\pi\ rad/sample$, is redesigned by Herrmann and Schuessler approach while instead of filter length, the passband magnitude response remains the same.

It should be noted that in general, designing the Herrmann and Schuessler filter is not an easy task. The Herrmann and Schuessler filter requires four design parameters including the passband edge, stopband edge, passband ripple, and stopband ripple. In such an application, selecting all the four parameters is a complicated task as there is no explicit relationship between the design parameters and the size of the battery and solar smoothness level. The proposed approach, by contrast, only relies on one parameter and the rest are optimized automatically to minimize the size of battery and maximize the smoothness. Therefore, one of the advantages of the proposed approach over traditional FIR filter design approaches is simplicity in design. In this experiment to achieve the same passband magnitude response, the passband edge of Herrmann and Schuessler filter is chosen equal to $\omega_p = 0.005370\,\pi\ rad/sample$, the stopband edge is $\omega_p = 0.007568\,\pi\ rad/sample$, the passband ripple is 0.29183, and stopband ripple is 0.05702 by trial and error. Figure 42 shows the magnitude response of the FIR filters designed by the proposed approach, and Herrmann and Schuessler approach. Although both filters have the same magnitude response in passband, the attenuation of proposed approach in high frequency is considerably higher which leads to smoother output.

The output of both filters to the solar signal is depicted in Figure 43. The group delay of the proposed filter, shown in Figure 44, is lower than the one of Herrmann and Schuessler filter with

the same passband magnitude response, which means smaller battery capacity. In fact, compared with the Herrmann and Schuessler filter, applying the proposed approach reduces the size of battery by almost 20 percent, from 19.9kWh to 16kWh.

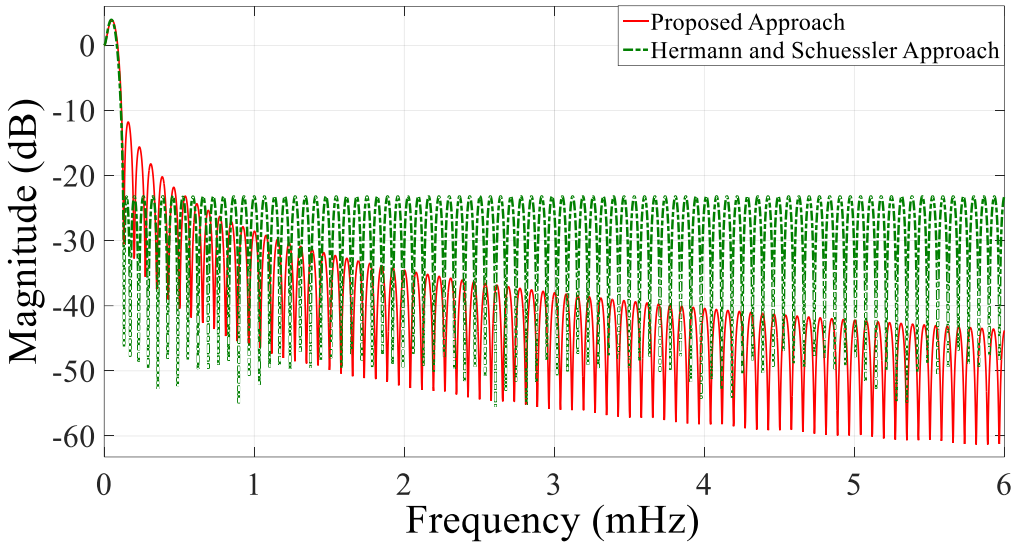

Figure 42 Magnitude response comparison of the proposed filter and Herrmann and Schuessler filter while the passband magnitude response is the same.

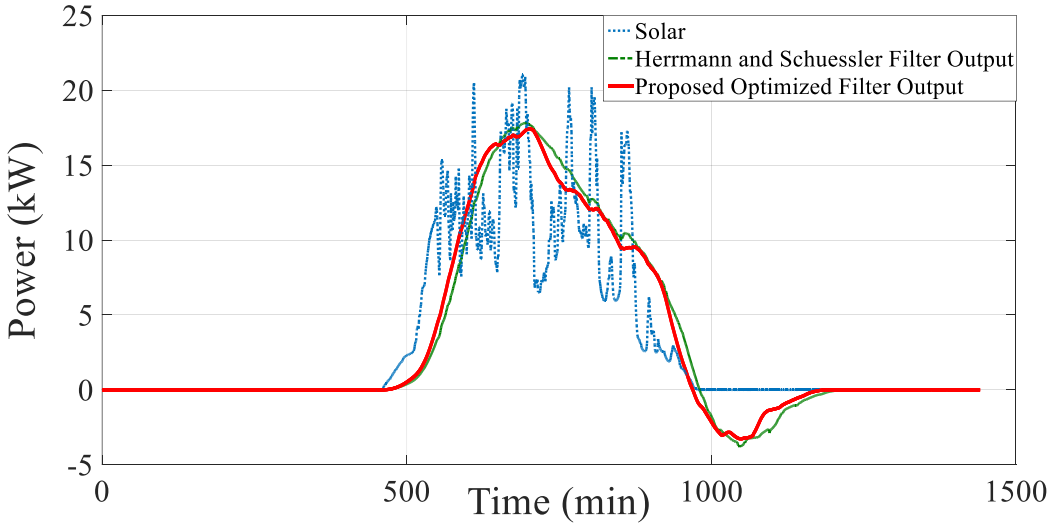

Figure 43 Reference signals obtained from proposed approach and Herrmann and Schuessler approach with the same passband magnitude response.

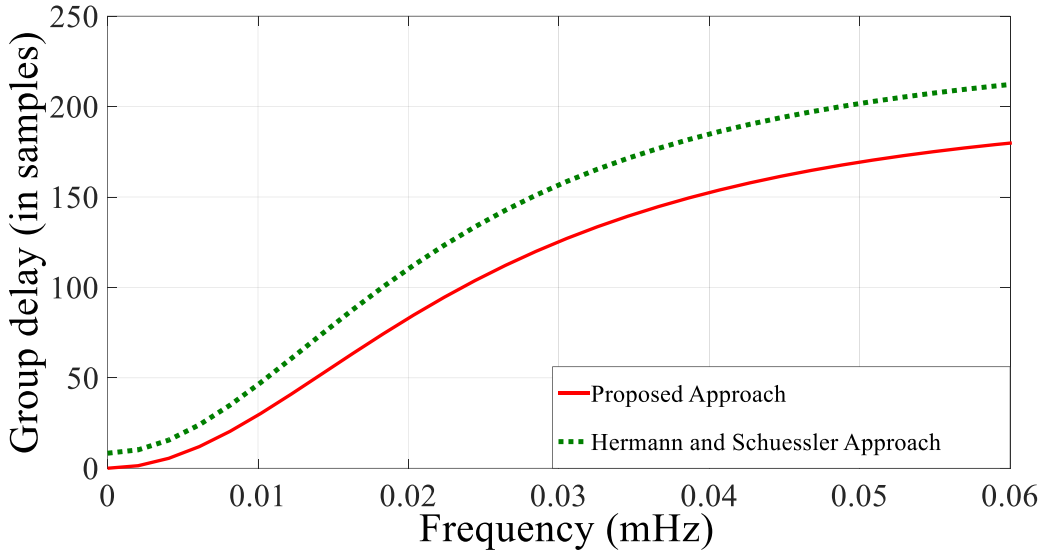

Figure 44 Group delay comparison of the proposed filter, and Herrmann and Schuessler filter with the passband magnitude response are the same.

In this scenario since the passband magnitude response and cut-off frequency of the filters are the same, it would be helpful to compare the percentage of fluctuation improvement. To this end, the fluctuation index of a curve defined based on the slope and curvature of the signal [124], is calculated as follows:

$$I_{fluctuation}(P_{solar}) = \sqrt{\sum_{k=2}^{M}[P_{solar}(k) - P_{solar}(k-1)]^2} + \sqrt{\sum_{k=2}^{M-1}[P_{solar}(k-1) - 2P_{solar}(k) + P_{solar}(k+1)]^2} \quad (37)$$

where M is the length of power time series. The comparison results between proposed filtering approach and Herrmann and Schuessler's one can be summarized in Table 6. Results in Table 6

validates the high smoothing performance of the proposed approach compared with Herrmann and Schuessler Filter, while the proposed approach deploys less battery capacity.

Table 6 Filters comparison

Filter Type	*Filter Length*	*Group Delay in Passband (samples)*	*Battery Capacity usage (kWh)*	*Output Fluctuation*
Proposed Filter	433	Starts from zero reaches 192	16	1553.3
Herrmann and Schuessler Filter	487	Starts from eight reaches 228	19.9	2492.6
Initial fluctuation index of solar power with no filtering				**3621.8**

In order to show the effect of the cut-off frequency on the size of the battery and solar power smoothness, the FIR filter is redesigned with (a) $\omega_c = 0.008\,\pi\ rad/sample$ and (b) $\omega_c = 0.004\,\pi\ rad/sample$.

The result for $\omega_c = 0.004\,\pi\ rad/sample$ is shown in Figure 45. Although by reducing the cut-off frequency the smoother curve is achieved, it costs more battery capacity. The optimum length of filter satisfying the cut-off frequency constraints increases to 650 which leads to a higher group delay. The required battery capacity for this level of smoothness is 26.8kWh.

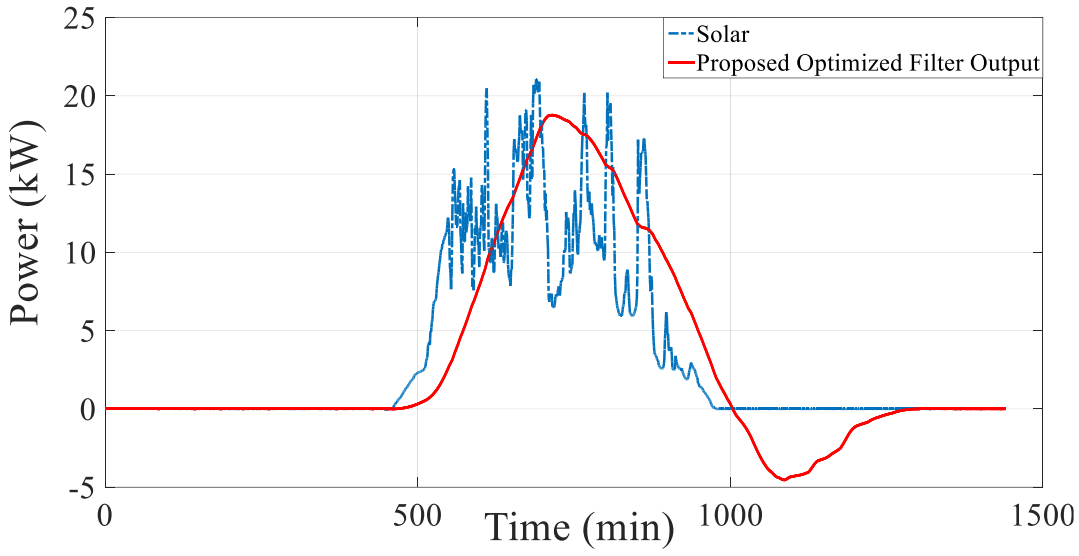

Figure 45 Solar output power and the reference signal obtained from proposed approach with $\omega_c = 0.004\,\pi\ rad/sample$.

The design result for $\omega_c = 0.008\,\pi\ rad/sample$ is shown in Figure 46. At the cost of reducing the smoothness of the output power, the required battery capacity is reduced to 11.1kWh and the optimum length of filter decreases to 326 which means less cost and complexity.

The simulation results validate the intended performance of the proposed approach and its simplicity where one can design the desired filtering level by just choosing one parameter (cut-off frequency) and finding the optimum solution in a trade-off between the investment (size of battery) and effectiveness (smoothness of the output). The higher cut-off frequency means lower battery capacity and lower level of smoothness and the lower cut-off frequency means higher battery capacity and higher level of smoothness. Therefore, the filter can be designed for a wide range of cut-off frequencies offline and then the user can select the level of solar output smoothness and dedicated battery storage capacity in real-time.

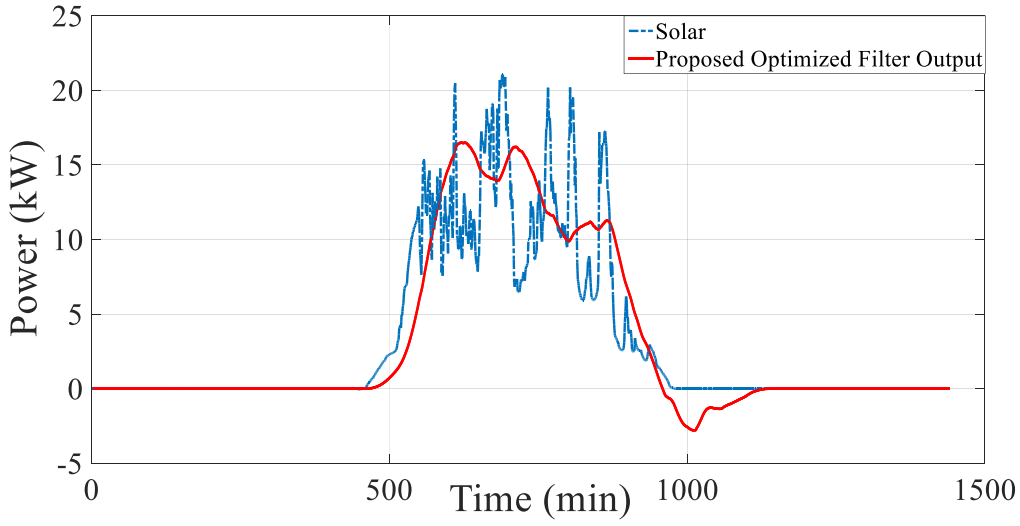

Figure 46 Solar output power and the reference signal obtained from proposed approach with $\omega_c = 0.008\,\pi\ rad/sample$

It should be noted that since the primary filter also meets the two conditions in lemma 3, the FIR filter maintains the area under the input and outputs signals unchanged. That is, the net energy exchanged by the battery during each cycle is zero. Therefore, when the solar generation becomes zero the battery automatically starts charging as much as it is discharged over smoothing process. In this context, according to Figs. 3, 6, 8, and 9, the power reference obtained from the primary filter has negative values (charging), seen as a pit, to recover the SOC of the battery. In order to avoid imposing extra burden on the grid, right after the solar generation is zero, the second filter can be added to distribute the charging load of the battery over time.

In the design for the second filter, $N = 1000$ and $a[n] = 1/1000$ for $n = 1, \cdots, 1000$ to satisfy both conditions in lemma 3. Figure 47 shows the simulation results of the double filter performance as compared with the single filter over several days. In Figure 47 the second filter helps to distribute the battery charging load over time and reduce the demand.

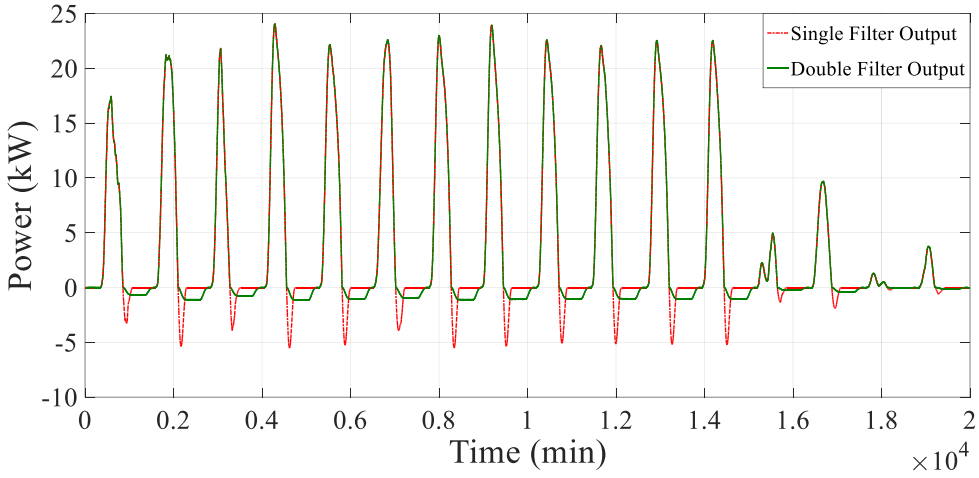

Figure 47 The simulation results of applying the proposed approach over two weeks and comparing the double filter technique and single filter technique

7.5.2 Experimental Results

The experimental setup to test the method proposed in this chapter includes a 62kWh lithium ion battery for energy storage, a 25kW solar PV panel, a 36kW grid-tie inverter, a PLC based local controller, and WINSmartGrid™ communication and control infrastructure.

The UCLA SMERC developed the WINSmartGrid™ platform that provides a smart grid architecture to enable remote monitoring, control, and bidirectional flow of information between a control center and devices, such as EV chargers, vehicle-to-grid units, grid-tied inverters, BESS, solar PV panels, and local controllers [72]. The platform is using a tri-layer design of Edgeware, Middleware and Centralware [125].

The experimental setup is shown in Figure 48 including the battery cabinet, grid-tie inverter, and the controller. The PLC based local controller is depicted in Figure 48 with more details including AC meter, DC meter, protection devices, and gateway. The power meter and solar panel installed at UCLA Ackerman union is also shown in Figure 48. The power meter is connected to

the output of solar panels' inverter. It is also connected to a gateway that includes a 3G dongle with a static IP address. The remote control center can retrieve power data using Modbus protocol from the gateway over the internet. The control center server receives data every 30 seconds and stores it into its local database. At the same time the control center runs the proposed algorithm, generates appropriate signal command and sends it to the BESS local controller via HTTP commands. There is a small delay between the time of measuring the solar power and the time of BESS response. Based on our experience this latency is about 3 to 4 seconds. The schematic of the experimental system including the grid integrated BESS and solar PV is shown in Figure 49.

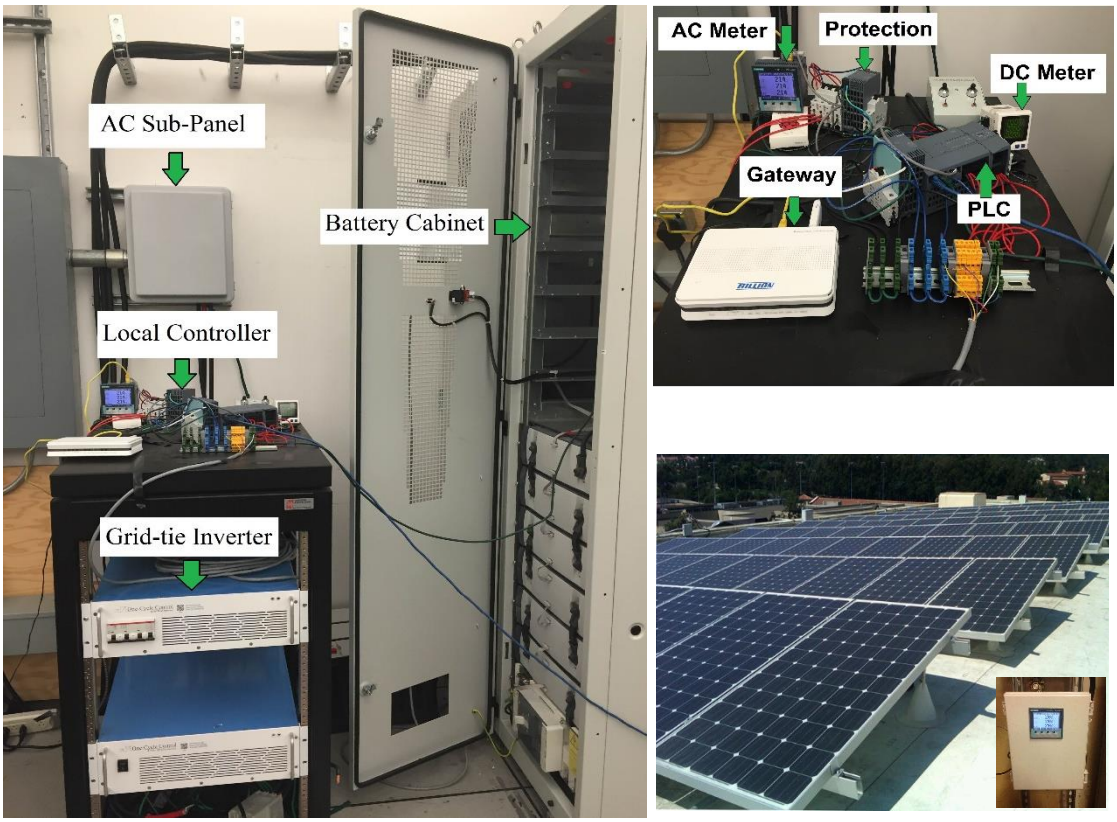

Figure 48 The BESS including the battery cabinet, grid-tie inverter, local controller, and AC panel

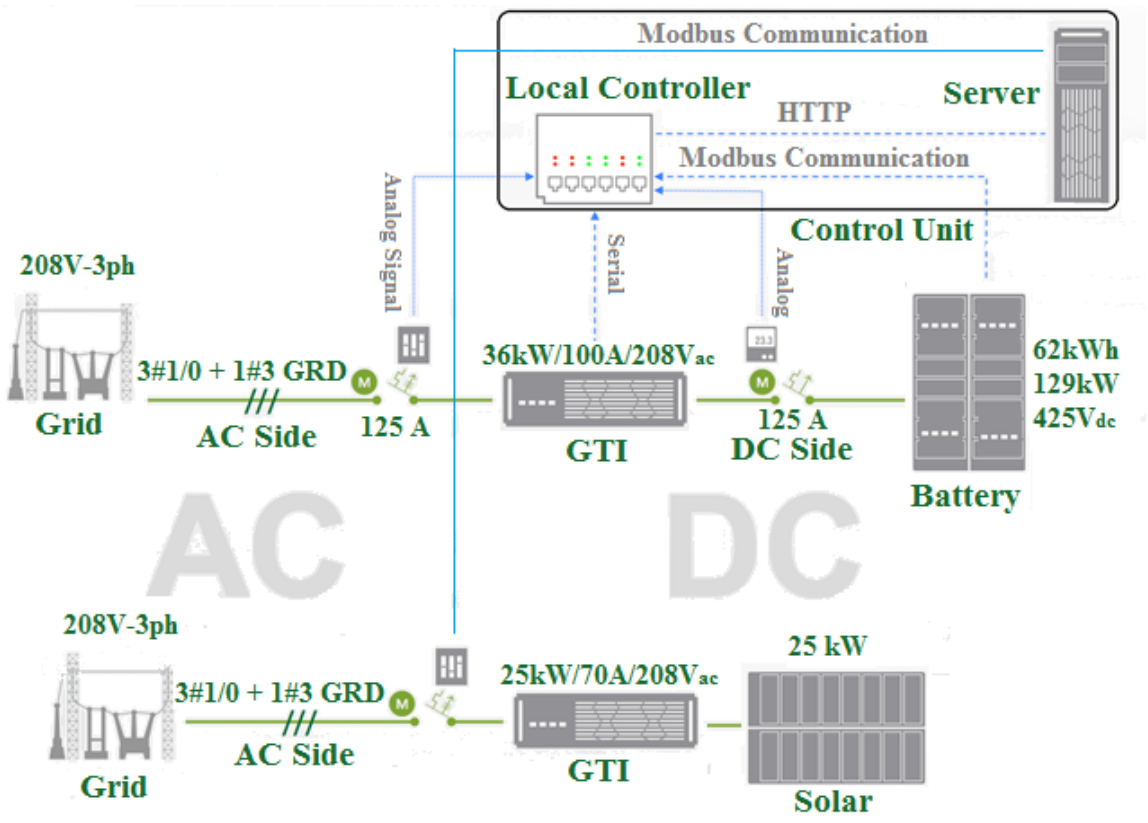

Figure 49 BESS and solar PV integration schematic

In this experiment, the battery and the solar unit are AC coupled as shown in Figure 49. That is, both the solar panels and battery are exchanging the energy with the grid. The battery storage system compensates the solar in real time based on the feedback from solar output power at each sampling time. The BESS can also receive power from the grid if the battery charge is running low. The Control of charging and discharging power of the battery energy storage system is performed through managing the grid-tie inverter power flow. The controller continuously communicates with the BMS, and measurement units to generate the control signal for the inverter. The controller based on the solar power data, received from the measurement unit, calculates the output of the filter at each sampling time. The output of the filter is the desired smoothed power curve. Then, using the desired power curve, the controller generates the reference signal for the

inverter. The reference signal is the difference between the desired output power given by the filter and the actual solar generation. The controller retrieves the voltage of the grid in real time and calculates the desired charging/discharging current. Before sending the reference signal to the inverter, the controller checks the available capacity of the battery and adjusts the reference signal according to the maximum allowable charging/discharging current calculated by BMS.

Inverter is internally equipped with a closed-loop feedback controller which tracks the reference signal with a fast dynamic. Figure 50 shows the control block diagram of the system.

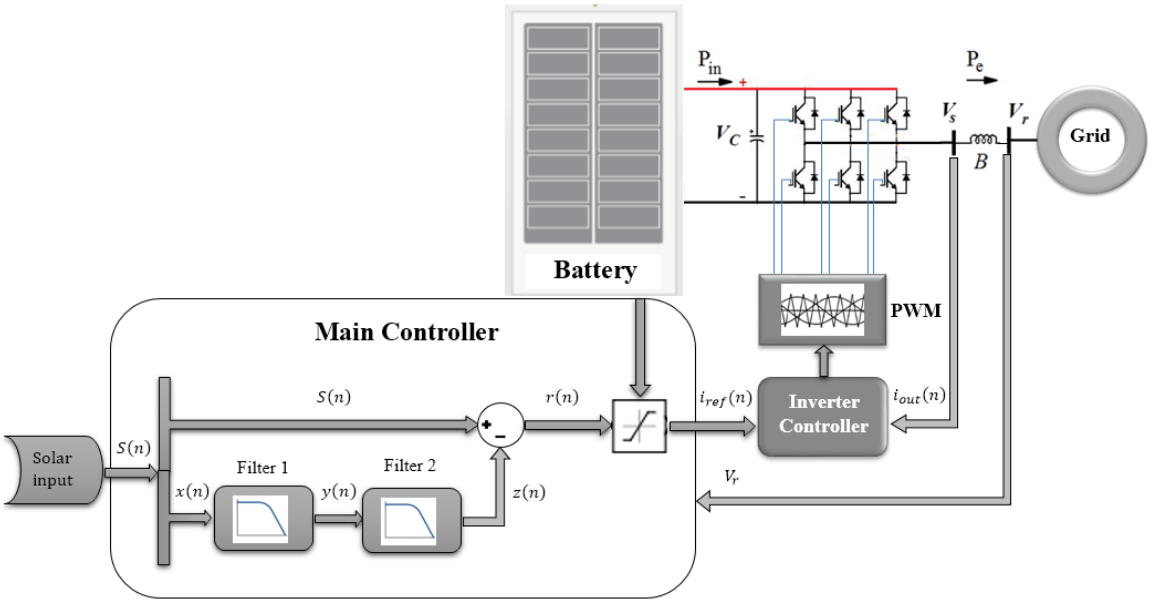

Figure 50 System control block

Showing the performance of the purposed approached, practical experiments are performed by using the same filter designed in subsection 7.5.1, with $\omega_c = 0.006\,\pi\ rad/sample$. In this experiment, the control center reads the solar data every 30 seconds. Then the control center generates the battery storage control signal based on the offline designed filter. The command is sent to the local battery storage system controller through HTTP command, and the local controller

executes the command by controlling the battery modules and grid-tie inverter. The measurement unit installed at the DC and AC side of the battery storage system send the output power of the BESS to the control center. Control center stores the output power of solar and battery storage system with timestamp. In the first experiment, the proposed cascade filter control approach is applied. Figure 51 shows the solar and smoothed curve. In order to compare the result, in the second experiment the Herrmann and Schuessler filter is also implemented.

The experiment result shows that the Herrmann and Schuessler filter requires 20.5kWh BESS which is 24 percent more than the capacity required by applying the proposed approach (16.5kWh). In addition, due to coupling the second filter, at the end of the day the battery is gradually being charged to bring back the SOC to the primary state. In fact, the second filter shape the battery load to reduce the grid demand.

In Figure 51 there is still some high frequency fluctuations in the output power. The spikes and high frequency fluctuations seen in the output are due to computational and execution delays of the controller and devices. In the physical system and practical experiment there is always a delay between the actual solar generation and battery reaction. This delay corresponds to the delay of the controller, inverter, battery and measurement units. The spikes seen in the experimental results stem from these computational and execution delays.

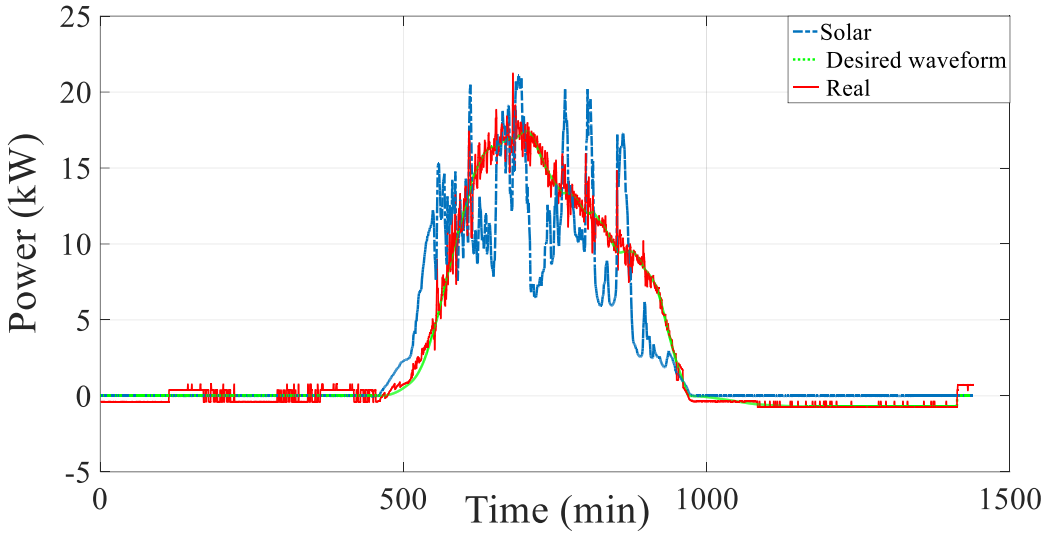

Figure 51 The experimental result obtained by applying the proposed approach with double filter: cloudy day.

The control signal is discrete and the controller has a zero-order hold. Due to the existing delay of the system, the control command is executed with 3-4 second delay and it is held till the next sampling interval, while the solar power has changed over that period. That is, although the battery power reaction is calculated for time interval *k*, it is seen in time interval *k+1*. In order to overcome the delay, one should predict the solar power for the next step with 100 percent accuracy and calculate the battery reaction based on the prediction. However, prediction of solar power with 100 percent accuracy is not theoretically feasible. The second solution which is more feasible is to choose a higher sampling frequency (act fast) to reduce the effect of the delay and zero-order holding.

In this context, a new experiment is run to show the effect of solar power sampling time on the quality of result. This time, we sample the solar power every 15 seconds instead of 30 seconds. Figure 52 shows the obtained results when the sampling time is changed from 30 seconds to 15 seconds. It can be seen that by reducing the sampling time the spikes in smoothed curve reduce considerably.

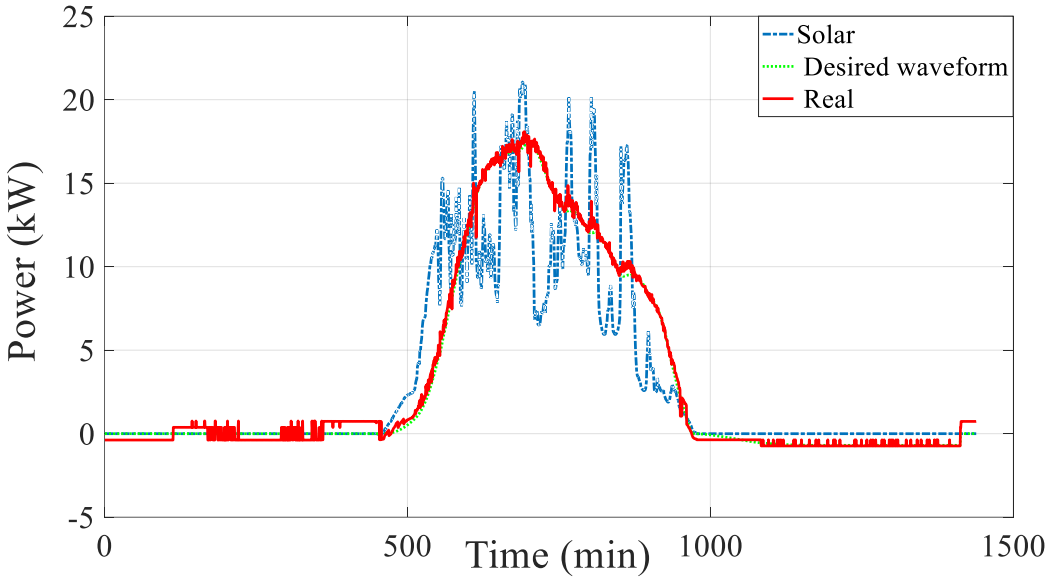

Figure 52 The experimental result of solar smoothing with sampling time of 15 seconds

The new experimental result shows how reducing the sampling time, as a viable solution, can mitigate the impact of system delay on output fluctuation.

The result of applying the proposed approach to a typical sunny day is shown in Figure 53. Although the solar generation is smooth by itself, the filter while maintain the smoothness adds a lag to the battery reference signal. The required battery capacity for this case is 17.8kWh.

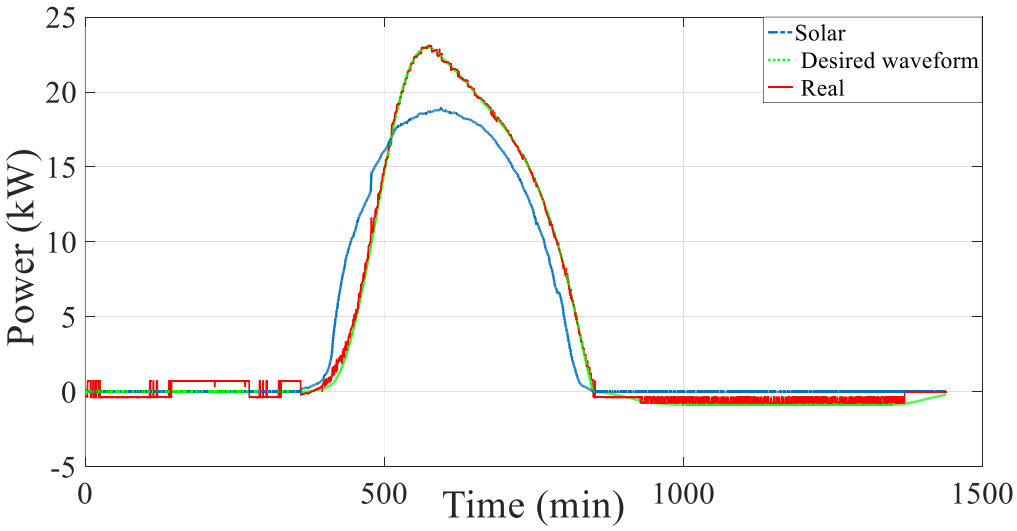

Figure 53 The experimental result of applying the proposed method: sunny day

7.6 Conclusion

In this chapter, a fast response controller for battery energy storage system is proposed to smooth the solar output power in real-time. The proposed controller is based on a two-stage filtering solution. The first stage filtering includes the minimum-phase, low-group-delay, minimum-length FIR filter designed by the convex and quasi-convex optimization technique. The minimum-phase low-group-delay feature of the filter reduces the capacity of the required battery considerably and the minimum-length feature simplifies the controller structure and reduces the cost. Another advantage of the proposed technique is to adjust the level of solar power smoothness directly by setting up the cut-off frequency while the other parameters of the filter are optimized automatically by the algorithm. The second stage filter is also designed to level the battery charging load by distributing the required charging energy over the entire night automatically. The proposed approach is implemented and applied to the UCLA solar PV output power over several days with different atmospheric conditions. The obtained results show a 45 percent reduction in the BESS

capacity compared with the common moving average technique. In addition, the developed FIR filter is well-adopted for this application while it is hard to design a well-behaved and appropriate filter by using other existing approaches and meet the design criteria for this application.

8 Voltage Regulation

This chapter proposes a new methodology to achieve voltage regulation in distributed power systems in the presence of solar energy sources and battery storage systems. The goal is to find the minimum size of battery storage and its corresponding location in the network based on the size and place of the integrated solar generation. The proposed method formulates the problem by employing the network impedance matrix to obtain an analytical solution instead of using a recursive algorithm such as power flow. The required modifications for modeling the slack and PV buses (generator buses) are utilized to increase the accuracy of the approach. The use of reactive power control to regulate the voltage regulation is not always an optimal solution as in distribution systems *R/X* is large. In this chapter, the minimum size and the best place of battery storage is achieved by optimizing the amount of both active and reactive power exchanged by battery storage and its GTI based on the network topology and *R/X* ratios in the distribution system. Simulation results for the IEEE 14-bus system verify the effectiveness of the proposed approach.

8.1 Introduction

Electric utility companies are concerned about potential difficulties due to the large scale penetration of PVs in the power grid. One of the challenges that may stem from the high penetration level of solar PVs and supply-demand imbalances is reverse power flow which may lead to voltage rise and variation. This issue will especially affect the distribution side of the grid where household PVs are connected [126], [127]. In addition, voltage variation due to uncontrollable nature of PVs can have a direct impact on the operation of load tap changers, voltage-controlled capacitor banks, and line voltage regulators, which may cause additional step-voltage changes. Based on the delays

(30-90s) in the control of the existing devices, minute-based step-voltage variations may be experienced. In addition, more frequent operation of these devices leads to more maintenance requirements, which consequently makes the expected life cycle of these devices short. Therefore, methods to improved voltage regulation have been developed to overcome the issue of overvoltage [128], [129], [130]. However, in distribution side and Low Voltage (LV) feeders the impedance is mostly resistive and the *R/X* ratio is considerable, as opposed to medium voltage feeder and transmission lines. Thus, the role of active power can be as important as reactive power on voltage variations and losses in a radial LV distribution feeder. This fact justifies the investigation to solve the voltage regulation problem by employing both active and reactive power and finding a tradeoff between these two parameters to optimally regulate the voltage [131]. One of the practical and effective solutions to achieve a flexible power control and solve the voltage issue is the deployment of energy storage systems [132]. Among all feasible types of energy storage technologies, a battery based energy storage system can be considered as widely used and fairly developed. Batteries in the form of stationary energy storage systems and mobile energy storage systems in electric vehicles (EVs) are being actively researched in the field of distributed generation [133], [134], [135], [136]. The application of battery storage system for voltage regulation and peak load shaving is investigated in previous works [137], [138]. It is shown in [128] how the BESS could help devices such as on-load tap changer and step voltage regulator to mitigate the overvoltage through reducing or eliminating the burden from these devices. The optimized size and best location of BESS has not been investigated in these researches. To expand the application of BESS in distribution systems, research on BESS size optimization and placement is important and beneficial for cost justification of their commercial applications in distribution systems.

Different algorithms have been proposed to minimize the size of battery storage system in [131], [139], [140], [141], [142]. While many of them focus on reducing cost or increasing revenue of bulk energy arbitrage [139], [140], some aim to compensate for intermittent nature and power fluctuation of renewable energy such as solar and wind [141], [142]. However, these studies have not concentrated on battery storage system capability to improve the voltage regulation in the distribution system and reduced workload on tap changer and voltage regulator. In addition, the optimal placement of battery storage system in distribution systems to affect the maximum number of node-voltages is yet a research topic to be addressed.

In this chapter, a new technique is presented to solve the overvoltage and under voltage issues in a distribution system with solar energy penetration. Based on the location of solar energy and amount of penetration, the size and place of battery storage system are obtained such that a BESS with minimum size is able to improve the voltage profile at maximum number of nodes in an optimal way. This approach benefits from active and reactive power control for voltage regulation, and based on the topology of distribution system the optimum ratio of exchanging active and reactive power by BESS and grid-tie inverter is calculated. In this method first the power system is presented in terms of impedance matrix which is a fast and powerful tool for power system analysis. Then, the minimum BESS active and reactive power is formulated as a function of solar power penetration, location of solar PV and battery, and the compensated node to regulate the voltage. For this purpose, new techniques are introduced to model the slack and PV buses in impedance matrix analysis to increase the accuracy of the proposed approach. In contrast to the approach in [131]- [143], in the proposed approach, instead of using load flow analysis which is a recursive algorithm, the modified impedance matrix analysis is employed which leads to an analytical solution. In this approach, the size and place of BESS is directly obtained and optimized

using the developed analytical functions, rather than using the time consuming scanning approaches.

The rest of the chapter is organized as follows. In Section 8.2, the principles of the proposed algorithm are described. Simulation results obtained from applying the proposed algorithm on IEEE 14-bus systems are presented in Section 8.3. Finally, concluding remarks are in Section 8.4.

8.2 Methodology

Grid integration of BESS through grid-tie inverter helps to improve the voltage profile at the point of connection as well as other buses in the network depending on the topology of the system. When a solar energy source injects power into the system, voltages in the network change depending on the location of the solar sources and impedances of the system. The problem arises when the voltage of one or several buses exceed the standard limit at high PV penetration level, or drop under standard limit at high load level. The focus of this chapter is to find the minimum size and best place for BESS to improve the voltage profile at the maximum possible number of nodes. This will allow benefiting from the maximum capacity of solar while reducing the overvoltage effect at high penetration levels.

Although reactive power control is assumed to be the most common method for voltage improvement, the *R/X* ratio of the distribution feeder limits its effectiveness. That means, the reactive compensation alone is not sufficient to achieve the desired voltage profile. As a result, there should be an optimum way to combine active and reactive power based on *R/X* of the network to achieve the desired voltage regulation for each node. This chapter is aiming to find that optimum point based on the developed analytical functions.

Developing the impedance matrix of the system (Z matrix) makes it easy to calculate the voltage change caused by PV and BESS penetration at each bus [144]. However, the impedance matrix of the system does not reflect the effect of slack bus which has always constant voltage, and PV buses with constant voltage amplitude and active power. This document utilizes a method to add the impact of the slack and PV buses on other buses in the impedance matrix. Note that, the advantages of this approach over power flow analysis are: first, the impedance matrix analysis calculates the voltage changes in each node avoiding any recursive algorithm so it is faster. Second, it allows developing the voltage changes of each bus as a function of penetrated current at other buses. Therefore, it makes it easier to analytically find the relationship between location of BESS and solar, and amount of exchanging power with specific node to regulate node-voltages. Finding this mathematical relationship helps with solving the sizing and placement optimization problem.

8.2.1 Problem Description

Suppose that $V_{k,S,B}$ represents the measured voltage at bus k affected by solar and BESS penetration where B is defined as $B = (j_{bess}, P_{bess}, Q_{bess})$ including the bus number, active and reactive power of BESS, respectively, and S is defined as $S = (i_{pv}, P_{pv})$ containing the bus number to which the solar is integrated (i_{pv}), and amount of injected active power to the grid (P_{pv}), respectively. Here, it is assumed that the solar grid-tie inverter is controlled such that the solar always inject active power under unity power factor to take the maximum benefit from the capacity of solar energy and GTI. Define $\Theta_{i_{pv}} = \{V_{k,S,B} \big| 1 \leq k, i_{pv}, j_{bess} \leq n, 0 \leq P_{pv} \leq P_{max}, P_{bess}\ and\ Q_{bess} \in \Re\}$ as a set of all possible $V_{k,S,B}$ for specific i_{pv}, where n is the total number of network busses. In addition, define $\Phi_{j_{bess}} \subseteq \Theta_{i_{pv}}$, where its members satisfy $V_{min} \leq$

$V_{k,S,B} \leq V_{max}$ with the minimum pair of (P_{bess}, Q_{bess}) for integrated BESS at node j_{bess} . $\Phi_{j_{bess}}$ is a subset of $\Theta_{i_{pv}}$ that can uniquely identify minimum (P_{bess}, Q_{bess}) that regulate the voltage of node *k* in the network when BESS is at node j_{bess} . Having $\Phi_{j_{bess}}$, the target is first to find the minimum unique (P_{bess}, Q_{bess}) that can regulate the voltage for maximum number of nodes in the network when BESS is in node j_{bess} (optimal solution for BESS at j_{bess}) and second, to find the best location (j_{bess}) for BESS to provide voltage regulation for the maximum number of nodes with minimum (P_{bess}, Q_{bess}).

8.2.2 Slack, PV, and PQ bus effects

The bus impedance matrix provides important information regarding the power system network, which can be used to facilitate network analysis [144]. Using the impedance matrix, the bus voltages corresponding to the initial values of bus currents I^0can be obtained from $V^0 = Z_{bus}I^0$. When the bus currents are changed from the initial values to new value $I^0 + \Delta I$, the new bus voltages can be obtain from the superposition equation:

$$V = Z_{bus}(I^0 + \Delta I\ ) = Z_{bus}I^0 + Z_{bus}\Delta I = V^0 + \Delta V \quad (38)$$

where ΔV expresses the bus voltage changes from their original values. Therefore, by having the initial voltages of the network V^0 at steady state from power flow, the voltage changes caused by adding renewable energy sources can be easily calculated from impedance matrix equation (38). However, the challenge is that in the real power system the voltage and angle of the slack bus are always constant which are not considered in this analysis. As a result the obtained results from this approach are not quite accurate. In order to overcome this challenge and model the effect of slack bus in impedance matrix analysis the new concept of "mirror current" is defined here. Suppose

that current I_i models the impact of a new added renewable source at bus i, then the network voltage changes (ΔV) can be calculated as:

$$\begin{bmatrix} \Delta V_1 \\ \vdots \\ \Delta V_i \\ \vdots \\ \Delta V_n \end{bmatrix} = \begin{bmatrix} Z_{11} & \dots & Z_{1i} & \dots & Z_{1n} \\ \vdots & \ddots & \vdots & \ddots & \vdots \\ Z_{i1} & \dots & Z_{ii} & \dots & Z_{in} \\ \vdots & \ddots & \vdots & \ddots & \vdots \\ Z_{n1} & \dots & Z_{ni} & \dots & Z_{nn} \end{bmatrix} \times \begin{bmatrix} 0 \\ \vdots \\ I_i \\ \vdots \\ 0 \end{bmatrix} \tag{39}$$

where $\{Z_{11}, \dots, Z_{nn}\}$ are the elements of impedance matrix and *n* is the number of buses. Equation (39) depicts that the voltage change of slack bus, normally the first bus is considered as slack bus (ΔV_1), is governed by $\Delta V_1 = Z_{1i} I_i$ while this voltage should not change. Therefore, the "mirror current" $I_1 = -(Z_{1i}/Z_{11}) I_i$ is added to compensate the effect of I_i and keep the V_1 constant. That is, for each new current source integrated to the network during the analysis, the "mirror current" term should be added to the first current element (I_1) to cancel out its impact on the slack bus voltage.

The same challenge exists for PV buses. In PV buses the active power and voltage amplitude are not changing. Therefore, adding a new source shouldn't affect the former parameters. However, modeling the PV buses in impedance matrix makes the analysis complicated. Here the proposed approach is applying current sources at those nodes such that the total resultant of existing current sources in the network changes neither voltage amplitude nor voltage angle. Then the active power can be modeled as constant impedance since by having constant voltage, the active power remains constant. Although this method ignores the voltage angle variation and consequently reactive power changing at PV buses, provides a reasonable accuracy through a simple approach. The third category of buses is PQ buses. The PQ buses which normally represent the load buses in the system can be modeled as constant impedances during the development of impedance matrix. Although

PQ buses are known as constant active (P) and reactive (Q) loads, since in this application the target is regulating the voltage, the constant impedance load (Z) can perfectly model this type of buses.

8.2.3 Current source modeling of solar source

In impedance matrix analysis in order to evaluate the voltage changes due to any modification of the network, those modifications should be reflected either in the impedance matrix or in the current vector. For example in case of adding/ removing loads or lines the impedance matrix is affected. However, when a new source is added to the system, the impact of this source should be modeled as a current source in current vector. In case of solar energy source, the grid-tie inverter is normally controlled to deliver maximum power under unity power factor [145]. Therefore, a solar energy source can be expressed as amount of active power generation. However, the proposed approach is looking for the current corresponding to the active power. Having constant active power the amount of solar current depends on the voltage of solar connected node while this voltage is a function of injected current. Suppose that the first node of the network is slack bus and there are *m* PV buses in the network. Therefore, referring to Section *8.2.2* description, adding the solar current at bus *i* leads to compensation currents for PV buses (bus 2 to bus *m*) and their mirror currents for slack bus.

$$\begin{bmatrix}\Delta V_1\\ \Delta V_2\\ \vdots\\ \Delta V_m\\ \vdots\\ \Delta V_i\\ \vdots\\ \Delta V_n\end{bmatrix}=\begin{bmatrix}Z_{11} & Z_{12} & \dots & Z_{1m} & \dots & Z_{1i} & \dots & Z_{1n}\\ Z_{21} & Z_{22} & \dots & Z_{2m} & \dots & Z_{2i} & \dots & Z_{2n}\\ \vdots & \vdots & \ddots & \vdots & \ddots & \vdots & \ddots & \vdots\\ Z_{m1} & Z_{m2} & \dots & Z_{mm} & \dots & Z_{mi} & \dots & Z_{mn}\\ \vdots & \vdots & \ddots & \vdots & \ddots & \vdots & \ddots & \vdots\\ Z_{i1} & Z_{i2} & \dots & Z_{im} & \dots & Z_{ii} & \dots & Z_{in}\\ \vdots & \vdots & \ddots & \vdots & \ddots & \vdots & \ddots & \vdots\\ Z_{n1} & Z_{n2} & \dots & Z_{nm} & \dots & Z_{ni} & \dots & Z_{nn}\end{bmatrix}$$

$$\times\begin{bmatrix}-\frac{Z_{1i}}{Z_{11}}I_i-\frac{Z_{12}}{Z_{11}}I_2-\dots-\frac{Z_{1m}}{Z_{11}}I_m\\ I_2\\ \vdots\\ I_m\\ \vdots\\ I_i\\ \vdots\\ 0\end{bmatrix} \tag{40}$$

Therefore, the solar voltage at bus *i* can be obtain as:

$$V_i=V_i^0+\left(Z_{i2}-Z_{i1}\frac{Z_{12}}{Z_{11}}\right)I_2+\dots+\left(Z_{im}-Z_{i1}\frac{Z_{1m}}{Z_{11}}\right)I_m+\left(Z_{ii}-Z_{i1}\frac{Z_{1i}}{Z_{11}}\right)I_i \tag{41}$$

where V_i^0 is initial voltage of node *i* before adding solar panel which is known.

Referring to the description in Section *8.2.2*, currents $I_2,\dots,I_m$ are calculated as a function of I_i such that voltages of buses 2 to *m* remain unchanged. That is, by making $\Delta V_j=0$ in (40) for $2\le j\le m$, $I_2,\dots,I_m$ can be written as a function of I_i as shown in (42).

$$\begin{bmatrix} \left(Z_{21}\frac{Z_{1i}}{Z_{11}} - Z_{2i}\right) I_i \\ \left(Z_{31}\frac{Z_{1i}}{Z_{11}} - Z_{3i}\right) I_i \\ \vdots \\ \left(Z_{m1}\frac{Z_{1i}}{Z_{11}} - Z_{mi}\right) I_i \end{bmatrix}$$

$$= \begin{bmatrix} \left(Z_{22} - Z_{21}\frac{Z_{12}}{Z_{11}}\right) & \left(Z_{23} - Z_{21}\frac{Z_{13}}{Z_{11}}\right) & \dots & \left(Z_{2m} - Z_{21}\frac{Z_{1m}}{Z_{11}}\right) \\ \left(Z_{32} - Z_{31}\frac{Z_{12}}{Z_{11}}\right) & \left(Z_{33} - Z_{31}\frac{Z_{13}}{Z_{11}}\right) & \dots & \left(Z_{3m} - Z_{31}\frac{Z_{1m}}{Z_{11}}\right) \\ \vdots & \vdots & \ddots & \vdots \\ \left(Z_{m2} - Z_{m1}\frac{Z_{12}}{Z_{11}}\right) & \left(Z_{m3} - Z_{m1}\frac{Z_{13}}{Z_{11}}\right) & \dots & \left(Z_{mm} - Z_{m1}\frac{Z_{1m}}{Z_{11}}\right) \end{bmatrix} \times \begin{bmatrix} I_2 \\ I_3 \\ \vdots \\ I_m \end{bmatrix} \quad (42)$$

Finding $I_2, \dots, I_m$ from (42) and substitute in (41) all elements on the right side of (41) are in terms of I_i. For operation under unity power factor:

$$I_i = S^*/V_i^* = P_{pv}/V_i^* \quad (43)$$

where S^* represents apparent power conjugate and V_i^* is conjugate of the solar node voltage. By replacing (43) in (41) and solving the equation (41) for V_i, the I_i corresponding to the desired solar P_{pv} can be obtained.

8.2.4 Optimal battery sizing

After modifying the impedance matrix to model the effects of slack, PV, and PQ buses and integrating the solar energy as a current source based on its injected active power, the voltage changes of each node can be obtained easily as a linear function of solar current through $\Delta V_{ki} = Z_{eq_{ki}} I_i$ where the coefficient $Z_{eq_{ki}}$ is an appropriate combination of impedance matrix elements. The same function can be developed for the BESS grid-tie inverter current connected at

node j_{bess} ($\Delta V_{kj} = Z_{eq_{kj}} I_j$). Therefore, the voltage of each node affected by both solar and battery storage system can be calculated as:

$$V_k = V_k^0 + Z_{eq_{ki}} I_i + Z_{eq_{kj}} I_j \tag{44}$$

Assume that the maximum and minimum allowable voltage are V_{max} and V_{min}, respectively. Then the optimum direction for bringing back the voltage from overvoltage and undervoltage zones to the acceptable range is aligned with the voltage vector $V_k^0 + Z_{eq_{ki}} I_i$ as it satisfies the minimum distance. As a result, the minimum required current injected by battery storage at node *j* to compensate overvoltage and undervoltage is calculated in (45) and (46), respectively.

$$(I_j)_{min}^k = -\frac{(\left|V_k^0 + Z_{eq_{ki}} I_i\right| - V_{max})}{Z_{eq_{kj}}} \times \frac{(V_k^0 + Z_{eq_{ki}} I_i)}{\left|V_k^0 + Z_{eq_{ki}} I_i\right|} \tag{45}$$

$$(I_j)_{min}^k = -\frac{(\left|V_k^0 + Z_{eq_{ki}} I_i\right| - V_{min})}{Z_{eq_{kj}}} \times \frac{(V_k^0 + Z_{eq_{ki}} I_i)}{\left|V_k^0 + Z_{eq_{ki}} I_i\right|} \tag{46}$$

Developing the minimum BESS current as a function of solar current provides a useful tool to control the BESS based on solar current feedback to improve voltage profile by minimum effort.

8.2.5 Best Placement

In Section *8.2.4* the minimum BESS current for improving the voltage of each node is calculated. Therefore, the proposed algorithm ends up with *n* (number of buses) minimum currents. Each current has both imaginary and real element. Therefore, the minimum resultant current $(I_j)_{min}$ that can satisfy the voltage regulation for all nodes is composed of maximum real part and maximum imaginary part among all currents $(I_j)_{min}^k$

$$(I_j)_{min} = \max\left\{real\ \left((I_j)_{min}^{k}\right) \middle| 0 \le k \le n\right\} + j.max\left\{image\ \left((I_j)_{min}^{k}\right) \middle| 0 \le k \le n\right\} \quad (47)$$

$(I_j)_{min}$ is the minimum current that contains all *n* current $\left(I_j\right)_{min}^{k}$ components required for each node voltage regulation. It should be noted that a BESS is able to improve either undervoltage or overvoltage issue at each time because the direction of required current for each task is different. Therefore, based on the number of nodes which are either in undervoltage zone or overvoltage zone, the function of BESS can be determined. In addition, there is a possibility that the BESS cannot regulate the voltage of all nodes, in such a case the nodes have less priority are eliminated from procedure of finding the minimum resultant current $(I_j)_{min}$.

Finally, the algorithm shown in Figure 54, finds the best BESS location to regulate the voltage of maximum number of nodes with the minimum battery capacity based on the obtained result from (47) for placement of BESS at each node. This algorithm checks the number of nodes that integrated BESS at node *j* can improve voltage profile. Then by changing the location of BESS, among all locations which lead to maximum regulated nodes, finds the one which requires the minimum current.

8.3 Simulation Results

The IEEE 14-bus benchmarks [146] are considered for the case studies as shown in Figure 55.

The proposed algorithm is applied to find the minimum BESS size and its best place to regulate node-voltages. The obtained results from proposed algorithm are compared with the results obtained from load flow analysis to validate the accuracy of the proposed methodology.

In the first scenario, without loss of generality the solar source is placed at node 5 in IEEE 14-bus while its power varies from 0 to 1pu with resolution of 0.1pu. The BESS is designed to regulate the node voltages for whole range of solar power variation. In addition, referring to ANSI C84.1 the acceptable voltage tolerance range is considered as ±5%. The results are shown in Table 7. As illustrated in Table 7, the best location for BESS is bus number 9 while 0.1196pu multiple by the desired time of voltage regulation at maximum solar penetration (1pu) defines the size of BESS. In addition, overrated inverters (0.3849pu) compared with BESS (0.1196pu) is proposed as the minimum size of inverter to regulate all node-voltages in the network. The extra capacity of inverter is due to the additional capacity for reactive power control. At each instant of time the BESS and GTI active and reactive power can be calculated from (45) as a function of solar penetration.

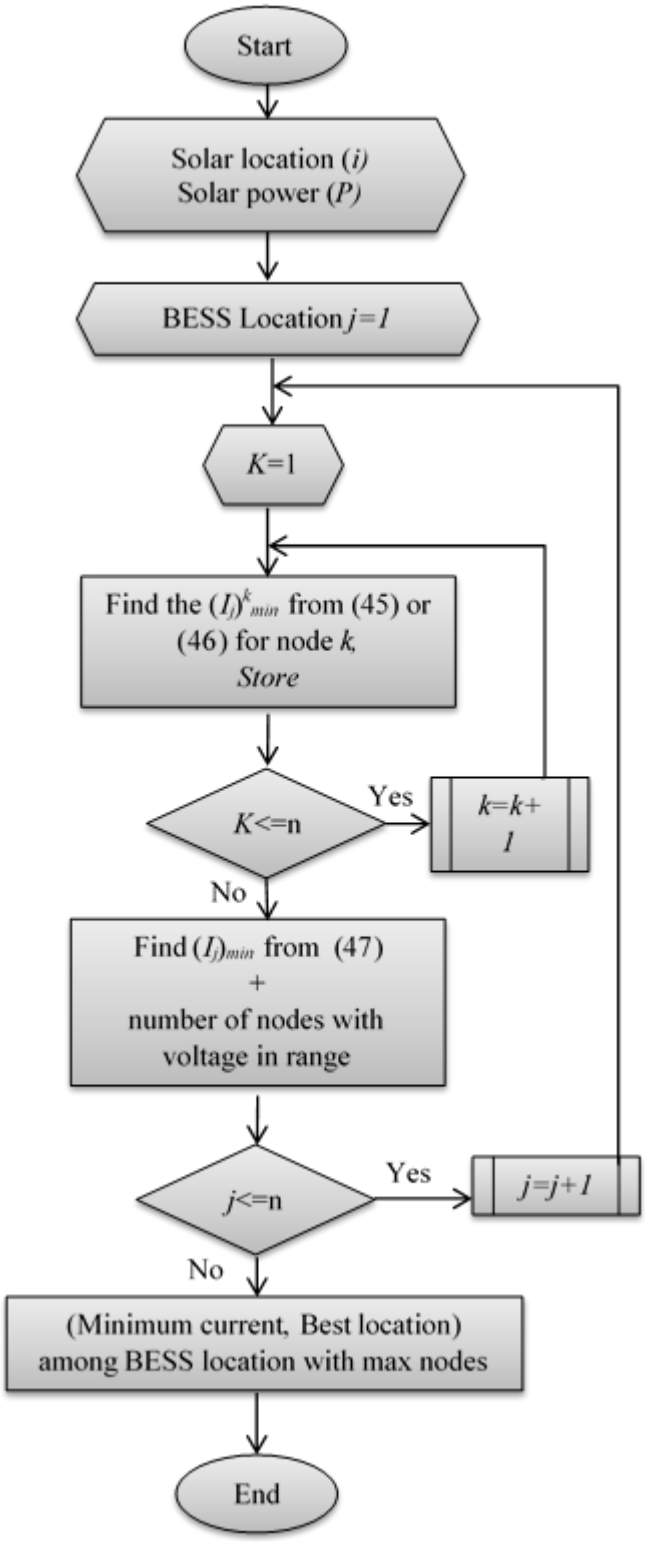

Figure 54 Algorithm of finding the best BESS placement

The voltage profile shown in Table 7, with 0.2pu P_{pv} resolution, validates the regulated voltage in range of 1±0.05pu. Note that the voltage of bus 1 and 2 (slack and PV bus) are always constant.

In the second scenario, 1pu solar is applied to the system but this time the total 1pu power is distributed between nodes 5 to 14. Since the nodes geographically are close to each other, it is assumed that all of them receive the same radiation and they have the identical capacity (0.1pu). The other conditions are as same as the first scenario. This scenario can represent integration of solar to a neighborhood's homes. Results are shown in Table 8. In this scenario the algorithm proposes bus 7 as the best location for BESS while less active power (0.0845pu) and more reactive power (0.4338pu) is required for voltage regulation.

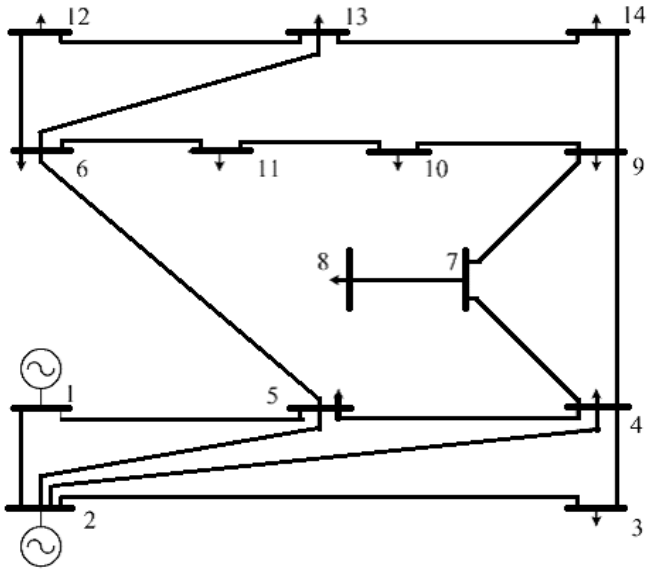

Figure 55 14 buses IEEE benchmark [146]

Table 7 Results after BESS integration with one unit solar source

Best Location for BESS				Bus number 9		
Minimum Active power (BESS)				0.1196 pu		
Minimum Reactive Power (GTI)				0.3566 pu		
Bus #	**Voltage profile**					
	P=0pu	***P=0.2pu***	***P=0.4pu***	***P=0.6pu***	***P=0.8pu***	***P=1p.u***
1	1.0600	1.0600	1.0600	1.0600	1.0600	1.0600
2	1.0450	1.0450	1.0450	1.0450	1.0450	1.0450
3	0.9978	0.9989	0.9998	1.0007	1.0014	1.0017
4	0.9982	1.0003	1.0023	1.0041	1.0057	1.0065
5	1.0032	1.0065	1.0096	1.0127	1.0154	1.0173
6	1.0362	1.0380	1.0396	1.0413	1.0424	1.0420
7	1.0157	1.0158	1.0159	1.0160	1.0156	1.0134
8	1.0450	1.0452	1.0453	1.0454	1.0449	1.0428
9	0.9964	0.9955	0.9946	0.9937	0.9922	0.9884
10	0.9955	0.9950	0.9946	0.9941	0.9930	0.9898
11	1.0118	1.0124	1.0130	1.0135	1.0135	1.0117
12	1.0202	1.0218	1.0233	1.0248	1.0258	1.0252
13	1.0143	1.0157	1.0170	1.0183	1.0190	1.0181
14	0.9879	0.9880	0.9880	0.9881	0.9875	0.9849

Table 8 Results after BESS integration with scattered solar source

Best Location for BESS	Bus number 7
Minimum Active power (BESS)	0.0845 pu

8.4 Conclusion

In this chapter, a new method for designing a BESS in distribution systems is developed. This method allows calculating the optimal size and place of BESS based on the size of integrated solar with the goal of voltage regulation in distributed system. The optimal BESS current is formulated as a function of solar current by employing modified impedance matrix analysis. Then, the required power from BESS to improve voltage profile is evaluated for all possible BESS locations. The proposed approach by utilizing the active power control along with the reactive power control improves the capability of voltage regulation in distribution system. The future work would be considering the effect of load variation and also the fact that the topology and parameter of distribution circuit might be unknown.

9 Model-Free Voltage Regulation

This chapter proposes and implements a model-free optimal methodology to regulate the voltage in distribution systems by controlling the power flow of battery energy storage systems. Reactive power control is not always an optimum solution to regulate the voltage especially at distribution systems where the ratio of *R/X* is considerable. This approach, with the aim of improving voltage regulation in distribution systems, optimally control active and reactive power exchanged by battery energy storage and grid-tie inverter in the grid. In this chapter an alternative method for voltage regulation is presented that does not require phase measurement, communication, and a system model which are barriers in behind-the-meter applications of BESSs. The proposed method formulates the problem of voltage regulation in form equilibrium map with optimum, without any restriction on system configuration, amount of reverse power flow and/or losses. Without an explicit model of distribution circuit this method coordinates the ratio of active and reactive power in real time, and adaptively controls the amount of exchanged power, using the extremum seeking control technique. Simulation results for a typical distribution circuit verify the effectiveness of the proposed approach to improve the voltage regulation. The experimental results also show a 20 percent reduction in use of BESS capacity for offering the desired voltage regulation performance.

9.1 Introduction

The proliferation of Distributed Energy Resources (DERs) and their integration to distribution systems can adversely impact on feeders' voltage profile at low/medium voltage networks, due to the reverse power flow [147], [148]. In addition the intermittent nature of renewable energy

resources such as solar and wind, and uncertain behavior of high demand loads such as EVs [149], [150]can cause voltage variation in distribution systems [151], [152].

The common practice to regulate the voltage within the normal range in distribution networks is employing equipment such as On-Load Tap Changer (OLTC) transformer, Step Voltage Regulator (SVR), and switch capacitor banks. However, these equipment might be less effective in the presence of power fluctuation of intermittent renewable resources, reverse power flow of DERs, and stochastic and concentrated power profile of dynamic loads [153]. The excessive work stress and frequent operation of conventional voltage control devices, accelerate the aging process of these devices and increase maintenance requirements, while their slow response, ranging from minutes to hours, prevents them to follow the high dynamics of renewables and loads variation. Therefore, they might eventually fail to provide the desired voltage regulation in distribution networks composed of DERs and high demand dynamic loads [154].

Although in many cases the system operators still manage the feeder voltage profile by curtailing the renewables generation or limiting the installed capacity of these resources, different methods are proposed to improve the voltage regulation in distribution systems under penetration of DERs [155], [156], [157], [158]. Some examples include 1) Controlling the reactive power of DG systems [155] or curtailing their generation during light load [156], 2) shifting and curtailing the energy consumption (load control) [157], 3) Controlling VAR compensators' reactive power [158].

The control structure to manage DGs, loads, or VAR compensators can be centralized, decentralized or distributed control scheme. Regarding the centralized control, in [159] voltage/VAR control scheme is formulated as a constrained optimization problem with an objective function minimizing the combined reactive power injection by DGs. The authors in [160] design a

generalized optimization problem to define the optimal reactive power references for each DG connected to distributed networks. In [161] the voltage control devices including OLTC transformer, SVR, shunt capacitor and reactor, and static VAR compensator are controlled in a coordinated manner to regulate the voltage in the distribution system. However, the centralized control scheme requires a communication channels and a significant investment in data sensing and collection infrastructure such as sensors and communication links.

The authors in [162] propose a multi-agent-based scheme to dispatch DGs' reactive power for voltage regulation application which uses quite modest communication compared with the centralized methods.

Although, in the literature a large number of approaches like the ones mentioned above focus on Volt/VAR control only, in distribution system unlike the transmission systems, reactive power compensation is less effective due to relatively high ratio of the R/X [163]. That is, the decoupling of voltage and frequency regulation through reactive and active power control, does not hold in distribution systems and active power control also plays an important role in voltage regulation. Therefore, the optimal coordination of active and reactive power to improve the voltage regulation would be an authentic subject to be pursued. BESS integrated to the distribution circuit through GTI is an asset which can effectively control both active and reactive power in the grid. The application of BESS for voltage regulation is investigated in previous works [163], [164], [165]. In [163] the optimal sizing and placement of BESS for voltage regulation in distribution system with solar energy penetration is investigated. Authors in [164] proposed a sparse optimization technique to develop a voltage regulation framework and control multiple dispersed BESSs in distribution systems. In [165] distributed BESS is proposed for voltage regulation and peak load shaving, and a sizing strategy under high PV penetration level is presented. However, these studies assume that

the perfect knowledge and model of the system including grid parameters, topology of the grid, and load and generation profiles are available, while in reality this information might not be accessible.

This chapter proposes a model-free optimal methodology to control active and reactive power of BESSs for voltage regulation in distribution system. The propose approach does not rely on the model of the system, communication, and sharing the information with control center. This method is a plug and play approach for the real-time control of BESSs with only measurement at the point of connection. In this context, a model free control methodology known as Extremum Seeking (ES) is employed. ES is an online optimization method and model-free based gradient search technique which dynamically seeks the extremum of a cost function. Providing the first rigorous stability analysis by Krstic and Wang [166] for a class of ES problems, ES method gains significant attention in control community. The recent applications of ES control are in fluid flow [167], robotics [168], combustion in thermal power plant [169], wind and solar energy conversion [170], [171], and biochemical [172].

To improve voltage regulation performance, the proposed approach, without the need of distribution system model, finds the optimum power factor for operation of GTI by using ES control technique. It also adaptively tune the PI controller to track the voltage reference by adjusting the magnitude of GTI current. The ES controllers apply the sinusoidal perturbation method to carry out real time optimization where its bounded convergence is guaranteed.

The contribution of this chapter can be summarized as follows. First, the voltage regulation problem in distribution systems is derived in form of equilibrium map with optimum, without any limits on the system configuration (e.g. radial vs. ring, balance vs. unbalance), the amount of reverse power flow and losses. Second, a new methodology is proposed that distributed BESSs can be controlled in a plug and play manner by only measuring the RMS voltage at the point of connection,

without any explicit information of the feeders, and any communication requirements. In fact, the active and reactive power of each BESS unit is independently controlled in an optimal manner such that the minimum capacity of battery energy storage and inverter is utilized.

The viewpoint assumed by the authors is that battery energy storage systems is considered by utilities primarily for functions such as diurnal load leveling rather than voltage regulation. However, the value stream of BESS can be extended to perform voltage regulation as an additional function. This function in distribution system also facilitates the accommodation of high DERs penetration.

The rest of the chapter is organized as follows: in Section 9.2, the background and the problem statement are presented. In Section 9.3, the principles of the proposed algorithm are described. Then, simulation and experimental results obtained from applying the proposed algorithm on a battery energy storage system are presented in Section 9.4. Finally, concluding remarks are given in Section 9.5.

9.2 Background

9.2.1 The Thevenin Impedance Model of the Grid

Assuming a power system network including k buses with the initial bus voltages, V_i^0 , $i = 1, \dots, k$. The voltages V_i^0 are the effective open-circuit voltages which are measured with respect to the network reference node. Figure 56 shows a schematic form of large-scale power system with k representative buses extracted along with the system reference node. If the current I_k is injected into the system from a current source connected between reference node and bus k, the voltage of each bus in the network changes.

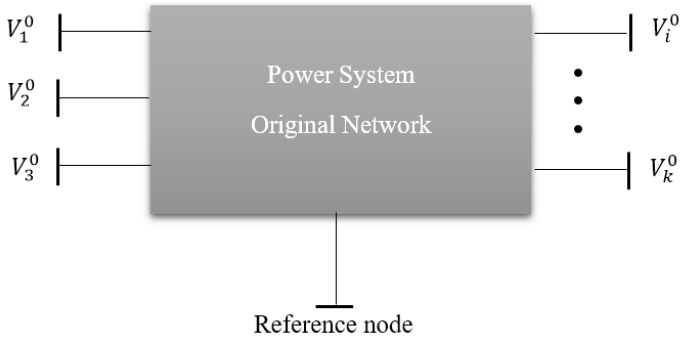

Figure 56 Schematic of a power system with *k* buses

The power system network can be represented by the Thevenin equivalent circuit at each bus. The Thevenin equivalent circuit corresponding to bus *k* and the injected current I_k is shown in Figure 57. The new voltage at bus *k* due to the injected current is calculated according to:

$$V_k = V_k^0 + Z_{th}I_k = V_k^0 + (R_{th}+jX_{th})I_k \tag{48}$$

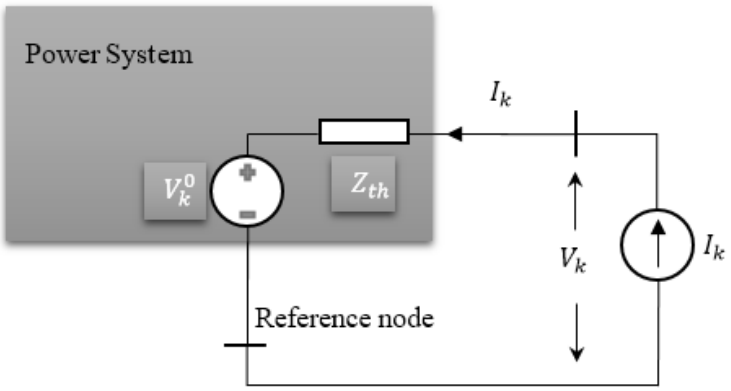

Figure 57 The Thevenin equivalent circuit corresponding to bus *k*

9.2.2 Phasor diagram of the voltage

The voltage at bus *k* can be expressed as phasors in form of $V_k = |V_k|\angle\varphi_k$, where $|V_k|$ is the magnitude of the phasor and φ_k is the angle of the phasor. Without loss of generality, the open circuit voltage at bus *k* (V_k^0) is considered as the reference phasor such that $V_k^0 = |V_k^0|\angle 0^\circ$. The

equivalent phasor of current source is defined $I_k = |I_k|\angle\theta_k$, where θ_k is the phase angle of lag of I_k measured with respect to open circuit voltage V_k^0. When the current I_k leads V_k^0 the angle θ_k is numerically negative; and when I_k lags V_k^0 the angle θ_k is numerically positive.

Phasor diagram of (48) is shown in Figure 58 for the case of lagging θ_k with respect to the open circuit voltage V_k^0 at bus *k*.

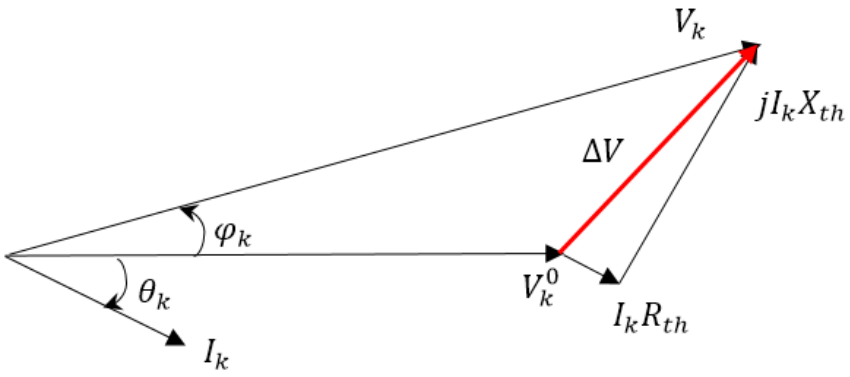

Figure 58 Phasor diagram of the terminal voltage at node *k*

9.2.3 Problem Statement

Suppose that BESS is connected to bus *k* in a distribution network through a grid-tie inverter, where phasor V_k^0 represents the measured voltage at bus *k* at no load, V_k is the measured terminal voltage, and set *B* is defined as $B = (|I_k|, \delta_k)$ including the current magnitude ($|I_k|$) exchanged by BESS at bus *k*, and the phase angle of the current with respect to the terminal voltage ($\delta_k = \theta_k + \varphi_k$). Define

$\Theta = \{V_k | \ 0 \le |I_k| \le I_{B_{max}} \ and \ \ 0 \le \delta_k \le 2\pi, \ \ |I_k| \in \Re\}$ as a set of all possible V_k for specific I_k, where $I_{B_{max}}$ is the maximum current capacity of integrated battery at point *k*. In addition, define $\Phi \subseteq \Theta$, where its members satisfy $V_{min} \le |V_k| \le V_{max}$, V_{min} and V_{max} are the minimum and

maximum allowable voltage magnitude in the network, respectively. The problem is to find the unique B_{opt} at each time with minimum $|I_k|$ and specific $0 \leq \delta_k \leq 2\pi$ that can regulate the voltage of node *k* such that $V_k \in \Phi$, while there is no information regarding the topology and parameters of the network except the RMS value of the terminal voltage $|V_k|$ at each time.

9.3 Methodology

In a power network, variations in load and generation impact on node voltages depending on the location and topology of the system. The problem arises when the voltage of one or several nodes exceeds the allowable range. A battery energy storage system integrated to the grid can improve the voltage profile of the connected node by a proper exchange of active and reactive power with the node through a grid-tie inverter. The inverter can be considered as a current source with controllable magnitude and angle.

According to (48) the magnitude of the terminal voltage due to injected current at node *k* can be calculated from:

$$|V_k|^2 = \left|V_k^0\right|^2 + |Z_{th}I_k|^2 + 2\left|V_k^0\right||Z_{th}I_k|\cos(\gamma_{th} + \theta_k) \tag{49}$$

where $|Z_{th}|\angle\gamma_{th}$ is the equivalent Thevenin impedance at node *k*. Equation (2) can be rewritten in form of (50) as below:

$$|V_k|^2 = \left(\left|V_k^0\right| + \left|Z_{thI_k}\right|\right)^2 + 2\left|V_k^0\right||Z_{th}I_k|[\cos(\gamma_{th} + \theta_k) - 1]$$

$$\Rightarrow |V_k|^2 = \left(\left|V_k^0\right| + \left|Z_{thI_k}\right|\right)^2 - 4\left|V_k^0\right|\left|Z_{thI_k}\right|\sin^2\left(\frac{\gamma_{th} + \theta_k}{2}\right) \tag{50}$$

In order to maximize the effect of injected current on the node voltage V_k, one can maximize the change in voltage magnitude by adjusting the angle of current source (θ_k) to be equal to $-\gamma_{th}$. When the voltage change vector (ΔV), in Figure 58, is aligned with the initial node voltage (V_k^0),

the maximum magnitude of terminal voltage for the given injected current is obtained. In this situation, the impact of injected current on the voltage would be maximized.

The magnitude of current source can be also controlled to adjust the voltage magnitude to the desired range. In this context, by controlling the magnitude and angle of inverter current the terminal voltage can be regulated with the minimum capacity of the battery, as a source of active power, and the minimum capacity of inverter, as a source of reactive power. Figure 59 shows how the terminal voltage can be pushed into the allowable range (region between parallel curve lines) at the time of voltage sag (solid lines) or overvoltage (dotted lines).

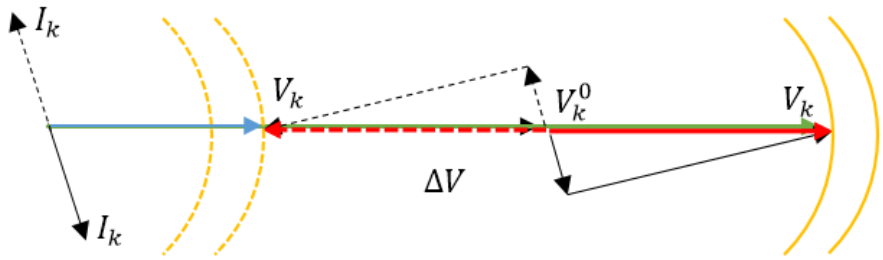

Figure 59 Voltage regulation with the minimum injected current

According to (49), in order to find the optimum inverter phase angle which maximizes the impact of exchanged current on the voltage, first the equivalent Thevenin impedance at the point of connection should be known. Second, the voltage phase angle at the node of connection should be measured. However, in practice the topology and parameters of the system are not necessarily known, specifically for behind the meter applications. In addition, measuring the phase of the voltage requires Phasor Measurement Units (PMUs) which might be costly or impractical to be installed at each node. In this context, the challenge is how to control the inverter effectively to minimize the size of storage and inverter for voltage regulation application, without having any

information about the distribution system parameters and network topology as well as the phase of the node voltages. The focus of this chapter is to perform voltage regulation with the minimum size of BESS and inverter by only measuring the RMS value of the voltage at the node of connection. To this end, this chapter proposes the extremum seeking-based approach for model-free control of inverter phase angle, and adaptive PI controller for model-free control of inverter current magnitude.

9.3.1 Extremum-Seeking Control

In the voltage regulation performed by energy storage systems, the current phase angle of inverter (θ_k) can be defined as the system control reference, and the change in terminal voltage magnitude as the output. In this system the reference-to-output map has a maximum such that:

$$\max_{\theta_k} |V_k|^2 = \left(\left|V_k^0\right| + |Z_{th} I_k|\right)^2 \tag{51}$$

The objective is to control the reference to keep the output at the maximum value. Since in (50), the equivalent Thevenin impedance ($Z_{th}\angle\gamma_{th}$) is unknown the reference-to-output map is uncertain. Addressing this problem, the extremum-seeking control (ESC) approach is a viable solution to find the optimum reference in such a system which maximizes the output.

In addition, in this application the extremum input (θ_k) and extremum output ($|V_k|^2$) are time-varying due to variation of open circuit voltage (V_k^0) over the time. The time variation of the open circuit voltage magnitude ($\left|V_k^0\right|$) changes the term $\left(\left|V_k^0\right| + |Z_{th} I_k|\right)^2$ which is the extremum output. Also variation in the phase of V_k^0 over the time changes the reference of phases and consequently the term θ_k which is the extremum input.

Therefore, the problem in this chapter is a time-varying extremum seeking control problem expressed as below.

Problem 1: By assuming a time-dependent plant with an output function $y = f\big(u(t), v(t)\big)$: $\mathbb{R} \times \mathbb{R} \to \mathbb{R}$: where $v(t)$ is time-varying and unknown vector, the time-varying extremum input $u^*(t)$ is defined such that:

$$f\big(u^*(t), v(t)\big) > f\big(u(t), v(t)\big), \qquad \forall\, u(t) \neq\ u^*(t) \tag{52}$$

Note that the functional description of the output function $f\big(u(t), v(t)\big)$ is unknown but measurable. The goal is to design a control method that the time-varying output function converges to the extremum value $f\big(u^*(t), v(t)\big)$ with the input variable at the extremum input $u^*(t)$.

Solution 1: The ESC shown in Figure 60 is a solution for Problem 1 [173]. In this solution, the output function is modulated and demodulated by using the sinusoidal perturbations in order to make the gradient of the output function extractable. The delay-based gradient estimation is employed to estimate the gradient. Due to time-varying nature of both extremum input and extremum value of the output function, the Robust Integral of the Sign of the Error (RISE) method is also utilized in the update law to estimate $\hat{u}(t)$.

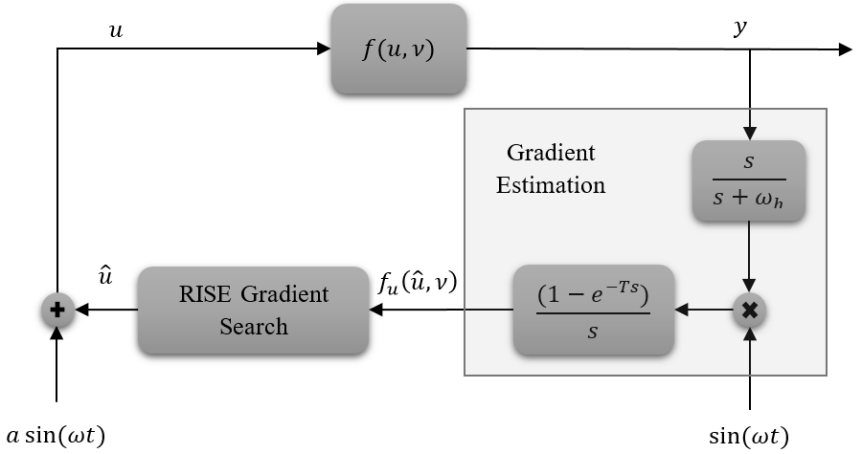

Figure 60 The ESC block diagram for phase control

In application of voltage regulation the plant $f = |V_k|^2$, the extremum input $u(t)=\theta_k$, and time-varying and unknown vector $v(t) = \left[\left(\left|V_k^0\right| + |Z_{th}I_k|\right)^2 \quad -4\left|V_k^0\right||Z_{th}I_k|\right]$.

Remark 1: In this application, the first partial derivative f_u exist and it is equal to zero at the extremum input $u^*(t)$. In addition, the second partial derivative f_{uu} exists at the extremum input $u^*(t)$ and is negative. Moreover,

$$f_u\left(u^* + \varepsilon, v(t)\right)\varepsilon < 0 \; for \; every \; \varepsilon \neq 0 \tag{53}$$

where $\varepsilon \in \mathbb{R}$ and is defined as $\varepsilon \triangleq \hat{u} - u^*$.

Remark 2: Here, the function $\gamma\left(\varepsilon, v(t)\right)$ defined as

$$\gamma\left(\varepsilon, v(t)\right) = \begin{cases} -\dfrac{f_u\left(u^* + \varepsilon, v(t)\right)}{\varepsilon}, & \varepsilon \neq 0 \\ -f_{uu}^*, & \varepsilon = 0 \end{cases} \tag{54}$$

is strictly greater than a positive value i.e., $\gamma > \gamma_0 > 0$, in a bounded interval containing origin. Moreover, the partial derivatives γ_ε, γ_v are bounded.

Remark 3: In the above application, the first three derivatives of $u^*(t)$ shown as $\dot{u}^*(t)$, $\ddot{u}^*(t)$, $\dddot{u}^*(t)$, and $\dot{v}(t)$ are bounded.

Theorem 1 [173]**:** Consider the plant $f\left(u(t), v(t)\right)$: $\mathbb{R} \times \mathbb{R} \rightarrow \mathbb{R}$ that satisfies Remarks 1-2. Suppose that u and v satisfy Remark 3. In the close loop system the update law is as follow

$$y = f(\hat{u} + a\sin(\omega t), v), \qquad y_h = \frac{s}{s + \omega_h} y \tag{55}$$

$$\mu = \frac{1}{2\pi}\frac{1 - e^{-Ts}}{s}[y_h \sin(\omega t)], \qquad e = 2\frac{\omega^2 + \omega_h^2}{a\omega}\mu \tag{56}$$

$$\dot{V} = c_1 k_1 e + k_2 sgn(e), \qquad \dot{\hat{u}} = k_1 e + V - c_2 \hat{u} \tag{57}$$

where $T = \frac{2\pi}{\omega}$, the signal $\hat{u}(t)$ reaches a small neighborhood of the optimal trajectory $u^*(t)$ provided that: the perturbation amplitude a is small, the perturbation frequency ω is high with respect to the variation of $v(t)$ and $\hat{u}(t)$, $k_1$is sufficiently large, and $c_1 > \frac{1}{2}$

Remark 4: The equilibrium map in (50) for $\theta_k \in [-\pi\ \pi]$ has a maximum at $\gamma_{th} + \theta_k = 0$, and a minimum at $\gamma_{th} + \theta_k = \pi$.

The ESC approach described in Theorem 1 seeks the maximum of the equilibrium map. In order to find the minimum, the negative of the estimated gradient (e) in (56) should be sent to the gradient search block. That is, when there is an under voltage problem in the system, it is required to find the current angle which optimally increase the voltage (maximizing). Therefore, the calculated gradient estimation is directly sent to the RISE gradient search block. However, at the time of overvoltage problem the negative of the estimated gradient is sent to the gradient search block to find the current angle which optimally decreases the voltage (minimizing). In this application, the sign of estimated gradient is automatically adjusted by comparing the network voltage and the voltage reference.

9.3.2 Extremum-Seeking based Auto-Tuning of PI Controller

In this Section an adaptive PI controller is proposed for model-free control of the inverter current magnitude. The control diagram of the PI feedback controller is shown in Figure 61. The RMS value of the terminal voltage is measured and compared to a voltage reference V_{ref}, which is the desirable and adjustable voltage. The error between the measured and reference voltage is fed back to adjust the reference of inverter current magnitude I_{ref}. The control law is indicated in (58)

$$I_{ref} = K_I \int_0^t [V_{ref} - V_{k,rms}]dt + K_P[V_{ref} - V_{k,rms}] \quad (58)$$

where K_I is the integral gain, and K_P is the proportional gain of the PI controller. The dynamics of the voltage regulation depend on the gains of PI controller. Therefore, in order to have an effective and efficient voltage regulation, it is imperative to optimize the performance of the PI controller by tuning the PI gains. However, since in this application the parameters of the system is unknown, this Chapter proposes the model-free ES algorithm to automatically tune the PI gains online.

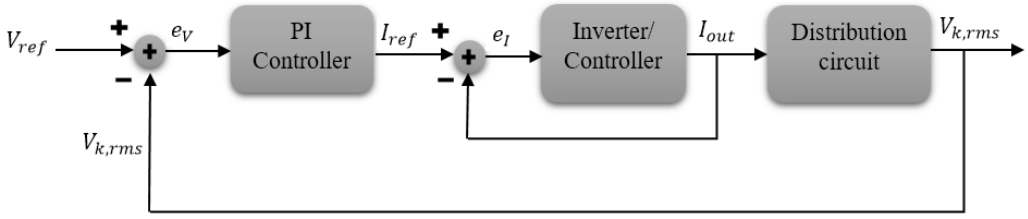

Figure 61 Control diagram of the PI feedback controller

In this Section, a scalar gradient-based ES control algorithm for the case of time-varying cost function is discussed [174]. The block diagram of the ES control algorithm is shown in Figure 62. In the proposed technique, unlike the basic ES control, there is no perturbation signal between the integral function and the cost function. The multi-parameter ES algorithm is presented in (59).

$$\dot{\hat{\theta}}_i = \alpha_i' \sqrt{\omega_i'} \cos(\omega_i' t) - k_i' \sqrt{\omega_i'} \sin(\omega_i' t)\, Q(\hat{\theta}, t) \quad (59)$$

where α_i' and k_i' are positive numbers, and $\omega_i' > \omega^*$, with ω^* large enough to ensure the convergence, while $\omega_i' \neq \omega_j' \; \forall \; i, j \; \in \{1,2, \dots, n\}$.

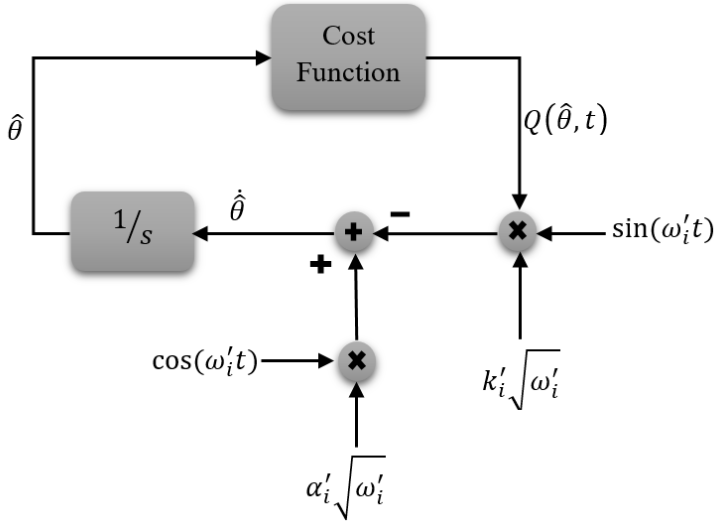

Figure 62 Block diagram of the ES for PI gains tuning

The cost function in this algorithm is given in (60).

$$Q(\theta,t) = \left[V_{ref}(t) - V_{k,rms}(t)\right]^2 \tag{60}$$

The ES algorithm uses the discrete value of the cost function generated at each sampling time in order to calculate the set of PI parameters for the next sampling time.

Figure 63 depicts the overall block diagram of ES-based PI controller scheme.

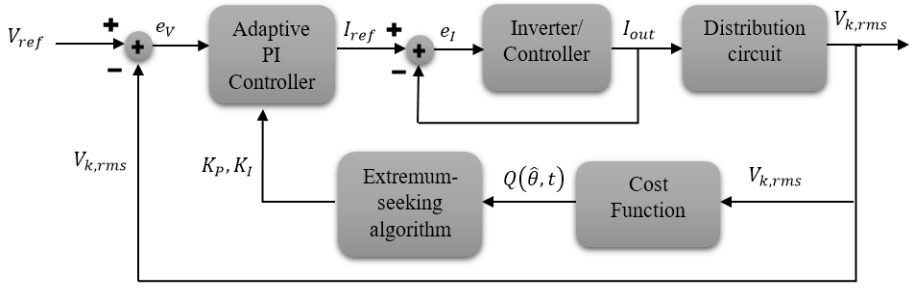

Figure 63 Block diagram of ES-based PI controller

Figure 64 demonstrates the entire system including battery energy storage, inverter, and controller.

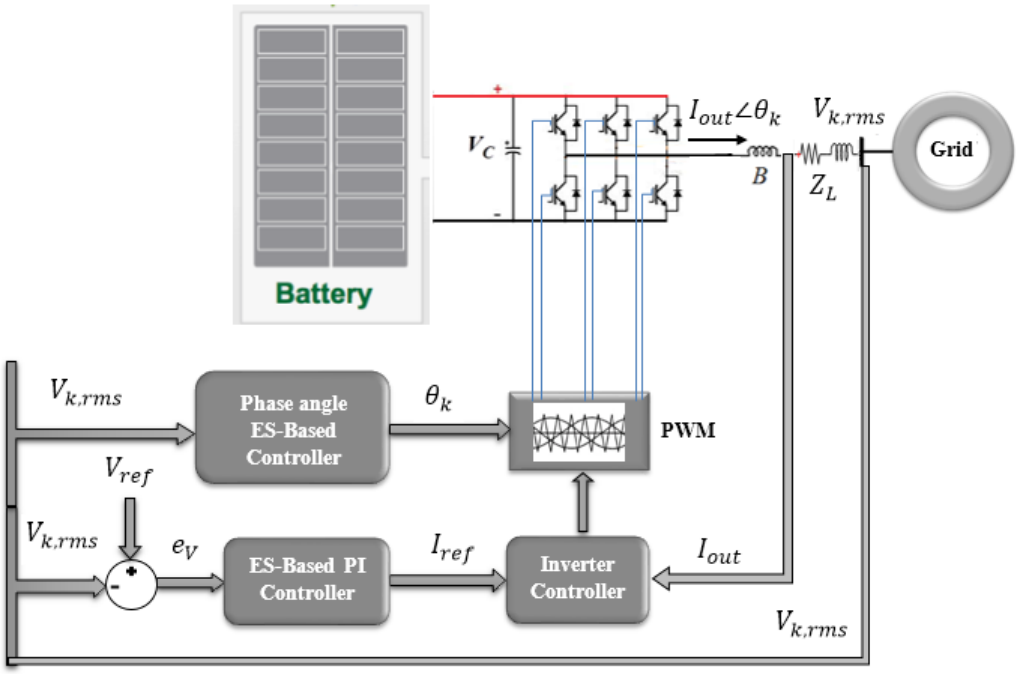

Figure 64 The entire unit including the equipment and controller

9.4 Case Studies

9.4.1 Simulation Results

In this Section the performance of the proposed control scheme managing a single unit BESS for voltage regulation is demonstrated. The simulation testbed, shown in Figure 65 is a typical single-phase three-wire distribution feeder in a residential area [175], [176]. The testbed includes three ordinary houses as the energy consumers, solar PV panels, and a battery energy storage system which all connected to the power network via a pole-mounted transformer. The pole-mounted distribution transformer rating is 6.6kV, 75kVA, and 60Hz on the primary side and 100V and 375A on the secondary side. The consumers' points of connection are linked together and to the distribution transformer through three low voltage wires with the length of 40m. Two consumers are equipped with solar panels and among them one with battery storage. The service-wires of

houses are 20m, 25m, and 30m. Table I shows the feeder model parameters. The load profile of consumers is driven based on demand data (kW) publicly available by Southern California Edison [177] while the filtered Gaussian noise added to the power demands. This data is interpolated for continuous simulation as shown in Figure 66. The solar power profile shown in Figure 67 is obtained from the UCLA Ackerman Union solar power measurement which is scaled for this case study.

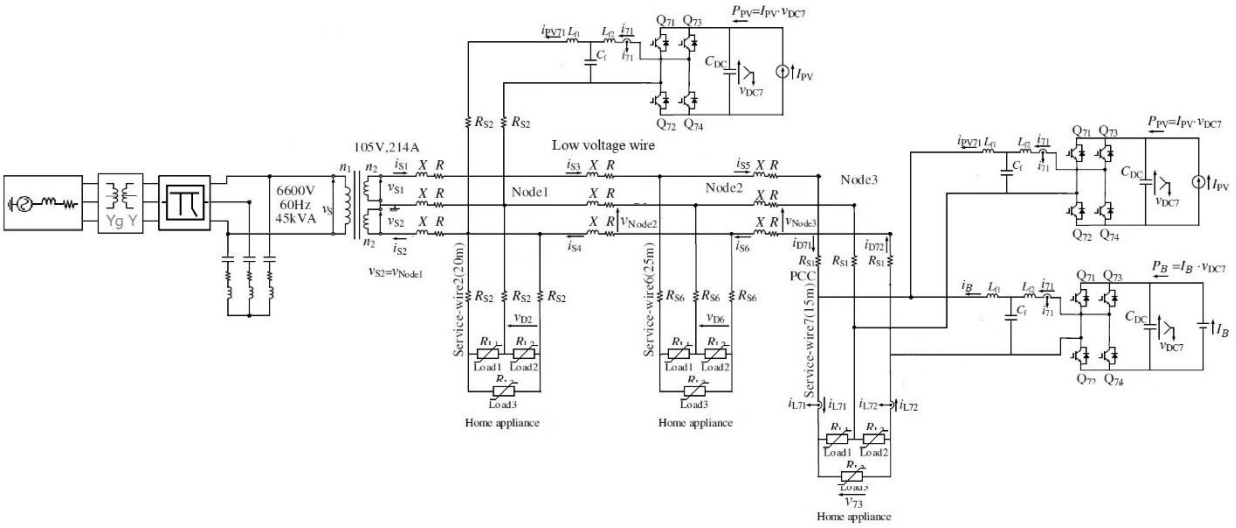

Figure 65 Typical single-phase three-wire distribution feeder in a residential area

Table 9 Testbed parameters

Item	Value
Low voltage wire resistance	0.484 Ω/km
Low voltage wire reactance	0.343 Ω/km
Service wire resistance	2.58 Ω/km
Maximum demand of consumer 1	2.5 kW
Maximum demand of consumer 2	2.5 kW
Maximum demand of consumer 3	2.5 kW
Capacity of solar panel 1	1kW
Capacity of solar panel 2	1kW

The proposed controller is designed and applied to the testbed for voltage regulation at the point of BESS connection. The controller parameters are given in Table 10. In this design, $\omega_i' \ll \omega$, to make sure that the dynamic of phase-control loop is faster than magnitude-control loop.

Table 10 Controller parameters

Parameter	Value	Parameter	Value
$\boldsymbol{\omega}\ (\boldsymbol{rad/s})$	10	$\boldsymbol{\omega_1'}\ (\boldsymbol{rad/s})$	1
$\boldsymbol{\omega_h}\ (\boldsymbol{rad/s})$	0.1	$\boldsymbol{\omega_2'}\ (\boldsymbol{rad/s})$	0.6
$\boldsymbol{a}$	0.005	$\boldsymbol{k_1'}$	2.4
$\boldsymbol{k_1}$	0.1	$\boldsymbol{k_2'}$	1
$\boldsymbol{k_2}$	0.05	$\boldsymbol{\alpha_1'}$	0.01
$\boldsymbol{c_1}$	0.6	$\boldsymbol{\alpha_2'}$	0.01
$\boldsymbol{c_2}$	10		

Figure 68 shows the net real power profile of the pole mounted transformer at the secondary side. Due to the intermittent solar power generation and time-varying load, there is a significant variation in the net load seen by the grid which adversary effects on the voltage profile.

The proposed control method is applied to the battery energy storage system connected to the end node which is subjected to the maximum voltage variation. The controller is enabled at t=300min. The desired voltage is set to 1pu. Simulation results provided in Figure 69 show the voltage profile of the end node before and after the BESS is activated. The proposed control method effectively coordinates the active and reactive power injected by BESS shown in Figure 70 to regulate the voltage with the minimum capacity of battery and inverter.

Figure 71 shows the net real power profile of transformer after enabling the BESS. The charging and discharging of BESS accordingly reduces the variation range of net real power profile seen by the grid and improves the load factor.

The phase angle and magnitude of inverter current is depicted in Figure 72. In order to verify the performance of ES-based controller in tracking the optimum current angle, the Thevenin equivalent circuit parameters of the testbed is calculated by performing the open circuit test, and short circuit test across the end node terminal. The phase angle of equivalent Thevenin impedance (γ_{th}) is calculated as 49 degree while the ES-based controller exactly converges to -49 degree.

The performance of the proposed method to control both active and reactive power for voltage regulation is compared with VAR compensation. Figure 73 illustrates the reactive power exchanged by inverter in order to regulate voltage at 1pu. Figure 74 depicts the regulated voltage with only VAR compensation while the power factor controller is disabled. The comparison between the system capacities is shown in Figure 75. The system capacity used by the proposed controlled is 2.5kVA, while for VAR compensation around 6.4kVA system is required.

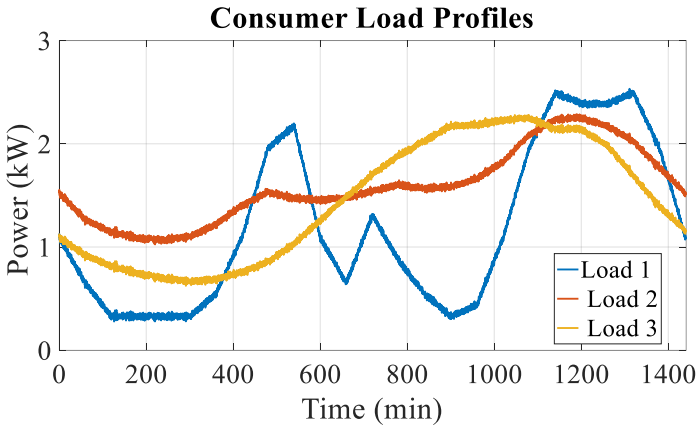

Figure 66 Load profile of consumers

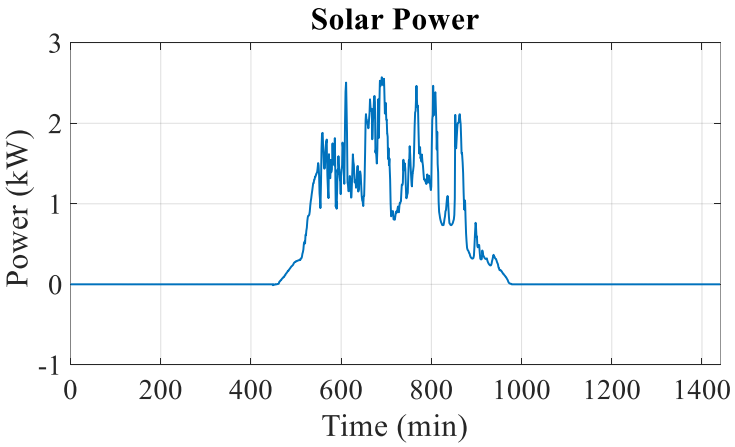

Figure 67 Solar power profile

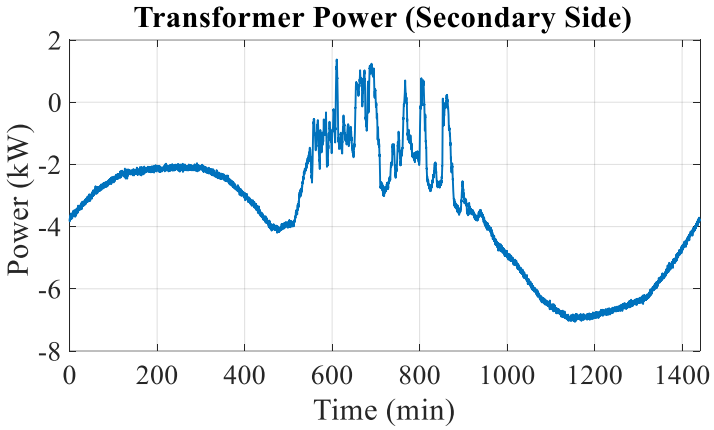

Figure 68 Net real power profile of the transformer before battery is activated

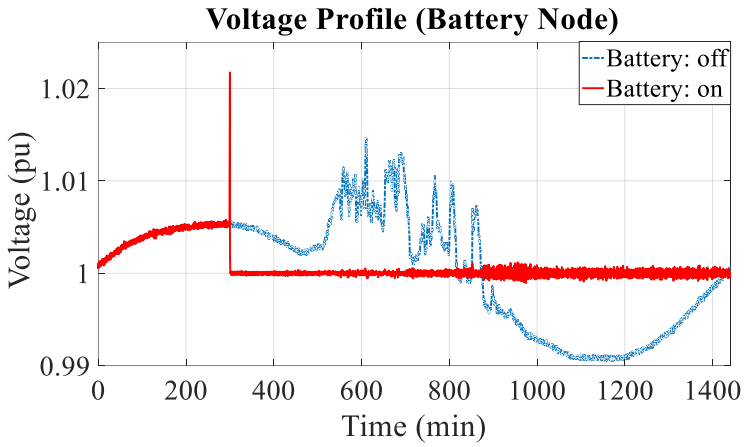

Figure 69 Voltage profile of end node before and after activation of the battery

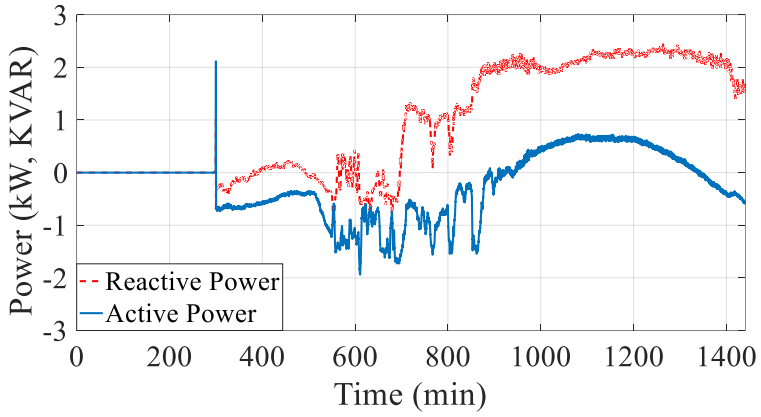

Figure 70 Active and reactive power exchange by BESS

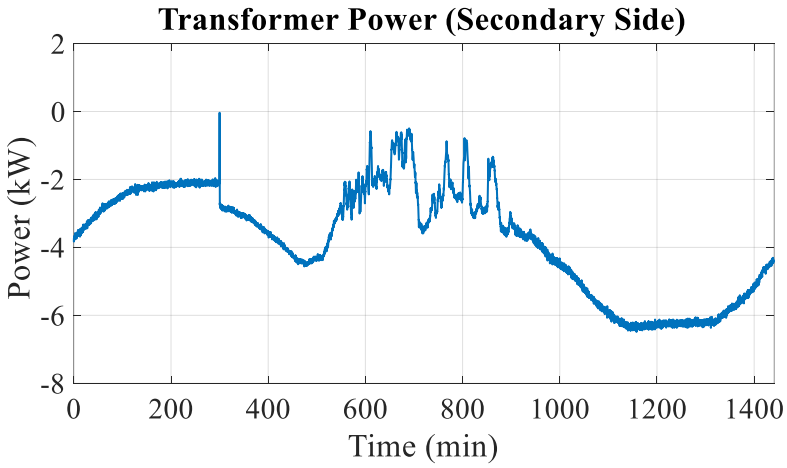

Figure 71 Net real power profile of the transformer after battery is activated

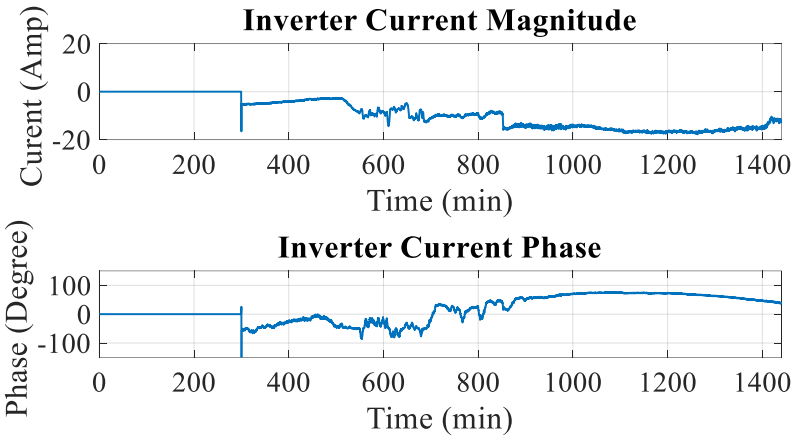

Figure 72 Magnitude and pahse of inverter current

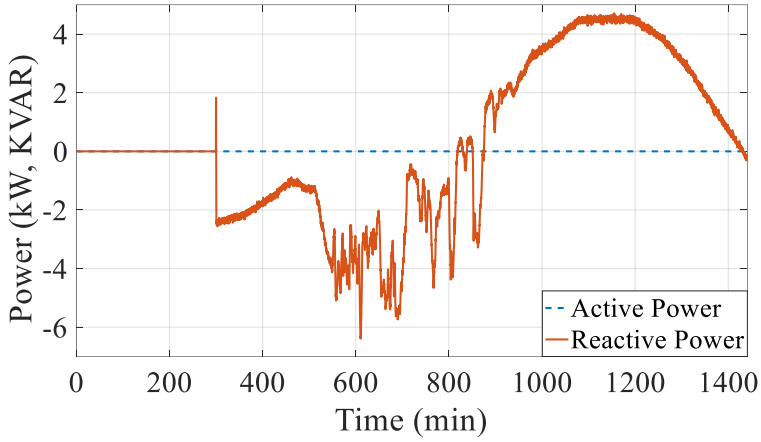

Figure 73 Reactive power exchange by BESS

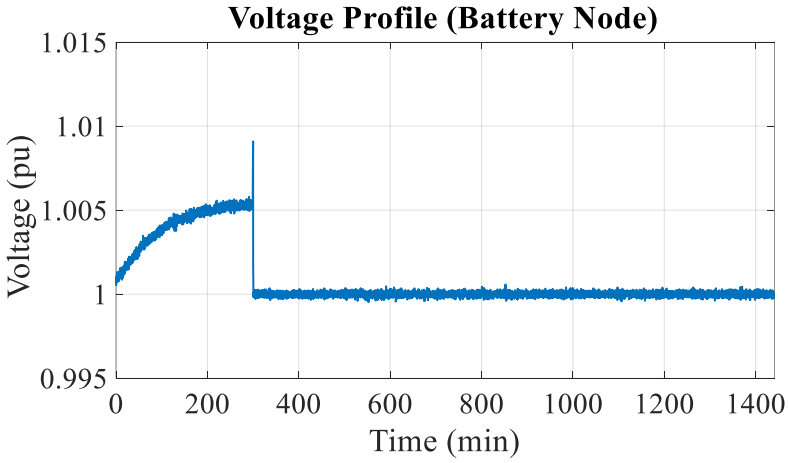

Figure 74 Voltage profile of end node after activation of only reactive power control

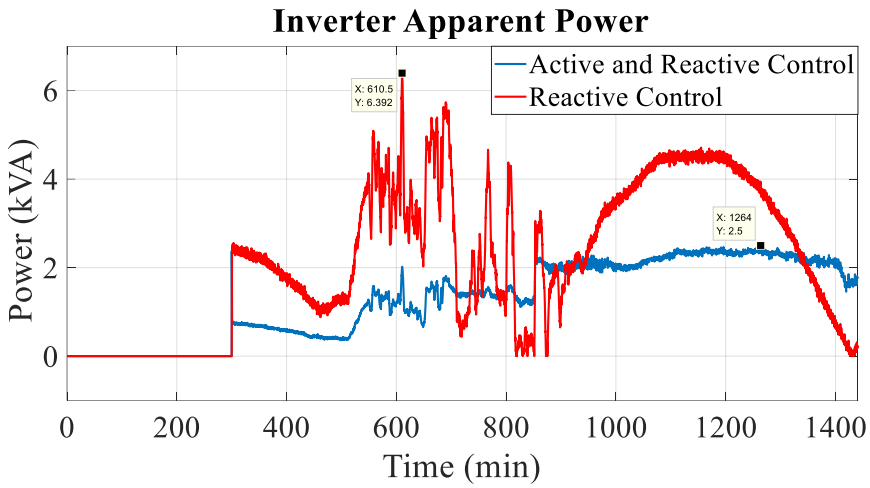

Figure 75 Apparent power of BESS during the voltage control

9.4.2 Experimental Results

In this section the performance of the proposed approach to regulate the voltage is demonstrated over an experimental implementation. The experimental setup includes a 62kWh lithium-ion battery energy storage, a 36kW grid-tie inverter, a control panel, and AC/DC measurement units.

The testbed system including battery cabinet, grid-tie inverter, AC panel, and the local controller is shown in Figure 76. The controller panel is also depicted with more details including AC meter, DC meter, protection devices, and Programmable Logic Controller (PLC). The AC meter measures the RMS voltage of the grid at the point of connection in real-time, and sends it to the PLC. The PLC runs the proposed algorithm, and generates appropriate command signals for gird-tie inverter including the current angle and magnitude. Then, the grid-tie inverter performs the command by operating in four quadrants. The schematic of the testbed system including the device ratings is shown in Figure 77.

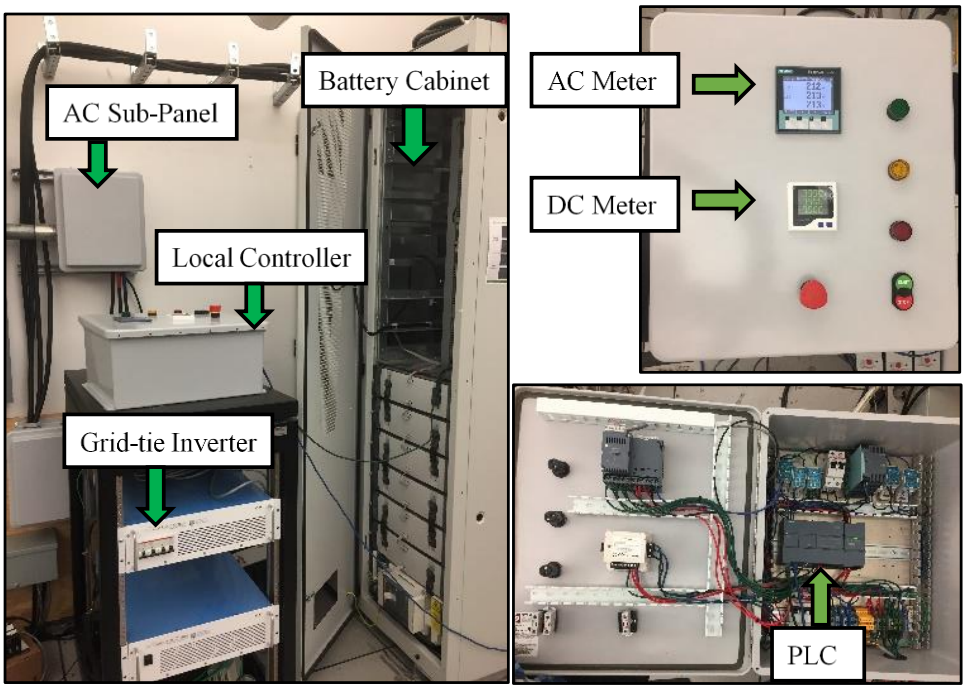

Figure 76 The BESS including the battery cabinet, grid-tie inverter, local controller, and AC panel

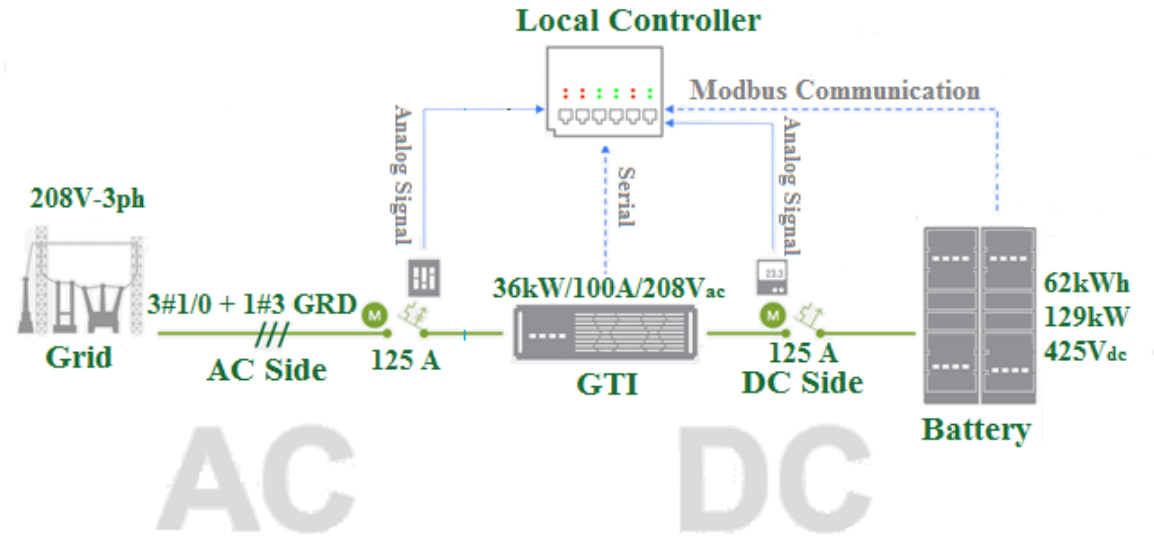

Figure 77 BESS integration schematic

The RMS voltage of the AC grid measured at the point of connection with BESS is depicted in Figure 78. The normal voltage of the grid is 212 V. The reference voltage is set to 213 V. By

activating the voltage regulation function at time $t = 1s$, the voltage gradually increases to reach the desired level. At time $t = 800s$, the voltage regulation function is deactivated and the voltage instantaneously drops to its initial value (212 V). The inverter power factor control can be either disabled, or enabled. When the power factor control is disabled the BESS including GTI works as a VAR resource and it regulates the voltage by injecting only reactive power. This mode can be recognized in Figure 80 where the power factor is shown as "zero" meaning that the power factor controller is switched off. However, when the model-free optimal controller is enabled, it seeks and sets the optimum power factor, BESS exchanges both active and reactive powers to maximize the impact of the injected current on the voltage magnitude. The proposed controller without the knowledge of the model of the distribution circuit automatically seeks and finds the optimum operation point to coordinate active and reactive power for voltage regulation application. This can be seen in Figure 79.

Figure 80 shows the active and reactive power of the battery system. In this experiment, since the voltage is regulated up from 212V to 213V, the battery is discharged and reactive power is leading. Therefore, both active and reactive power are shown with positive value.

Figure 81 demonstrates the amount of apparent power exchanged by the system for voltage regulation which reflects the size of the system. In Figure 81, when the power factor control is enabled, and both active and reactive power is controlled in an optimum manner, less apparent power is used to maintain the voltage at the desired level. Figure 81 shows the apparent power of the system increases from 20kVA to 25kVA when only reactive power is exchanged with the grid and power factor control is disabled. Therefore, in this case study, the proposed power factor control method reduces the size of system by 20 percent from 25kVA to 20kVA. However, the percentage

of capacity reduction varies case by case based on optimum power factor value depending on the topology, and parameters of the circuit.

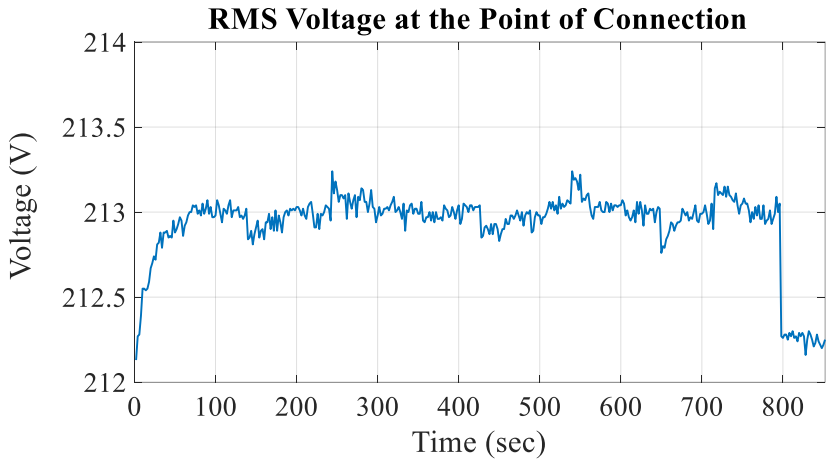

Figure 78 The RMS voltage at the point of connection

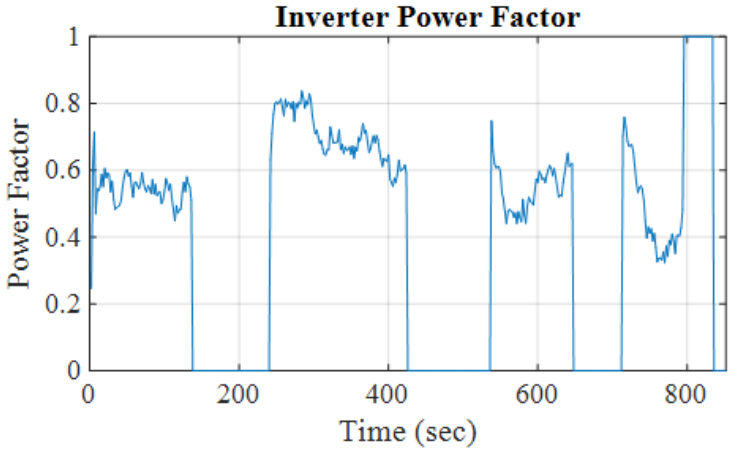

Figure 79 Inverter power factor

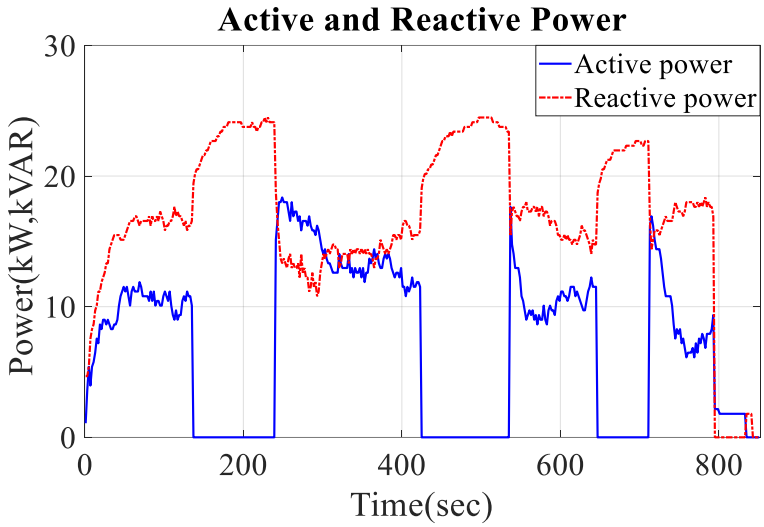

Figure 80 Active and reactive power exchanged by battery system

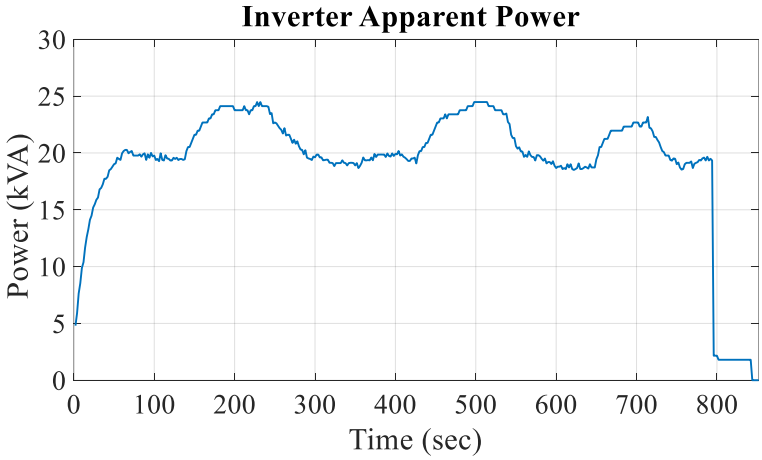

Figure 81 Inverter apparent power

9.5 Conclusions

This paper proposes a new framework for model-free control of BESS and grid-tie inverter to provide voltage regulation. The developed methodology incorporates extremum-seeking-based control technique to find the optimal operating point of BESS without an explicit model of

distribution circuit. The proposed approach by coordinating the active power along with the reactive power improves the capability of voltage regulation in distribution system and minimize the use of battery capacity. To this end, the voltage regulation problem is modeled in the form of an equilibrium map with an optimum. The extremum seeking algorithm and adaptive PI controller are used to control the phase angle and magnitude of the inverter current in an optimal manner. The simulation results show 60 percent improvement in the deployed battery and inverter capacity for voltage regulation compared with VAR compensation. The experimental results also show a 20 percent reduction in the use of the battery capacity.

10 Conclusion and Future Work

This dissertation has been conducting research on energy storage system integration and control as part of the DOE's $120M Smart Grid Demonstration project in collaboration with USC, CALTECH and LADWP. To this end, a framework for real-time control and efficient operation of BESS and power electronic converter is developed to compensate for the intermittency of renewables and provide grid services. In order to address the scalability concern, the framework is designed to be plug-and-play and operate independent of topology and parameters of the power grid. This framework is based on model-free optimal control methodology with fast dynamics. It optimizes the use of BESS capacity for applications such as solar power smoothing and voltage regulation. It also improves the controllability of solar power generation by super-short term prediction.

In this research also a testbed platform is designed and setup consists of 64kWh battery energy storage system, 36kW inverter, and control/communication panel which interacts with 50kW DC fast charger and 25kW solar panel. The proposed control framework has been implemented on the testbed platform and commissioned at the SMERC lab. The results show the proposed framework compared with its control counterparts reduces the use of BESS capacity by 45 percent for solar smoothing application, improves the voltage regulation by 20 percent for defined battery capacity, and reduce the mean absolute value error of the super short-term solar prediction by 11 percent.

The contribution of this dissertation can be summarized as follows:

1) Provide a new hybrid method for super short-term solar power prediction which unlike most exiting approaches in the literature, only relies on current and past values of the solar power time series.

2) Provide a systematic way to optimize the size of the battery capacity for the desired level of solar power smoothing by proposing a new method for an optimal design of minimum-length, low-group-delay FIR filter with maximum stopband attenuation for a given level of smoothness.
3) Drive an explicit formula to calculate the required BESS current as a function of solar PV current and location in a power grid for real-time voltage regulation applications.
4) Derive the voltage regulation problem in distribution systems, consist of renewable energy resources and dynamic loads, in form of an equilibrium map with optimum, without any limits on the system configuration (e.g. radial vs. ring, balance vs. unbalance), amount of reverse power flow, and losses.
5) Provide a new voltage regulation methodology using battery energy storage systems in which distributed BESSs are controlled in a plug and play manner by only measuring the RMS voltage at the point of connection, without any explicit information of the feeders, and any communication requirements.

This research project identifies utilities' concerns and technical challenges due to high penetration of renewable energy resources and stochastic behavior of high demand loads such as EVs. It proposes a mitigation solution by deploying battery energy storage system and power electronic device as well as control and integration methodology which optimizes the use of battery capacity. This research demonstrates incorporating advanced control technologies and solutions customized for different applications of energy storage provide efficient, high performance, and reliable solution while it considerably reduces the deployment cost. In specific, this project will benefit utilities to accommodate more battery energy storage capacity in power system, to facilitate utilization of high renewable penetration, and avoid the cost of power system expansion.

In this research, the new control technique for smoothing solar power consists of fast-acting minimum-phase, low-group-delay discrete FIR filter could reduce the size of battery capacity by 45% compared with moving average smoothing control. In addition, the extremum seeking–based model free control methodology reduces the battery capacity use by 20% for voltage regulation application compared with VAR compensation techniques. These performance improvements contribute in lower cost energy storage deployment.

In addition, this research by smoothing the renewables power generation addresses the intermittency of renewable energy resources which is the fundamental challenge of renewables integration. It also minimizing the impact of high penetration of renewables on distribution system voltage which is one of the main concerns of utilities. To this end, this research paves the way for accommodation of high renewable penetration.

Finally, this research by combining battery energy storage system, renewable energy resource, and EV charger maximizes the local power utilization (self-supply), and consequently provides the grid with congestion relief. It can also delay, reduce, or entirely avoid utility investments in distribution system upgrades necessary to supply projected load growth on particular nodes in the power system.

As the future work to enhance the performance of the proposed control methodology, there is an interested to advance the capability of BESS to perform multi tasks/services in an optimal manner. Multi-task/service capability faces complicated multi-objective optimization problem, where the global optimum of any individual objective function might not be in satisfactory range of the others. However, solving such a problem helps to justify the value stream of BESS deployment in the power grid.

Finally, during this research we realized some barriers to broad deployment of energy storage system in power system. Addressing these challenges helps with widespread utilization of energy storage system within grid. These barriers can be summarized as 1) Cost, 2) Type, size, and placement 3) Rules, regulation, and standards.

Cost: One of the main factors to promote the deployment of energy storage systems is to be cost competitive with other alternatives available to power system. To this end, the value stream and extra revenue that energy storage systems can create within a grid should be explored and clearly quantified. Moreover, the cost of energy storage deployment should be reduced. It should be noted that the total cost of energy storage systems is not limited to the cost of technology but also the cost of supplementary equipment, installation, integration, and commissioning. In some cases the secondary cost reaches up to 60-70 percent of the total cost [66], which shows the importance of targeting all aspects of energy storage deployment cost.

Type, size, and placement: The existence of a wide range of energy storage technologies in the market, each with its own characteristics, makes the energy storage users confused to select the best suited technology for their applications. Even if they select one technology, it would be hard to properly size the required energy storage. Therefore, in order to facilitate the energy storage utilization, creating comprehensive standards to evaluate and compare the quality and performance of energy storage systems is the first step. The second step is to develop a transparent guideline to help energy storage users with optimally selection of energy storage type and size and location in order to gain the maximum benefit.

Rules, regulation, and standards: Proper rules and regulation can encourage stakeholders to invest more in the energy storage industry. This regulatory environment should provide investors with clear market models as well as incentives, while removing the regulatory restrictions which

prevent stakeholders to collect revenue. Moreover, the stakeholders require clear and accurate vision about the performance of available energy storage systems before they could perform investment calculation. Therefore, in order to alleviate the existing uncertainties over the energy storage capabilities and make the stakeholders confident for investment, a unified framework for reporting and evaluation of energy storage performance, and also codes and standards which define the desired performance criteria are required.

11 References

[1] H. Nazaripouya, C. Chu, H. R. Pota and R. Gadh, "Battery Energy Storage System Control for Intermittency Smoothing Using Optimized Two-Stage Filter," *IEEE Transactions on Sustainable Energy*, no. 99, pp. 1-1, 2017.

[2] H. Nazaripouya, B. Wang, Y. Wang, P. Chu, H. R. Pota and R. Gadh, "Univariate Time Series Prediction of Solar Power Using a Hybrid Wavelet-ARMA-NARX Prediction Method," in *2016 IEEE/PES Transmission and Distribution Conference and Exposition (T&D)*, Dallas, TX, USA, 2016.

[3] M. Benaouadj, A. Aboubou, M. Becherif, M.-Y. Ayad and M. Bahri, "Recharging of batteries/supercapacitors hybrid source for electric vehicles application using photovoltaic energy in a stand-alone point," in *2012 First International Conference on Renewable Energies and Vehicular Technology (REVET)*, Hammamet, Tunisia, 2012.

[4] K. Wang, F. Ciucu, C. Lin and S. H. Low, "A Stochastic Power Network Calculus for Integrating Renewable Energy Sources into the Power Grid," *IEEE Journal on Selected Areas in Communications*, vol. 30, no. 6, pp. 1037 - 1048, 2012.

[5] Y. Ru, J. Kleissl and S. Martinez, "Storage Size Determination for Grid-Connected Photovoltaic Systems," *IEEE Transactions on Sustainable Energy*, vol. 4, no. 1, pp. 68 - 81, 2013.

[6] K. Yoshimi, M. Osawa, D. Yamashita, T. Niimura, R. Yokoyama, T. Masuda, H. Kondou and T. Hirota, "Practical storage and utilization of household photovoltaic energy by electric vehicle battery," in *2012 IEEE PES Innovative Smart Grid Technologies (ISGT)*, Washington, DC, USA, 2012.

[7] L. Roggia, C. Rech, L. Schuch, J. Baggio, H. Hey and J. Pinheiro, "Design of a sustainable residential microgrid system including PHEV and energy storage device," in *Proceedings of the 2011 14th European Conference on Power Electronics and Applications*, Birmingham, UK, 2011.

[8] F. Soto and E. Prieto, "Spanish experience in the integration of wind and solar energy into the electric power system," in *2009 CIGRE/IEEE PES Joint Symposium Integration of Wide-Scale Renewable Resources Into the Power Delivery System*, Calgary, AB, Canada, 2009.

[9] S. R. Bull, "Renewable energy today and tomorrow," *Proceedings of the IEEE,* vol. 89, no. 8, pp. 1216 - 1226, 2001.

[10] M. K. Hossain and M. H. Ali, "Small scale energy storage for power fluctuation minimization with spatially diverged PV plants," in *2013 Proceedings of IEEE Southeastcon*, Jacksonville, FL, USA, 2013.

[11] "Global Trends in Renewable Energy Investment 2011," United Nations Environment Programme (UNEP), July 2011.

[12] P. Thounthong, "Model Based-Energy Control of a Solar Power Plant With a Supercapacitor for Grid-Independent Applications," *IEEE Transactions on Energy Conversion,* vol. 26, no. 4, pp. 1210 - 1218, 2011.

[13] W. A. Omran, M. Kazerani and M. M. A. Salama, "Investigation of Methods for Reduction of Power Fluctuations Generated From Large Grid-Connected Photovoltaic Systems," *IEEE Transactions on Energy Conversion,* vol. 26, no. 1, pp. 318 - 327, 2011.

[14] S. D. G. Jayasinghe, D. M. Vilathgamuwa and U. K. Madawala, "Direct Integration of Battery Energy Storage Systems in Distributed Power Generation," *IEEE Transactions on Energy Conversion,* vol. 26, no. 2, pp. 677 - 685, 2011.

[15] M. Black and G. Strbac, "Value of Bulk Energy Storage for Managing Wind Power Fluctuations," *IEEE Transactions on Energy Conversion,* vol. 22, no. 1, pp. 197 - 205, 2007.

[16] J. P. Barton and D. G. Infield, "Energy storage and its use with intermittent renewable energy," *IEEE Transactions on Energy Conversion,* vol. 19, no. 2, pp. 441 - 448, 2004.

[17] S.-J. Lee, J.-H. Kim, C.-H. Kim, S.-K. Kim, E.-S. Kim, D.-U. Kim, K. K. Mehmood and S. U. Khan, " Coordinated Control Algorithm for Distributed Battery Energy Storage Systems for Mitigating Voltage and Frequency Deviations," *IEEE Transactions on Smart Grid,* vol. 7, no. 3, pp. 1713 - 1722, 2016.

[18] R. Sebastián, " Battery energy storage for increasing stability and reliability of an isolated Wind Diesel power system," *IET Renewable Power Generation,* vol. 11, no. 2, pp. 296 - 303, 2017.

[19] Y. Chen, Y. Zheng, F. Luo, J. Wen and Z. Xu, "Reliability evaluation of distribution systems with mobile energy storage systems," *IET Renewable Power Generation,* vol. 10, no. 10, pp. 1562 - 1569, 2016.

[20] F. Y. Melhem, O. Grunder, Z. Hammoudan and N. Moubayed, "Optimization and Energy Management in Smart Home Considering Photovoltaic, Wind, and Battery Storage System With Integration of Electric Vehicles," *Canadian Journal of Electrical and Computer Engineering*, vol. 40, no. 2, pp. 128 - 138, 2017.

[21] R. Margolis, D. Feldman and D. Boff, "Q4 2016/Q1 2017 Solar Industry Update," 2017.

[22] M. Munsell, June 07 2017. [Online]. Available: https://www.greentechmedia.com/articles/read/us-solar-market-adds-2-gw-of-pv-in-q1-2017.

[23] "SunShot Vision Study," U.S. Department of Energy, 2012.

[24] F. Katiraei and J. R. Aguero, "Solar PV integration challenges," *IEEE Power and Energy Magazine*, vol. 9, no. 3, pp. 62-71, 2011.

[25] C. A. Hill, M. C. Such, D. Chen, J. Gonzalez and W. M. Grady, "Battery Energy Storage for Enabling Integration of Distributed Solar Power Generation," *IEEE Transactions on Smart Grid*, vol. 3, no. 2, pp. 850 - 857, 2012.

[26] M. J. E. Alam, K. M. Muttaqi and D. Sutanto, "A Novel Approach for Ramp-Rate Control of Solar PV Using Energy Storage to Mitigate Output Fluctuations Caused by Cloud Passing," *IEEE Transactions on Energy Conversion*, vol. 29, no. 2, pp. 507 - 518, 2014.

[27] H. Nazaripouya, Y. Wang, P. Chu, H. R. Pota and R. Gadh, "Optimal sizing and placement of battery energy storage in distribution system based on solar size for voltage regulation," in *2015 IEEE Power & Energy Society General Meeting*, Denver, CO, USA, 2015.

[28] A. S. Anees, "Grid integration of renewable energy sources: Challenges, issues and possible solutions," in *2012 IEEE 5th India International Conference on Power Electronics (IICPE)*, Delhi, India, 2012.

[29] Y. S. Lim and J. H. Tang, "Creating a Dynamic Load Controller to Mitigate Flickers Caused by Photovoltaic Systems in Cloudy Regions".

[30] V. Klonari, F. Vallée, O. Durieux, Z. D. Grève and J. Lobry, "Probabilistic modeling of short term fluctuations of photovoltaic power injection for the evaluation of overvoltage risk in low voltage grids," in *2014 IEEE International Energy Conference (ENERGYCON)*, Cavtat, Croatia, 2014.

[31] R. Huang, T. Huang, R. Gadh and N. Li, "Solar generation prediction using the ARMA model in a laboratory-level micro-grid," in *2012 IEEE Third International Conference on Smart Grid Communications (SmartGridComm)*, Tainan, Taiwan, 2012.

[32] T. Kato, T. Inoue and Y. Suzuoki, "Estimation of total power output fluctuation of high penetration photovoltaic power generation system," in *2011 IEEE Power and Energy Society General Meeting*, Detroit, MI, USA, 2011.

[33] Y. Riffonneau, S. Bacha, F. Barruel and S. Ploix, "Optimal Power Flow Management for Grid Connected PV Systems With Batteries," *IEEE Transactions on Sustainable Energy*, vol. 2, no. 3, pp. 309 - 320, 2011.

[34] X. Li, D. Hui and X. Lai, " Battery Energy Storage Station (BESS)-Based Smoothing Control of Photovoltaic (PV) and Wind Power Generation Fluctuations," *IEEE Transactions on Sustainable Energy*, vol. 4, no. 2, pp. 464 - 473, 2013.

[35] W. Shuyun and Y. Yue, "Research on the application of storage battery to restrain the photovoltaic power fluctuation," in *Power Engineering Conference (UPEC), 2013 48th International Universities'*, Dublin, Ireland, 2013.

[36] Y. Miyamoto and Y. Hayashi, "Evaluating improved generation efficiency: One year using residential PV voltage control with a clustered residential grid-interconnected PV," in *2012 3rd IEEE PES Innovative Smart Grid Technologies Europe (ISGT Europe)*, Berlin, Germany, 2012.

[37] M. Fleckenstein, M. Eisenreich and G. Balzer, "Energy storage system in the medium-voltage network," in *2013 12th International Conference on Environment and Electrical Engineering*, Wroclaw, Poland, 2013.

[38] M. Ptacek, "The definition of input parameters for modelling of energetic subsystems," in *EPJ Web of Conferences*, 2013.

[39] M. Kopicka, M. Ptacek and P. Toman, "Analysis of the power quality and the impact of photovoltaic power plant operation on low-voltage distribution network," in *Electric Power Quality and Supply Reliability Conference (PQ)*, Rakvere, Estonia, 2014.

[40] M. Farhoodnea, A. Mohamed, H. Shareef and H. Zayandehroodi, "Power quality impact of grid-connected photovoltaic generation system in distribution networks," in *2012 IEEE Student Conference on Research and Development (SCOReD)*, Pulau Pinang, Malaysia, 2012.

[41] A. R. Malekpour and A. Pahwa, "A Dynamic Operational Scheme for Residential PV Smart Inverters," *IEEE Transactions on Smart Grid*, vol. 8, no. 5, pp. 2258 - 2267, 2017.

[42] P. A. B. Block, H. L. L. Salamanca, M. D. Teixeira, D. B. Dahlke, O. M. Shiono, A. R. Donadon and J. C. Camargo, "Power quality analyses of a large scale photovoltaic system," in *2014 5th International Renewable Energy Congress (IREC)*, Hammamet, Tunisia, 2014.

[43] R. Kumar, A. Mohanty, S. R. Mohanty and N. Kishor, "Power quality improvement in 3-Φ grid connected photovoltaic system with battery storage," in *2012 IEEE International*

Conference on Power Electronics, Drives and Energy Systems (PEDES), Bengaluru, India, 2012.

[44] Y. Pan, I. Voloh and W. Ren, "Protection issues and solutions for protecting feeder with distributed generation," in *2013 66th Annual Conference for Protective Relay Engineers*, College Station, TX, USA, 2013.

[45] W. Yang, X. Zhou and F. Xue, " Impacts of Large Scale and High Voltage Level Photovoltaic Penetration on the Security and Stability of Power System," in *2010 Asia-Pacific Power and Energy Engineering Conference*, Chengdu, China, 2010.

[46] B. Hussain, S. M. Sharkh, S. Hussain and M. A. Abusara, "Integration of distributed generation into the grid: Protection challenges and solutions," in *10th IET International Conference on Developments in Power System Protection (DPSP 2010). Managing the Change*, Manchester, UK, 2010.

[47] T. M. d. Britto, D. R. Morais, M. A. Marin, J. G. Rolim, H. H. Zurn and R. F. Buendgens, "Distributed generation impacts on the coordination of protection systems in distribution networks," in *2004 IEEE/PES Transmision and Distribution Conference and Exposition: Latin America*, Sao Paulo, Brazil, 2004.

[48] S. Bhattacharya, T. Saha and M. J. Hossain, "Fault current contribution from photovoltaic systems in residential power networks," in *2013 Australasian Universities Power Engineering Conference (AUPEC)*, Hobart, TAS, Australia, 2013.

[49] S. Kwon, C. Shin and W. Jung, "Evaluation of protection coordination with distributed generation in distribution networks," in *10th IET International Conference on Developments in Power System Protection (DPSP 2010). Managing the Change*, Manchester, UK, 2010.

[50] F. R. Yu, P. Zhang, W. Xiao and P. Choudhury, "Communication systems for grid integration of renewable energy resources," *IEEE Network*, vol. 25, no. 5, pp. 22 - 29, 2011.

[51] C.-Y. Chung, A. Shepelev, C. Qiu, C.-C. Chu and R. Gadh, "Design of RFID mesh network for Electric Vehicle smart charging infrastructure," in *2013 IEEE International Conference on RFID-Technologies and Applications* , Johor Bahru, Malaysia, 2013.

[52] E.-K. Lee, R. Gadh and M. Gerla, "Energy Service Interface: Accessing to Customer Energy Resources for Smart Grid Interoperation," *IEEE Journal on Selected Areas in Communications*, vol. 31, no. 7, pp. 1195 - 1204, 2013.

[53] O. Haas, O. Ausburg and P. Palensky, "Communication with and within Distributed Energy Resources," in *2006 4th IEEE International Conference on Industrial Informatics*, Singapore, Singapore, 2006 .

[54] M. Starke, A. Herron, D. King and Y. Xue, "Implementation of a Publish-Subscribe Protocol in Microgrid Islanding and Resynchronization with Self-Discovery," *IEEE Transactions on Smart Grid*, no. 99, pp. 1-1, 2017.

[55] H. Guozhen, C. tao, C. Changsong and D. Shanxu, "Solutions for SCADA system communication reliability in photovoltaic power plants," in *2009 IEEE 6th International Power Electronics and Motion Control Conference*, Wuhan, China, 2009.

[56] R. Huang, Y. Wang, C.-C. Chu, R. Gadh and Y.-j. Song, "Optimal Configuration of Distributed Generation on Jeju Island Power Grid Using Genetic Algorithm: A Case Study," *Journal of Communication Software and Systems*, vol. 10, no. 2, pp. 135-144, 2014.

[57] B. Kroposki, P. K. Sen and K. Malmedal, "Optimum Sizing and Placement of Distributed and Renewable Energy Sources in Electric Power Distribution Systems," *IEEE Transactions on Industry Applications*, vol. 49, no. 6, pp. 2741 - 2752, 2013.

[58] R. Prenc, D. Škrlec and V. Komen, "Optimal PV system placement in a distribution network on the basis of daily power consumption and production fluctuation," in *Eurocon 2013*, Zagreb, Croatia, 2013.

[59] M. Ettehadi, H. Ghasemi and S. Vaez-Zadeh, "Voltage Stability-Based DG Placement in Distribution Networks," *IEEE Transactions on Power Delivery*, vol. 28, no. 1, pp. 171 - 178, 2013.

[60] Y. Tang and S. H. Low, "Optimal Placement of Energy Storage in Distribution Networks," *IEEE Transactions on Smart Grid*, no. 99, pp. 1-1, 2017.

[61] "Renewables 2017 Global Status Report," Paris, 2017.

[62] "World Energy Resources Solar 2016," 2016.

[63] "Trends 2016 in Photovoltaic Applications," 2016.

[64] "Solar Market Insight Report 2016 Year In Review," 2017.

[65] "25X25', "White House launches plan to broaden solar access, energy efficiency", Weekly REsource, 22 July 2016".

[66] "Grid Energy Storage," U.S. Department of Energy, 2013.

[67] G. Fitzgerald, J. Mandel, J. Morris and H. Touati, "The Economics of Battery Energy Storage," Boulder, CO, 2015.

[68] NISSAN Motor Company, "QUICK CHARGER INSTALLATION DIGEST.," 2012.

[69] F. Katiraei and J. Agüero, "Solar PV Integration Challenges," *Power and Energy Magazine, IEEE*, vol. 9, no. 3, pp. 62-71, 2011.

[70] H. Nazaripouya, Y. Wang, P. Chu, H. R. Pota and R. Gadh, "Optimal Sizing and Placement of Battery Energy Storage in Distribution System Based on Solar Size for Voltage Regulation," in *2015 IEEE PES General Meeting*, Denver, Colorado, US, 2015.

[71] S. Jafarzadeh, M. S. Fadali and C. Y. Evrenosoglu, "Solar Power Prediction Using Interval Type-2 TSK Modeling," *IEEE Transactions on Sustainable Energy*, vol. 4, no. 2, pp. 333 - 339, 2013.

[72] Y. Wang, H. Nazaripouya, C.-C. Chu, R. Gadh and H. R. Pota, " Vehicle-to-grid automatic load sharing with driver preference in micro-grids," in *IEEE PES Innovative Smart Grid Technologies, Europe*, Istanbul, Turkey, 2014.

[73] U. Nalina, V. Prema, K. Smitha and K. Rao, "Multivariate regression for prediction of solar irradiance," in *2014 International Conference on Data Science & Engineering (ICDSE)*, Kochi, India, 2014.

[74] G. R. Kishore, V. Prema and K. U. Rao, " Multivariate wind power forecast using artificial neural network," in *2014 IEEE Global Humanitarian Technology Conference - South Asia Satellite (GHTC-SAS)*, Trivandrum, India, 2014.

[75] A. Ghanbarzadeh, A. R. Noghrehabadi, E. Assareh and M. A. Behrang, " Solar radiation forecasting based on meteorological data using artificial neural networks," in *2009 7th IEEE International Conference on Industrial Informatics*, Cardiff, Wales, UK, 2009.

[76] S. Srivastava, S. Bhardwaj and O. S. Sastri, "A novel hybrid model for solar radiation prediction," in *2012 International Conference on Emerging Trends in Electrical Engineering and Energy Management (ICETEEEM)*, Chennai, India, 2012.

[77] A. Assi, M. Al-Shamisi and M. Jama, "Prediction of monthly average daily global solar radiation in Al Ain City–UAE using artificial neural network," in *25th European photovoltaic solar energy conference*, Valencia, Spain, 2010.

[78] J. Liu, W. Fang, X. Zhang and C. Yang, "An Improved Photovoltaic Power Forecasting Model With the Assistance of Aerosol Index Data," *IEEE Transactions on Sustainable Energy,* vol. 6, no. 2, pp. 434 - 442, 2015.

[79] R. Huang, T. Huang, R. Gadh and N. Li, "Solar generation prediction using the ARMA model in a laboratory-level micro-grid," in *2012 IEEE Third International Conference on Smart Grid Communications (SmartGridComm),* ainan, Taiwan, 2012.

[80] W.-Y. Zhang, Z.-B. Zhao, T.-T. Han and L.-B. Kong, "Short Term Wind Speed Forecasting for Wind Farms Using an Improved Autoregression Method," in *2011 International Conference on Information Technology, Computer Engineering and Management Sciences (ICM),* , Nanjing, Jiangsu, China, 2011.

[81] J. Zeng and W. Qiao, "Short-term solar power prediction using a support vector machine," *Renewable Energy,* vol. 52, pp. 118-127, 2013.

[82] R. Iqdour and A. Zeroual, "A rule based fuzzy model for the prediction of solar radiation," *Revue des energies renouvelables,* vol. 9, no. 2, pp. 113-120, 2006.

[83] G. Capizzi, F. Bonanno and C. Napoli, "A wavelet based prediction of wind and solar energy for Long-Term simulation of integrated generation systems," in *2010 International Symposium on Power Electronics Electrical Drives Automation and Motion (SPEEDAM),* , Pisa, Italy, 2010.

[84] A. Ajabshirizadeh, N. M. Jouzdani and S. Abbassi, "Neural network prediction of solar cycle 24," *Research in Astronomy and Astrophysics,* vol. 11, no. 4, p. 491, 2011.

[85] Y. Wang, B. Wang, R. Huang, C.-C. Chu, H. R. Pota and R. Gadh, "Two-tier prediction of solar power generation with limited sensing resource," in *2016 IEEE/PES Transmission and Distribution Conference and Exposition (T&D)*, Dallas, TX, USA, 2016.

[86] S. M. Ruffing and G. K. Venayagamoorthy, "Short to Medium Range Time Series Prediction of Solar Irradiance Using an Echo State Network," in *2009 15th International Conference on Intelligent System Applications to Power Systems*, Curitiba, Brazil, 2009.

[87] M. Majidpour, C. Qiu, P. Chu, R. Gadh and H. R. Pota, "Fast Prediction for Sparse Time Series: Demand Forecast of EV Charging Stations for Cell Phone Applications," *IEEE Transactions on Industrial Informatics*, vol. 11, no. 1, pp. 242 - 250, 2015.

[88] M. Majidpour, C. Qiu, P. Chu, R. Gadh and H. R. Pota, "Modified pattern sequence-based forecasting for electric vehicle charging stations," in *2014 IEEE International Conference on Smart Grid Communications (SmartGridComm)*, Venice, Italy, 2014.

[89] T. R. Sumithira and A. N. Kumar, "Prediction of monthly global solar radiation using adaptive neuro fuzzy inference system (ANFIS) technique over the State of Tamilnadu (India): a comparative study," *Applied Solar Energy*, vol. 48, no. 2, pp. 140-145, 2012.

[90] J. Cao and X. Lin, "Application of the diagonal recurrent wavelet neural network to solar irradiation forecast assisted with fuzzy technique," *Engineering Applications of Artificial Intelligence*, vol. 21, no. 8, pp. 1255-1263, 2008.

[91] J. Kleissl, Solar Energy Forecasting and Resource Assessment, Academic Press, 2013.

[92] J. Zeng and W. Qiao, "Short-term solar power prediction using an RBF neural network," in *2011 IEEE Power and Energy Society General Meeting*, Detroit, MI, USA, 2011.

[93] M. Shafie-Khah, M. P. Moghaddam and M. K. Sheikh-El-Eslami, "Price forecasting of day-ahead electricity markets using a hybrid forecast method," *Energy Conversion and Management*, vol. 52, no. 5, pp. 2165-2169, 2011.

[94] W. Ji and K. C. Chee, "Prediction of hourly solar radiation using a novel hybrid model of ARMA and TDNN," *Solar Energy*, vol. 85, no. 5, pp. 808-817, 2011.

[95] C. Stolojescu, I. Railean, S. M. P. Lenca and A. Isar, "A wavelet based prediction method for time series," in *Stochastic Modeling Techniques and Data Analysis (SMTDA2010) International Conference*, Chania, Greece, 2010.

[96] P. Fryzlewicz, S. Van Bellegem and R. Von Sachs, "Forecasting non-stationary time series by wavelet process modelling," *Annals of the Institute of Statistical Mathematics*, vol. 55, no. 4, pp. 737-764, 2003.

[97] T. W. Joo and S. B. Kim, "Time series forecasting based on wavelet filtering," *Expert Systems with Applications*, vol. 42, no. 8, pp. 3868-3874, 2015.

[98] L. M. Bruce, C. H. Koger and J. Li, "Dimensionality reduction of hyperspectral data using discrete wavelet transform feature extraction," *IEEE Transactions on Geoscience and Remote Sensing*, vol. 40, no. 10, pp. 2331 - 2338, 2002.

[99] H. T. Siegelmann, B. G. Horne and C. L. Giles, "Computational capabilities of recurrent NARX neural networks," *IEEE Transactions on Systems, Man, and Cybernetics, Part B (Cybernetics)*, vol. 27, no. 2, pp. 208 - 215, 1997.

[100] P. Derewonko and J. M. Pearc, "Optimizing design of household scale hybrid solar photovoltaic + combined heat and power systems for Ontario," in *Photovoltaic Specialists Conference (PVSC), 2009 34th IEEE*, Philadelphia, PA, 2009.

[101] A. Agrawal, K. Rahimi, R. P. Broadwater and J. Bank, "Performance of PV generation feedback controllers: Power factor versus Volt-VAR control strategies," in *North American Power Symposium (NAPS), 2015*, Charlotte, NC, 2015.

[102] J. Marcos, I. d. l. Parra, M. García and L. Marroyo, "Control strategies to smooth short-term power fluctuations in large photovoltaic plants using battery storage systems," *Energies*, vol. 7, no. 10, pp. 6593-6619, 2014.

[103] V. Gevorgian and S. Booth, "Review of PREPA technical requirements for interconnecting wind and solar generation," National Renewable Energy Laboratory, Golden, CO, USA, 2013.

[104] J. Marcos, I. d. l. Parra, M. García and L. Marroyo, "Simulating the variability of dispersed large PV plants," *Progress in Photovoltaics*, vol. 24, no. 5, p. 680–691, 2016.

[105] K. S. Tam, P. Kumar and M. Foreman, "Enhancing the utilization of photovoltaic power generation by superconductive magnetic energy storage," *IEEE Transactions on Energy Conversion*, vol. 4, no. 3, pp. 314 - 321, 1989.

[106] X. Li, D. Hui and X. Lai, "Battery Energy Storage Station (BESS)-based smoothing control of Photovoltaic (PV) and wind power generation fluctuations," *IEEE Transactions on Sustainable Energy,* vol. 4, no. 2, pp. 464-473, 2013.

[107] C. A. Hill, M. C. Such, D. Chen, J. Gonzalez and W. M. Grady, "Battery energy storage for enabling integration of distributed solar power generation," *IEEE TRANSACTIONS ON SMART GRID,* vol. 3, no. 2, pp. 850-857, 2012.

[108] G. Wang, M. Ciobotaru and V. G. Agelidis, "Power smoothing of large solar PV plant using hybrid energy storage," *IEEE Transactions on Sustainable Energy,* vol. 5, no. 3, pp. 834-842, 2014.

[109] Y. Ghiassi-Farrokhfal, S. Keshav, C. Rosenberg and F. Ciucu, "Solar power shaping: an analytical approach," *IEEE Transactions on Sustainable Energy,* vol. 6, no. 1, pp. 162-170, 2015.

[110] I. de la Parra, J. Marcos, M. García and L. Marroyo, "Dynamic ramp-rate control to smooth short-term power fluctuations in large photovoltaic plants using battery storage systems," in *IECON 2016 - 42nd Annual Conference of the IEEE Industrial Electronics,* Florence, 2016.

[111] M. J. E. Alam, K. M. Muttaqi and D. Sutanto, "A novel approach for ramp-rate control of solar PV using energy storage to mitigate output fluctuations caused by cloud passing," *IEEE Transactions on Energy Conversion,* vol. 29, no. 2, pp. 507-518, 2014.

[112] R. P. Sasmal, S. Sen and A. Chakraborty, "Solar photovoltaic output smoothing: Using battery energy storage system," in *2016 National Power Systems Conference (NPSC)*, Bhubaneswar, 2016.

[113] E. Balamurugan and S. Venkatasubramanian, "Analysis of double moving average power smoothing methods for photovoltaic systems," *International Research Journal of Engineering and Technology (IRJET),* vol. 3, no. 2, pp. 1260-1262, 2016.

[114] Y. Moumouni, Y. Baghzouz and R. F. Boehm, "Power “smoothing” of a commercial-size photovoltaic system by an energy storage system," in *2014 16th International Conference on Harmonics and Quality of Power (ICHQP)*, Bucharest, 2014.

[115] M. Brenna, F. Foiadelli, M. Longo and D. Zaninelli, "Energy storage control for dispatching photovoltaic power," *IEEE Transactions on Smart Grid,* no. 99, pp. 1-1, 2016.

[116] X. Fang, S. Ma, Q. Yang and J. Zhang, "Cooperative energy dispatch for multiple autonomous microgrids," *Energy,* vol. 99, pp. 45-57, 2016.

[117] W. Su, J. Wang and J. Roh, "Stochastic energy scheduling in microgrids with intermittent renewable energy resources," *IEEE Transactions on Smart Grid,* vol. 5, no. 4, pp. 1876 - 1883, 2014.

[118] A. V. Oppenheim, R. W. Schafer and J. R. Buck, Discrete-time signal processing, Upper Saddle River, NJ: Prentice Hall, 1999.

[119] G. Calvagno, G. M. Cortelazzo and G. A. Mian, "A technique for multiple criterion approximation of FIR filters in magnitude and group delay," *IEEE Transactions on Signal Processing,* vol. 43, no. 2, pp. 393 - 400, 1995.

[120] V. D. Blondel, M. Gürbüzbalaban, A. Megretski and M. L. Overton, "Explicit solutions for root optimization of a polynomial family with one affine constraint," *IEEE TRANSACTIONS ON AUTOMATIC CONTROL,* vol. 57, no. 12, pp. 3078-3089, 2012.

[121] S. P. Wu, S. Boyd and L. Vandenberghe, "FIR filter design via spectral factorization and convex optimization," in *Applied and computational control, signals, and circuits*, Birkhäuser Boston, 1999.

[122] S. P. Wu, S. Boyd and L. Vandenberghe, "FIR filter design via semidefinite programming and spectral factorization," in *Decision and Control, Proceedings of the 35th IEEE Conference on*, Kobe, 1996.

[123] O. Herrmann and W. Schuessler, "Design of nonrecursive digital filters with minimum phase," *Electronics Letters,* vol. 6, no. 11, pp. 329-330, 1970.

[124] T. Wang, H. Kamath and S. Willard, "Control and optimization of grid-tied photovoltaic storage systems using model predictive control," *IEEE Transactions on Smart Grid,* vol. 5, no. 2, pp. 1010-1017, 2014.

[125] "UCLA WINSmartGrid," UCLA, [Online]. Available: http://winmec.ucla.edu/smartgrid/.

[126] A. Masoum, P. Moses, M. Masoum and A. Abu-Siada, "Impact of rooftop PV generation on distribution transformer and voltage profile of residential and commercial networks,"

in *Innovative Smart Grid Technologies (ISGT), 2012 IEEE PES*, Washington, DC, USA, 2012.

[127] R. Tonkoski, D. Turcotte and T. El-Fouly, "Impact of High PV Penetration on Voltage Profiles in Residential Neighborhoods," *IEEE Transactions on Sustainable Energy*, vol. 3, no. 3, pp. 518-527, 2012.

[128] X. Liu, A. Aichhorn, L. Liu and H. Li, "Coordinated control of distributed energy storage system with tap changer transformers for voltage rise mitigation under high photovoltaic penetration," *IEEE Transactions on Smart Grid ,* vol. 3, no. 2, p. 897–906, 2012.

[129] A. Kanchanaharuthai, V. Chankong and K. Loparo, "Transient Stability and Voltage Regulation in Multimachine Power Systems Vis-à-Vis STATCOM and Battery Energy Storage," *IEEE Transactions on Power Systems*, vol. 30, no. 5, pp. 2404 - 2416, 2015.

[130] D. Ranamuka, A. Agalgaonkar and K. Muttaqi, "Online Voltage Control in Distribution Systems With Multiple Voltage Regulating Devices," *IEEE Transactions on Sustainable Energy*, vol. 5, no. 2, pp. 617-628, 2014.

[131] Y. Yang, H. Li, A. Aichhorn, J. Zheng and M. Greenleaf, "Sizing Strategy of Distributed Battery Storage System With High Penetration of Photovoltaic for Voltage Regulation and Peak Load Shaving," *IEEE Transactions on Smart Grid*, vol. 5, no. 2, pp. 982 - 991, 2014.

[132] F. Marra, G. Yang, C. Træholt, J. Østergaard and E. Larsen, "A Decentralized Storage Strategy for Residential Feeders With Photovoltaics," *IEEE Transactions on Smart Grid*, vol. 5, no. 2, pp. 974 - 981, 2014.

[133] S. Mal, A. Chattopadhyay, A. Yang and R. Gadh, "Electric vehicle smart charging and vehicle-to-grid operation," *International Journal of Parallel, Emergent and Distributed Systems*, vol. 27, no. 3, pp. 249-265, 2012.

[134] Y. Wang, W. Shi, B. Wang, C.-C. Chu and R. Gadh, "Optimal operation of stationary and mobile batteries in distribution grids," *Applied Energy*, vol. 190, p. 1289–1301, 2017.

[135] Y. Wang, B. Wang, C.-C. Chu, H. Pota and R. Gadh, "Energy management for a commercial building microgrid with stationary and mobile battery storage," *Energy and Buildings*, vol. 116, p. 141–150, 2016.

[136] Y. Wang, B. Wang, T. Zhang, H. Nazaripouya, C.-C. Chu and R. Gadh, "Optimal energy management for Microgrid with stationary and mobile storages," in *2016 IEEE/PES Transmission and Distribution Conference and Exposition (T&D)*, Dallas, TX, USA, 2016 .

[137] M. Zillmann, R. Yan and T. K. Saha, "Regulation of distribution network voltage using dispersed battery storage systems: A case study of a rural network," in *2011 IEEE Power and Energy Society General Meeting*, Detroit, MI, USA, 2011.

[138] V. Khadkikar, R. K. Varma and R. Seethapathy, "Grid voltage regulation utilizing storage batteries in PV solar — Wind plant based distributed generation system," in *2009 IEEE Electrical Power & Energy Conference (EPEC)*, Montreal, QC, Canada, 2009.

[139] A. Aichhorn, M. Greenleaf, H. Li and J. Zheng, "A cost effective battery sizing strategy based on a detailed battery lifetime model and an economic energy management strategy," in *2012 IEEE Power and Energy Society General Meeting*, San Diego, CA, USA, 2012.

[140] Y. Ru, J. Kleissl and S. Martinez, "Storage Size Determination for Grid-Connected Photovoltaic Systems," *IEEE Transactions on Sustainable Energy,* vol. 4, no. 1, pp. 68-81, 2103.

[141] L. Xu, X. Ruan, C. Mao, B. Zhang and Y. Luo, " An Improved Optimal Sizing Method for Wind-Solar-Battery Hybrid Power System," *IEEE Transactions on Sustainable Energy,* vol. 4, no. 3, pp. 774 - 785, 2013.

[142] T. K. A. Brekken, A. Yokochi, A. v. Jouanne, Z. Z. Yen, H. M. Hapke and D. A. Halamay, "Optimal Energy Storage Sizing and Control for Wind Power Applications," *IEEE Transactions on Sustainable Energy,* vol. 2, no. 1, pp. 69 - 77, 2011.

[143] F. Yahyaie and T. Soong, "Optimal operation strategy and sizing of battery energy storage systems," in *Electrical & Computer Engineering (CCECE), 2012 25th IEEE Canadian Conference on*, Montreal, QC, Canada, 2012.

[144] J. J. Grainger and W. D. Stevenson, Power System Analysis, New York: McGraw-Hill, 1994.

[145] Y. Liu, B. Ge and H. Abu-Rub, "Modelling and controller design of quasi-Z-source cascaded multilevel inverter-based three-phase grid-tie photovoltaic power system," *Renewable Power Generation, IET,* vol. 8, no. 8, pp. 925-936, 2014.

[146] H. Nazaripouya and S. Mehraeen, "Optimal PMU placement for fault observability in distributed power system by using simultaneous voltage and current measurements," in *Power and Energy Society General Meeting (PES)*, Vancouver, BC, Canada, 2013.

[147] P.-C. Chen, R. Salcedo, Q. Zhu, F. d. Leon, D. Czarkowski, Z.-P. Jiang, V. Spitsa, Z. Zabar and R. E. Uosef, "Analysis of Voltage Profile Problems Due to the Penetration of Distributed Generation in Low-Voltage Secondary Distribution Networks," *IEEE Transactions on Power Delivery,* vol. 27, no. 4, pp. 2020 - 2028, 2012.

[148] M. Hasheminamin, V. G. Agelidis, V. Salehi and Remus, "Index-Based Assessment of Voltage Rise and Reverse Power Flow Phenomena in a Distribution Feeder Under High PV Penetration," *IEEE Journal of Photovoltaics,* vol. 5, no. 4, pp. 1158 - 1168, 2015.

[149] B. Wang, Y. Wang, H. Nazaripouya, C. Qiu, C.-C. Chu and R. Gadh, "Predictive Scheduling Framework for Electric Vehicles With Uncertainties of User Behaviors," *IEEE Internet of Things Journal,* vol. 4, no. 1, pp. 52 - 63, 2017.

[150] B. Wang, R. Huang, Y. Wang, H. Nazaripouya, C. Qiu, C.-C. Chu and R. Gadh, "Predictive scheduling for Electric Vehicles considering uncertainty of load and user behaviors," in *2016 IEEE/PES Transmission and Distribution Conference and Exposition (T&D)*, Dallas, TX, USA, 2016.

[151] S. Shivashankar, S. Mekhilef, H. Mokhlis and M. Karimi, "Mitigating methods of power fluctuation of photovoltaic (PV) sources – A review," *Renewable and Sustainable Energy Reviews,* vol. 59, p. 1170–1184, 2016.

[152] A. Dubey, S. Santoso and M. P. Cloud, "Understanding the effects of electric vehicle charging on the distribution voltages," in *2013 IEEE Power & Energy Society General Meeting*, Vancouver, BC, Canada, 2013.

[153] J. Petinrin and M. Shaaban, "Impact of renewable generation on voltage control in distribution systems," *Renewable and Sustainable Energy Reviews,* vol. 65, p. 770–783, 2016.

[154] I.-K. Song, W.-W. Jung, C.-M. Chu, S.-S. Cho, H.-K. Kang and J.-H. Choi, "General and Simple Decision Method for DG Penetration Level in View of Voltage Regulation at Distribution Substation Transformers," *Energies,* vol. 6, no. 9, pp. 4786-4798, 2013.

[155] B. A. Robbins and A. D. Domínguez-García, "Optimal Reactive Power Dispatch for Voltage Regulation in Unbalanced Distribution Systems," *IEEE Transactions on Power Systems,* vol. 31, no. 4, pp. 2903 - 2913, 2016.

[156] M. Džamarija and A. Keane, "Autonomous Curtailment Control in Distributed Generation Planning," *IEEE Transactions on Smart Grid,* vol. 7, no. 3, pp. 1337 - 1345, 2016.

[157] N. C. Scott, D. J. Atkinson and J. E. Morrell, "Use of load control to regulate voltage on distribution networks with embedded generation," *IEEE Transactions on Power Systems,* vol. 17, no. 2, pp. 510 - 515, 2002.

[158] A. Boynuegri, B. Vural, A. Tascikaraoglu, M. Uzunoglu and R. Yumurtacı, "Voltage regulation capability of a prototype Static VAr Compensator for wind applications," *Applied Energy,* vol. 93, p. 422–431, 2012.

[159] S. Deshmukh, B. Natarajan and A. Pahwa, "Voltage/VAR Control in Distribution Networks via Reactive Power Injection Through Distributed Generators," *IEEE TRANSACTIONS ON SMART GRID,* vol. 3, no. 3, pp. 1226 - 1234, 2012.

[160] A. Bonfiglio, M. Brignone, F. Delfino and R. Procopio, "Optimal Control and Operation of Grid-Connected Photovoltaic Production Units for Voltage Support in Medium-Voltage Networks," *IEEE Transactions on Sustainable Energy,* vol. 5, no. 1, pp. 254 - 263, 2014.

[161] T. Senjyu, Y. Miyazato, A. Yona, N. Urasaki and T. Funabashi, "Optimal Distribution Voltage Control and Coordination With Distributed Generation," *IEEE Transactions on Power Delivery,* vol. 23, no. 2, pp. 1236 - 1242, 2008.

[162] M. E. Baran and I. M. El-Markabi, "A Multiagent-Based Dispatching Scheme for Distributed Generators for Voltage Support on Distribution Feeders," *IEEE Transactions on Power Systems,* vol. 22, no. 1, pp. 52 - 59, 2007.

[163] H. Nazaripouya, Y. Wang, P. Chu, H. R. Pota and R. Gadh, "Optimal sizing and placement of battery energy storage in distribution system based on solar size for voltage regulation," in *2015 IEEE Power & Energy Society General Meeting*, Denver, CO, USA, 2015.

[164] Y. Zhang, J. Li, K. Meng, Z. Y. Dong, Z. Yu and K. P. Wong, "Voltage regulation in distribution network using battery storage units via distributed optimization," in *2016 IEEE International Conference on Power System Technology (POWERCON)*, Wollongong, NSW, Australia, 2016.

[165] Y. Yang, H. Li, A. Aichhorn, J. Zheng and M. Greenleaf, "Sizing Strategy of Distributed Battery Storage System With High Penetration of Photovoltaic for Voltage Regulation and Peak Load Shaving," *IEEE Transactions on Smart Grid,* vol. 5, no. 2, pp. 982 - 991, 2014.

[166] K. B. Ariyur and a. M. Krstic., Real-time optimization by extremum-seeking control, New Jersey: John Wiley & Sons, 2003.

[167] R. D. Brackston, A. Wynn and J. F. Morrison, "Extremum seeking to control the amplitude and frequency of a pulsed jet for bluff body drag reduction," *Experiments in Fluids,* vol. 57, no. 10, p. 159, 2016.

[168] V. Koropouli, A. Gusrialdi, S. Hirche and D. Lee, "An extremum-seeking control approach for constrained robotic motion tasks," *Control Engineering Practice,* vol. 52, pp. 1-14, 2016.

[169] A. Marjanović, M. Krstić, Ž. Đurović and B. Kovačević, "Control of Thermal Power Plant Combustion Distribution Using Extremum Seeking," *IEEE Transactions on Control Systems Technology,* vol. 25, no. 5, pp. 1670 - 1682, 2017.

[170] I. Munteanu and A. I. Bratcu, "MPPT for grid-connected photovoltaic systems using ripple-based Extremum Seeking Control: Analysis and control design issues," *Solar Energy,* vol. 111, pp. 30-42, 2015.

[171] A. Ghaffari, M. Krstić and S. Seshagiri, "Power Optimization and Control in Wind Energy Conversion Systems Using Extremum Seeking," *IEEE Transactions on Control Systems Technology,* vol. 22, no. 5, pp. 1684 - 1695, 2014.

[172] O. Trollberg and E. W. Jacobsen, "Greedy Extremum Seeking Control with Applications to Biochemical Processes," *IFAC-PapersOnLine,* vol. 49, no. 7, pp. 109-114, 2016.

[173] F. D. Sahneh, G. Hu and L. Xie, "Extremum Seeking Control for Systems with Time-Varying Extremum," in *31st Chinese Control Conference,* Hefei, China, 2012.

[174] C. Wei and M. Benosman, "Extremum seeking-based adaptive voltage control of distribution systems with high PV penetration," in *2016 IEEE Power & Energy Society Innovative Smart Grid Technologies Conference (ISGT),* Minneapolis, MN, USA, 2016.

[175] H. Tanaka, F. Ikeda, T. Tanaka, H. Yamada and M. Okamoto, "Novel Reactive Power Control Strategy Based on Constant DC-Capacitor Voltage Control for Reducing the Capacity of Smart Charger for Electric Vehicles on Single-Phase Three-Wire Distribution Feeders," *IEEE Journal of Emerging and Selected Topics in Power Electronics,* vol. 4, no. 2, pp. 481 - 488, 2016.

[176] M. Ushiroda, T. Wakimoto, H. Yamada, T. Tanaka, M. Okamoto and K. Kawahara, "Voltage rise suppression and load balancing by PV-PCS with constant dc-capacitor

voltage control based strategy on single-phase three-wire distribution feeders," in *2015 18th International Conference on Electrical Machines and Systems (ICEMS)*, Pattaya, Thailand, 2015.

[177] "SCE Load Profiles," 2017. [Online]. Available: https://www.sce.com/wps/portal/home/regulatory/load-profiles/!ut/p/b1/nVJNc4IwFPwtPXDEPD4GsDdGOxQ62qp1KrkwIYSPDiQIUeq_b2y9OFNr7TvlZXZfsvsWYbRBmJN9VRBZCU7qY4-dJAqnvhHYZhi40RT8l6k7XS8dw34yFCBWALhQPlzjvyGMMOWylSWKe8oSKrhkXCaMa3A6a9CxYlcTKbqDBrUgmd52Iq9q1h_ZL.

[178] H. Nazaripouya, Y. Wang, P. Chu, H. R. Pota and R. Gadh, "Optimal sizing and placement of battery energy storage in distribution system based on solar size for voltage regulation," in *2015 IEEE Power & Energy Society General Meeting*, Denver, CO, 2015.